

University of Louisville

## ThinkIR: The University of Louisville's Institutional Repository

---

Electronic Theses and Dissertations

---

8-2021

### Development and evaluation of a body weight support treadmill for use with locomotor training on pediatric spinal cord injury patients.

Winston T Rauch  
*University of Louisville*

Follow this and additional works at: <https://ir.library.louisville.edu/etd>



Part of the [Other Biomedical Engineering and Bioengineering Commons](#), and the [Other Rehabilitation and Therapy Commons](#)

---

#### Recommended Citation

Rauch, Winston T, "Development and evaluation of a body weight support treadmill for use with locomotor training on pediatric spinal cord injury patients." (2021). *Electronic Theses and Dissertations*. Paper 3911. <https://doi.org/10.18297/etd/3911>

This Master's Thesis is brought to you for free and open access by ThinkIR: The University of Louisville's Institutional Repository. It has been accepted for inclusion in Electronic Theses and Dissertations by an authorized administrator of ThinkIR: The University of Louisville's Institutional Repository. This title appears here courtesy of the author, who has retained all other copyrights. For more information, please contact [thinkir@louisville.edu](mailto:thinkir@louisville.edu).

DEVELOPMENT AND EVALUATION OF A BODY WEIGHT SUPPORT TREADMILL  
FOR USE WITH LOCOMOTOR TRAINING ON PEDIATRIC SPINAL CORD INJURY  
PATIENTS

by

Winston T Rauch

B.S. Bioengineering, University of Louisville, 2015

A Thesis

Submitted to the Faculty of the

University of Louisville

J. B. Speed School of Engineering

as Partial Fulfillment of the Requirements

for the Professional Degree

MASTER OF ENGINEERING

Department of Bioengineering

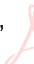
August 2021

DEVELOPMENT AND EVALUATION OF A BODY WEIGHT SUPPORT TREADMILL FOR  
USE WITH LOCOMOTOR TRAINING ON PEDIATRIC SPINAL CORD INJURY PATIENTS

A Thesis Approved on

23 August 2021

by the Following Reading and Examination Committee:

Thomas J. Roussel,  Digitally signed by Thomas J.  
Roussel, Jr.  
Date: 2021.08.23 14:58:52 -04'00'

Thomas Roussel, PhD, Thesis Director

Andrea Behrman  Digitally signed by Andrea  
Behrman  
Date: 2021.08.23 15:23:15 -04'00'

Andrea Behrman, PhD, PT, FAPTA

Claudia Angeli  Digitally signed by Claudia Angeli  
Date: 2021.08.23 15:25:15 -04'00'

Claudia Angeli, PhD

## **ACKNOWLEDGMENTS**

To my beloved grandmother who taught me the value of hard work and perseverance. I truly can't thank you enough.

I want to express my deepest gratitude to Dr. Thomas Roussel, my thesis director and mentor, for his unwavering support, guidance, and invaluable advice throughout this project and my career.

I would like to also extend my sincere thanks to Dr. Andrea Behrman and the entire team at the Kentucky Injury Spinal Cord Research Center for the opportunity to participate in such an incredible and rewarding project.



## **ABSTRACT**

The consequences of spinal cord injury (SCI) are devastating regardless of the age of a patient. When the injury occurs in children five years old or younger, however, the impact is magnified due to the inevitable development of scoliosis (96%) and hip dysplasia (57%) (Schottler et al., 2012). To reduce occurrence of these complications and improve the quality of life for these patients, specialized activity-based therapies such as locomotor training (LT) are being increasingly used to improve overall trunk control and muscle activity in the lower extremities (Harkema et al., 2012; Howland et al., 2014). The aim of this therapy is to activate the neuromuscular networks below and across the level of the lesion via intense practice and repetition of the task of walking and standing. To conduct LT, the re-training of the neuromuscular network occurs during training on a specialized treadmill with an integrated system for monitoring, controlling, and recording the patient's body weight support (BWS) (via a patented force feedback system) and manual trainers that promote a task-specific, sensorimotor experience. While body weight support treadmills (BWST) exist for LT with adults, none have been developed specifically for children. Adult systems are neither suited to the needs of the pediatric population, nor to the needs of the physical therapist and trainers providing the therapy. This thesis reports on the development of a body weight support treadmill specifically designed to enable pediatric LT. Evaluation of this prototype will lead to further system development with the end goal to develop a marketable clinical ready body weight support treadmill for use with the pediatric population.

## TABLE OF CONTENTS

ACKNOWLEDGMENTS .....	ii
ABSTRACT .....	iii
TABLE OF CONTENTS .....	iv
LIST OF TABLES .....	vii
LIST OF FIGURES .....	viii
I. INTRODUCTION .....	1
1.1 Specific Aims.....	1
II. BACKGROUND & SIGNIFICANCE.....	3
2.1 Spinal Cord Injury and Anatomy .....	3
2.2 Paradigm Shift in Rehabilitation Strategies .....	5
2.3 Locomotor Training .....	7
2.4 LT translation to Pediatric Population .....	9
2.5 Clinical Need .....	10
2.6 Prior Work and System Limitations.....	14
III. MATERIALS & METHODS .....	16
3.1 Overview .....	16
3.2 User Needs Evaluation and Design Criteria Development .....	17
3.2.1 User Needs .....	17
3.2.2 Quality Function Deployment.....	18
3.2.3 Design Ideation and Design Criteria Creation .....	19
3.2.4 Design Failure Mode and Effects Analysis (DFMEA) .....	23
3.3 Engineering Methods for Initial Design Evaluation .....	24
3.4 Beta Prototype – Re-design for Manufacturability .....	26
3.4.1 Overall System Design Requirements and Layout Development.....	26
3.4.2 Motion Analysis Tipping Scenario .....	30
3.4.3 Fabrication and Assembly.....	33
3.4.4 Verification Testing .....	33
3.5 Treadmill.....	35
3.5.1 Treadmill Design Requirements and Development .....	35
3.5.2 Treadmill Deck FEA Simulation .....	43
3.5.3 Fabrication and Assembly.....	46
3.5.4 Verification Testing .....	48

3.6	Integrated Seating and Footrest System.....	49
3.6.1	Seating/Footrest Design Requirements and Development.....	49
3.6.2	Safety FEA Evaluation of Trunk and Side Seating.....	57
3.6.3	Fabrication and Assembly.....	62
3.6.4	Verification Testing .....	63
3.7	Stabilizing Decks .....	63
3.7.1	Fore and Aft Deck Design Requirements and Development .....	63
3.7.2	Fabrication and Assembly.....	70
3.7.3	Verification Testing .....	72
3.8	Crane .....	73
3.8.1	Rotating Crane Design Requirements and Development.....	73
3.8.2	Gusset/Non-gusset Design Comparison and Crane Safety FEA Evaluation .....	77
3.8.3	Fabrication and Assembly.....	86
3.8.4	Verification Testing .....	87
3.9	Body Weight Support and Control System.....	87
3.9.1	BWS and Control System Design Requirements and Development.....	87
3.9.2	Fabrication and Assembly.....	93
3.9.3	Verification Testing .....	94
IV.	RESULTS & DISCUSSION.....	97
4.1	QFD Results.....	97
4.2	DFMEA Results.....	98
4.3	Overall System.....	99
4.3.1	Modularity and Dimensional adjustment to Pediatric Population .....	99
4.3.2	Tipping Scenario Verification and Motion Analysis Results.....	101
4.3.3	Footprint Reduction and Ease of Installation.....	103
4.3.4	Overall System Stability Testing .....	104
4.4	Treadmill.....	105
4.4.1	Dimensional and Visual Analysis of Central Treadmill .....	105
4.4.2	Treadmill Deck Static FEA and Weight Testing Results.....	107
4.4.3	Treadmill Functionality Testing Results .....	110
4.5	Integrated Seating and Footrest System.....	112
4.5.1	Seating and Footrest Dimensional Verification and Visual Analysis Results .	112
4.5.2	Trunk and Side Trainer Seating Static FEA Results and Weight Testing .....	114
4.5.3	Trainer Feedback on Seating/Footrests and Subsequent Iterations.....	119
4.6	Stabilizing Decks .....	123
4.6.1	Front/Rear Deck Dimensional Verification and Visual Analysis Results .....	123

4.6.2	Front/Rear Deck TRESPA Install and Weight Testing Results .....	125
4.7	Crane .....	127
4.7.1	Crane Dimensional Verification and Slew Ring Functionality Testing.....	127
4.7.2	Gusset vs. Non-gusset Static FEA results .....	128
4.7.3	Non-gusset Modal Frequency Analysis and Linear Dynamic FEA Results ....	134
4.7.4	Crane Weight Testing and Subsequent Electric Cylinder Support Box Redesign 136	
4.8	Body Weight Support and Control System.....	140
4.8.1	BWS Dimensional Verification .....	140
4.8.2	BWS Functionality Testing.....	143
4.8.3	Load Cell Installation and Verification Testing.....	145
V.	CONCLUSION & FUTURE WORK .....	147
5.1	Considerations for Further Development and Validation .....	147
5.2	Conclusion .....	147
VI.	REFERENCES .....	149
VII.	APPENDIX I: DFMEA .....	152
VIII.	APPENDIX II: Overall BWST Design Criteria and Verification Results .....	153
IX.	APPENDIX III: Treadmill Design Criteria and Verification Results .....	155
X.	APPENDIX IV: Seating/Footeast Design Criteria and Verification Results .....	157
XI.	APPENDIX V: Front/Rear Decks Design Criteria and Verification Results .....	159
XII.	APPENDIX VI: Crane Design Criteria and Verification Results.....	161
XIII.	APPENDIX VII: BWS/Control System Design Criteria and Verification Results .	163
XIV.	APPENDIX VIII: Original Patient Force Data for FEA Dynamic Analysis .....	165
XV.	APPENDIX IX: Crane Modal Time History von Mises Stress Graphs.....	166
XVI.	APPENDIX X: High-level Cost Structure .....	168
XVII.	APPENDIX XI: Pediatric SCI Patient Metrics Reference.....	169
XVIII.	APPENDIX XII: BWST Control System Schematic.....	170

## LIST OF TABLES

Table 3.1 - Established BWST User Needs .....	17
Table 3.2 – Further Refined Design Criteria Based on Established BWST User Needs .....	20
Table 3.3 - Simulated System Sub-Assembly Weights in Pounds.....	30
Table 3.4 - Free Weights Used for Weight testing .....	34
Table 3.5 - Treadmill Deck FEA Properties .....	45
Table 3.6 – Side Seat Cantilever Arm FEA Properties.....	59
Table 3.7 - Trunk Trainer Seat FEA Properties .....	62
Table 3.8 - Gusset Crane Static FEA Properties .....	79
Table 3.9 – Non-Gusset Crane Static FEA Properties .....	80
Table 3.10 - Non-Gusset Crane Linear Dynamic FEA Properties.....	84
Table 3.11 - Load Cell Calibration Min/Max Weight Used .....	94
Table 3.12 - Load Cell Linearity Testing Weights .....	95

## LIST OF FIGURES

Figure 2.4: Adult Body weight support treadmill.....	8
Figure 2.5: Lokomat with pediatric addon module.....	11
Figure 2.6: ErgoTrainer gantry system with treadmill.....	12
Figure 2.8: Alpha Iteration Pediatric BWST CAD Model.....	14
Figure 2.9: Fully Functional Prototype of Alpha Unit Pediatric BWST.....	15
Figure 3.1: QFD Format (adapted from REF) .....	18
Figure 3.2: Concept Solid Model Renderings of Beta Prototype.....	22
Figure 3.3: Concept Rendering of Beta Prototype Showing Modularity and Symmetry .....	22
Figure 3.4: Full system (top), Full system exploded view with each sub assembly labeled (bottom) .....	27
Figure 3.5: Top view of system showing orientation (left) and exploded view (right) .....	28
Figure 3.6: Full System with Patient Showing Patient Orientation .....	29
Figure 3.7: Treadmill and Complete BWST Center of Mass.....	31
Figure 3.8: Simplified CAD Model Showing Center of Mass for Motion Analysis .....	32
Figure 3.9: Motion Analysis BWST with Floor Setup .....	32
Figure 3.10: Isometric View of Treadmill Showing Rear Flanges and Leveling Feet .....	35
Figure 3.11: Central Treadmill Highlighted and Translucent Front and Back Stabilizing Decks .	36
Figure 3.12: Rear Flanges for Rear Stabilizing Deck Attachment.....	37
Figure 3.13: Treadmill Motor Housing.....	38
Figure 3.14: Treadmill Motor Location (Right) and BWST Power Breaker Box (Left).....	39
Figure 3.15: Treadmill with Exposed Treadmill Deck Highlighted in Orange .....	40

Figure 3.16: Treadmill Top View of Belt .....	41
Figure 3.17: Treadmill Rear Roller (Left) Without the Belt Showing "V" Groove and Rear Pillow Blocks (Right).....	42
Figure 3.18: Isometric Treadmill View with Exposed Internal Seating Adjustment Components	43
Figure 3.19: FEA of Treadmill Deck Showing Load and Fixture Locations.....	44
Figure 3.20: Treadmill Deck Mesh.....	46
Figure 3.21: Treadmill bottom view – note internal crossbeam supports.....	47
Figure 3.22: Highlighted Right/Left Trunk Trainer Seats and Right/Left Footrests .....	50
Figure 3.23: Side View of “Floating” Side Seat and Footrest Design.....	50
Figure 3.24: Side Leg Trainer Seat and Cantilever Mounting Arm.....	51
Figure 3.25: Side Seat Positioning and Adjustability Range .....	51
Figure 3.26: Seating and Footrest Linear Bearing and Rack System .....	52
Figure 3.27: Side Seating Rotational Movement to Disengage Rack for Fore and Aft Movement .....	53
Figure 3.28: Highlighted Seating and Footrest Cantilever Arms Mounted to Linear Bearing and Rack/Pinion Adjustability System.....	53
Figure 3.29: Trunk Trainer Seat (Left) and Trunk Trainer Seat Installed Location (Right).....	54
Figure 3.30: Trunk Trainer Seat Attachment points .....	55
Figure 3.31: Trunk Trainer Seat Swivel Movement and Modularity.....	55
Figure 3.32: Side Leg Trainer Footrest.....	56
Figure 3.33: Footrest Adjustability Range.....	57
Figure 3.34: Force Location (Left) and Fixed Geometry Location (Right) of Seating Cantilever Arm FEA Simulation .....	58
Figure 3.35: Mesh Density of Seating Cantilever Arm FEA .....	60
Figure 3.36: Force Location (Left) and Fixed Geometry Location (Right) of Trunk Trainer Seat FEA Simulation .....	61
Figure 3.37: Mesh Density of Trunk Trainer Seat FEA .....	61

Figure 3.38: Front and Rear Stabilizing Decks Highlighted.....	64
Figure 3.39: Isometric View of Front and Rear Decks Including a Center Axis Line Showing Symmetry.....	65
Figure 3.40: Front and Rear Stabilizing Decks Exploded View Showing Modularity.....	65
Figure 3.41: Front Stabilizing Deck with Steps to Treadmill Motor Housing Platform.....	66
Figure 3.42: Front Deck Dimensions.....	67
Figure 3.43: Front Deck Exploded View Showing Mounting Brackets.....	68
Figure 3.44: Rear Stabilizing Deck Dimensions.....	68
Figure 3.45: Exploded Rear Deck View.....	69
Figure 3.46: Rear Stabilizing Deck Showing Crane Mounting Locations.....	70
Figure 3.47: Beatty Tube Bending Machine at Winston Industries.....	71
Figure 3.48: Tube Bending Die for 1”x3” Steel Tube.....	71
Figure 3.49: Tube Bender for Support Struts on Rear Deck.....	72
Figure 3.50: Profile View of Two-Piece Support Crane (Left) and Exploded View Including BWS Bracketry (Right).....	73
Figure 3.51: Slew Ring (Left) and Transport Slew ring Casing Showing Internal Gear (Right) ..	75
Figure 3.52: Crane Mounting Location on Aft/Rear Deck.....	75
Figure 3.53: Top View Showing Clockwise Crane Rotation of 150 Degrees.....	76
Figure 3.54: Gusseted Solid Static FEA Model (Left) and Non-Gusset Solid Static FEA Model (Right).....	77
Figure 3.55: Crane FEA Force placement (Left) and Crane FEA Fixed Geometry (Right).....	78
Figure 3.56: Mesh Density of Gusset Crane for Static FEA Analysis.....	78
Figure 3.57: Mesh Density of Non-Gusset Crane for Static FEA Analysis.....	81
Figure 3.58: Non-Gusset Shell Linear FEA Model.....	82
Figure 3.59: Crane FEA Force placement (Left) and Crane FEA Fixed Geometry (Right).....	83
Figure 3.60: Mesh Density of Non-Gusset Crane for Linear Dynamic FEA Analysis.....	85



Figure 3.61: Node Location for von Mises Stress Data Analysis from Modal Time History Analysis .....	85
Figure 3.62: Trumpf Trulaser Tube 7000 Steel Tube Laser Cutter at Hafendorfer Machine, Inc.	86
Figure 3.63: Electric and pneumatic control system.....	88
Figure 3.64: BWS Pulley System and BWS Labeled Components .....	89
Figure 3.65: BWS Pulley System Setup .....	91
Figure 3.66: PCB layout for slew ring control.....	92
Figure 3.67: Slew Ring Control Switch.....	93
Figure 4.1: QFD for complete BWST.....	97
Figure 4.2: QFD technical requirements prioritized as percentage of total points .....	98
Figure 4.3: Complete BWST Assembled for Testing .....	100
Figure 4.4: Complete BWST System with 3’ 3’ Child Manikin (Left) and 4’ 9” Child Manikin (Right).....	101
Figure 4.5: Crane Weight Testing.....	102
Figure 4.6: Complete BWST Tipping Motion Analysis Results .....	102
Figure 4.7: Assembled Beta Prototype Showing Symmetry and System Footprint .....	103
Figure 4.8: Shipping Pallet Containing Top/bottom Crane Mast, Back Deck, Front Deck and Crane Plate.....	104
Figure 4.9: Assembled Central Treadmill.....	105
Figure 4.10: Treadmill Motor Housing Showing Motor, Electrical Panel, and VFD.....	106
Figure 4.11: Integrated Linear Bearing and Rack System for Side Seat/Foxtrest within Central Treadmill.....	107
Figure 4.12: Treadmill Deck and Mounting Brackets von Mises Stress Plot (psi) – Zero Deformation Scale .....	108
Figure 4.13: Treadmill Mounting Bracket von Mises Stress Plot (psi) – Zero Deformation Scale .....	108
Figure 4.14: Treadmill Deck and Mounting Brackets Displacement Plot (in) – 30 Deformation Scale.....	109

Figure 4.15: Weight Testing of Motor Housing - 309.96 lbs. (E, F, G, H, I, J, K) for 10 mins. .	110
Figure 4.16: Rear View of Treadmill Showing Open Back End and Roller Tensioning Bolts ...	111
Figure 4.17: Installed Rev. 1 Footrest Arm and Rev. 1 Side Seating Arms .....	112
Figure 4.18: Assembled Rev. 1 Right and Left Side Seats and Rev. 1 Footrests .....	113
Figure 4.19: Trunk Trainer Seat Installation.....	113
Figure 4.20: Side Seat Cantilever Arm and Treadmill Side Panel von Mises Stress Plot (psi) – Zero Deformation Scale.....	114
Figure 4.21: Close-up Side Seat Bracketry von Mises Stress Plot (psi) – Zero Deformation Scale .....	115
Figure 4.22: Profile View Side Seat Cantilever Arm Displacement Plot (in) – 50 Deformation Scale.....	116
Figure 4.23: Side Seat Linear Bearing Displacement Plot (in) – 50 Deformation Scale.....	117
Figure 4.24: Trunk Trainer Seat von Mises Stress Plot (psi) – Zero Deformation Scale .....	118
Figure 4.25: Trunk Trainer Displacement Plot (in) – 50 Deformation Scale .....	119
Figure 4.26: Rev. 2 Cantilever Side Seating Arm (Left) and Installed Rev. 2 Side Seating (Right) .....	120
Figure 4.27: Updated Rev. 3 Side Seat Design.....	121
Figure 4.28: Rev. 3 Cantilever Side Seating Arm (Left) and Installed Rev. 3 Side Seating (Right) .....	122
Figure 4.29: Rev. 1 Footrest Installed (Left) and Rev. 2 Footrest Installed (Right).....	123
Figure 4.30: Modular Front Deck Install (Left) and Installed Front Deck (Right).....	123
Figure 4.31: Modular Back Deck Install (Left) and Back Deck Leveling Feet with Crane Plate (Right).....	124
Figure 4.32: Installed Front and Back Decks.....	125
Figure 4.33: TRESPA Ball Sockets (Left) and Rear Deck TRESPA Installed Showing Patient Stairs (Right).....	126
Figure 4.34: Rear Deck Patient Stairs Weight Testing .....	126
Figure 4.35: Fully Assembled Crane (Left) and BWS Support Brackets and Pulley Brackets (Right).....	127

Figure 4.36: Slew Ring and Crane Attachment Point to Rear Deck.....	128
Figure 4.37: Gusset Crane Static FEA von Mises Stress Plot (psi) – Zero Deformation Scale...	129
Figure 4.38: Gusset Crane Close-up von Mises Stress Plot (psi) – Zero Deformation Scale.....	130
Figure 4.39: Gusset Crane Static FEA Displacement Plot (in) – 50 Deformation Scale.....	131
Figure 4.40: Non-gusset Crane Static FEA von Mises Stress Plot (psi) – Zero Deformation Scale .....	132
Figure 4.41: Non-gusset Crane Close-up von Mises Stress Plot (psi) – Zero Deformation Scale .....	133
Figure 4.42: Non-gusset Crane Static FEA Displacement Plot (in) – 50 Deformation Scale.....	134
Figure 4.43: Non-gusset Crane Mode Shape 1 (19.57Hz)(Left) and Mode Shape 2 (19.89Hz)(Right).....	135
Figure 4.44: Assembled Crane Weight Testing.....	136
Figure 4.45: Rev. 1 Cylinder Support Box Bracket Failure.....	137
Figure 4.46: Rev. 2 Static FEA Fixture Points and Force Location (Left) and Mesh Density (Right).....	138
Figure 4.47: Rev. 2 Cylinder Support Box von Mises Stress Plot (psi) – Zero Deformation Scale .....	139
Figure 4.48: Installed Rev. 2 Cylinder Support Box Bracket.....	140
Figure 4.49: Installed Complete BWS, Control System, and Computer.....	141
Figure 4.50: Yoke Height Dimensional Verification – High Point (Left) and Low Point (Right) .....	142
Figure 4.51: Yoke Height Low Point Dimensional Verification in Patient Pickup Location.....	142
Figure 4.52: Completed BWST Pneumatic and Electrical Control System.....	143
Figure 4.53: Slew Ring Control Circuit Board.....	144
Figure 4.54: Whisker Limit Switch (Left) and positioning Switch (Right).....	145
Figure 4.55: Installed Load Cell (Left) and Pneumatic Small cylinder (Right).....	145
Figure 4.56: Load Cell Linearity and Verification Test Results.....	146

## I. INTRODUCTION

It is an unfortunate reality that the parents of children diagnosed with severe spinal cord injuries (SCI) and the resulting paralysis are often told that their children are never expected to get better. However, the intervention of emerging *activity-based* therapies, specifically locomotor training (LT), has shown promising results related to the recovery of pediatric SCI patients. These types of therapies have provided the rehabilitation community with evidence of increased mobility and improved muscle activity which is promoting a paradigm shift in how these patients are treated.

To further enhance recovery in children with paralysis by providing enhanced LT options, the overall goal of this thesis is to design, build, and test a body weight support treadmill specific to the needs of children. The system will incorporate ergonomic considerations for the trainers that are not routinely provided or even considered in activity-based therapy equipment. The system will ultimately allow for optimal delivery of the unique therapeutic intervention of LT specifically within the pediatric population. The project was supported through the Wallace H. Coulter Translational Research Partnership which “promotes the utilization of best practices of industry to accelerate academic innovations to the market to improve patient care”.

### 1.1 Specific Aims

To achieve this goal, the project was organized into three primary aims:

Specific Aim 1: Develop system design criteria based on user needs

User needs will be developed through dialogue with trainers and researchers, observation of therapy sessions, analysis of prior completed work and a product development methodology translating user needs to technical design requirements called a quality function deployment

(QFD). Design criteria will be developed based on the previously established user needs and an ideation phase will occur to construct concept drawings of the updated system.

Specific Aim 2: Develop a body weight support treadmill for use with locomotor training that is specifically developed for the pediatric population

A high-precision, three-dimensional computer aided design (CAD) model will be developed based on established design criteria and concept drawings created during the ideation phase.

Design for manufacturability will be integrated into the design by coordinating with specialized manufacturers. The final CAD design will be evaluated using FEA simulation software for safety and functionality. A prototype will be fabricated and assembled for verification testing using contract manufactures.

Specific Aim 3: Complete overall system verification testing and end-user evaluation

A design failure mode and effect analysis risk (DFMEA) will be created to identify potential design risk to the patient and develop individual test methods to verify design safety and meeting of user needs. Then, testing for the final assembled prototype will be conducted using dimensional analysis, pre-patient functionality testing, visual inspection, and mechanical safety testing. Design and usability feedback sessions will be conducted to ensure the design meets user needs and changes will be iterated as needed.

Completing these three aims will provide a safe, robust, and manufacturable pediatric body weight support treadmill specifically modified to the requirements of performing LT on the pediatric population. By implementing this BWST at multiple clinics, researchers will be able to further pursue and replicate the clinical outcomes across standardized clinical pediatric sites furthering characterizing the positive patient outcomes seen using activity-based therapies such as LT on children.

## **II. BACKGROUND & SIGNIFICANCE**

### **2.1 Spinal Cord Injury and Anatomy**

Spinal cord injury (SCI) is defined as a mechanical injury to the spinal column that disrupts the nerve pathways causing various primary and secondary complications, most significantly motor function loss.

The pathophysiology of SCI begins with the primary point of mechanical or traumatic injury which is essentially the physical damaging of axons, the severing of blood vessels and cell membranes. Typical traumatic SCIs are a compressive type of injury where the displacement of the vertebral column bones exert force onto the central spinal cord causing compressive damage (Rowland et al., 2008). This initial injury imposes loads directly on the spinal cord disrupting axon conduction, physically cutting off various nerve pathways. This primary mechanical injury typically does not necessarily transect (sever) the spinal cord which would completely and catastrophically cut off all nerve pathways; rather, spared axons cross through the injury site and ultimately permit innovative therapeutic rehabilitation possibilities that will be discussed later. After the initial injury, the first secondary complication seen is the general swelling and hemorrhaging of the spinal cord within the grey matter and white matter. This causes immediate cell necrotic death, disruption of cell membranes, and hemorrhaging (Rowland et al., 2008). The injury vascular disruption and hemorrhaging causes ischemia which is the predecessor to the resulting cascade of secondary injuries. The ischemia causes cytotoxic cell swelling that affects the neurons, axons, and glia (form myelin and protect neurons). This axonal swelling causes a blocking of action potentials from crossing the axons (Rowland et al., 2008). The continued ischemia causes free radical production contributing to cell membrane degradation or cell lysis ultimately shutting down cell organelles and causing cell necrosis in neurons and glia. The injury

site also sees a loss of ion homeostasis in the form of excitotoxicity which causes cell death due to excessive activation of glutamate leading to an influx of calcium ions (Rowland et al., 2008). Demyelination of neurons is seen due to inflammation. This causes impairment of the conduction of action potential signals in the affected nerves. These neurological damages are presented in Figure 2.1.

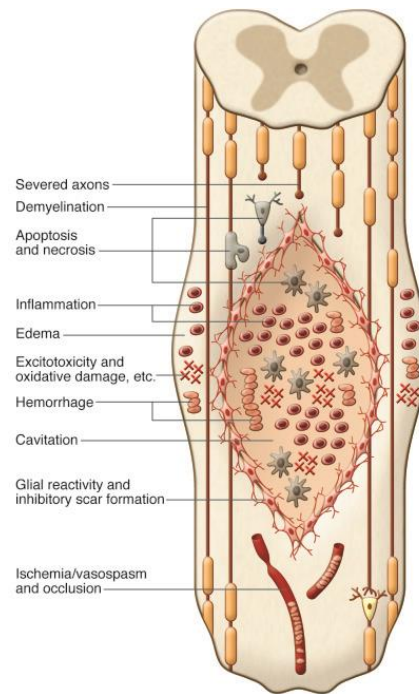


Figure 2.1: Pathophysiology of SCI (Mothe & Tator, 2012)

Injury site nerve damage and cell death causes neurological pathways to be altered triggering a deficiency in nerve function and action potential propagation. This leads to loss of sensation, movement, cognition, or other functions throughout the body based on the nerve pathways involved in the SCI. SCIs can occur at varying positions along the spinal column affecting different nerve pathways as shown in Figure 2.2. For example, SCIs occurring in the cervical spine region would have various function loss below the injury site in areas such as leg muscles, trunk, or abdominal muscles, and even arm muscles. SCIs can also occur at varying positions within the spinal column affecting different nerve paths. Incomplete SCI posterior cord

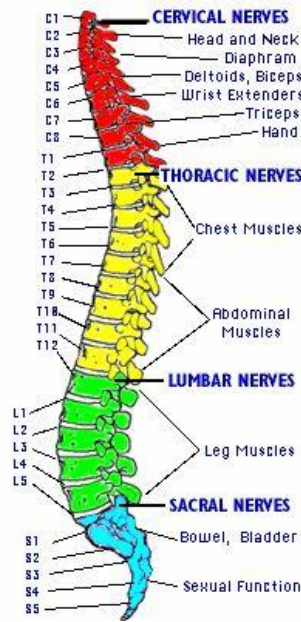


Figure 2.2: Regions of the spinal cord

syndrome is an injury in the back part of the spine causing loss of sensory function while motor function is preserved, while incomplete SCI anterior cord syndrome is an injury in the most inner region of the spine causing loss of leg motor function while proprioception (sense of position) is preserved (McKinley et al., 2007). Overall, the SCI pathophysiology leads to obstructed nerve pathways severely limiting or possibly eliminating supraspinal (above the spinal cord) input from the premotor and primary motor cortices of the brain to the peripheral nerves controlling movement and bodily function (Roy et al., 2012). Collectively, these conditions result in the patient suffering some form of paralysis. Important consideration needs to be taken when discussing the pathophysiology of a SCI and rehabilitation needs of the patient; because every SCI is unique and has varying resulting complications dependent on multiple variables. Therefore, rehabilitation strategies for incomplete SCI patients need to be taken on an individual, case-by-case basis (Harkema et al., 2011).

## 2.2 Paradigm Shift in Rehabilitation Strategies

Rehabilitation strategies for SCI patients have been based on the knowledge that the central nervous system is hardwired and irreparable after the resulting damage to the nerve pathways



caused by the injury mechanism. Spinal nerve tissue does not heal or regenerate compared to peripheral nerves (<http://dx.doi.org/10.1016/j.cell.2010.08.039>) This assumption has caused clinicians to compensate for the function deficits by using wheelchairs, braces, and assistive devices to achieve mobility and a decent standard of living for the patient (Harkema et al., 2011). Recent research has contradicted this way of thinking and has shown that the spinal cord is malleable, can learn, and respond to input causing a reassessment of existing rehabilitation strategies. This is supported through multiple animal studies involving cats with spinal transections (simulated SCI) and their response to intensive walking therapy. When spinal transected cats were provided with truncal support, manually assisted loading, and stepping kinematics over a treadmill, the animals were shown to generate a stepping response in the absence of supraspinal input (Behrman et al., 2006). Although the mechanism is not thoroughly understood, this outcome is believed to come from the capability of the spinal cord to respond to afferent input such as proprioception, muscle length, or load fed back by various sensory receptors. This sensory feedback travels from the afferent nerves to central pattern generators (networks of spinal interneurons that produce rhythmic movements such as walking) within the spinal cord that interpret and generate a response that travels the efferent nerve pathways back creating a motor response (MacKay-Lyons, 2002) (Figure 2.3).

This feedback loop is the foundation for the natural ability of the neural network within the spinal cord to integrate and interpret incoming information and respond with a motor output fundamentally making the spinal cord “smart” (Behrman et al., 2006). Because of this, further research has been done to explain the role of specific afferent sensory feedback during walking. For example, in animal models a vibration of the hip flexor muscle (iliopsoas) during stance

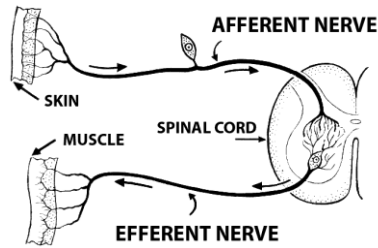


Figure 2.3: Nerve pathways

phase led to an onset of swing phase during walking. It is believed that this vibration stimulated the primary and secondary endings of the muscle spindle within the hip flexor muscles. This stimulation sends afferent sensory feedback to the spinal cord ultimately exciting a stretch that occurs when the hip is extended during the late stance stage of walking thus triggering the forward swing of the limb (Behrman et al., 2006). It has also been shown that afferent input from ankle extensors leads to a self-generated excitation by way of the variation of extensor load receptors or Golgi tendon organs (Harkema et al., 2011). Rehabilitation strategies have been designed to key in on these afferent sensory feedback mechanisms to help therapists create intrinsic sensory information for the central pattern generator during walking rehabilitation therapy. This leads to the conclusion that the central pattern generators use an ensemble of sensory information (speed, inter-limb and intra-limb coordination, kinematics) to create a complete walking pattern within the spinal cord (Harkema et al., 2011). This idea of using sensory feedback to create a walking pattern from the central pattern generator, has been translated into a clinical rehabilitation therapy called “Locomotor Training” providing a recovery path for incomplete spinal cord injury patients (Behrman et al., 2006).

### 2.3 Locomotor Training

Locomotor training is an activity-based training therapy used with SCI patients for the rehabilitation of mobility, posture, standing, and walking. This rehabilitation therapy uses task specific retraining of the nervous system by motivating neural plasticity (Harkema et al., 2011). To provide the necessary function rehabilitation, locomotor training is used on patients with

incomplete spinal cord injury and utilizes the remaining supraspinal nerve input carried through the “spared” axons around the injury site as mentioned early. The essential philosophy behind the therapy is to provide the patient with the intrinsic necessary sensory feedback seen in normal standing or walking patterns by increasing the challenges placed on the nervous system to adapt (Harkema et al., 2011). The training uses four core principles to maximize recovery of the patient: maximize weight bearing on the legs, optimize sensory input cues, optimize the kinematics (i.e., transition from stance to swing phase in walking), and maximize the recovery strategies and eliminate compensation strategies (Harkema et al., 2011).

Locomotor training implores the use walking of the patient on a specialized system for monitoring, controlling, and recording the patient’s body weight called a body weight support treadmill (BWST) (Figure 2.4) and trainers manually supporting the patient with a task specific sensorimotor experience. A BWST uses a patented closed-loop force feedback system (Gordon et al., 2008)U.S. Patent 7,381,163) by implementing a small and large pneumatic air cylinder to



Figure 2.4: Adult Body weight support treadmill

adjust the body weight support (BWS) of the patient. This system will safely hold the patient in a vertical position and offset the weight experienced by the legs. The body weight control can be adjusted to allow the patient to feel varying amounts of load while standing depending on individual level of progression. Three trainers (one in the back that controls the trunk and one on each side interacting with the legs of the patient) physically move the trunk and legs to simulate and provide the necessary sensory feedback (i.e., pressure, loads) to extremities of the patient to create a natural walking gait that ignites the spinal central pattern generators.

Known benefits for adults with SCI include improved standing, walking, balance, endurance, and walking speed (Harkema et al., 2012). The recovery process using locomotor training follows a very nonlinear trend due to variations among patients; therefore, there is not a designated timeline of sessions. Instead, the therapy uses qualitative observation (i.e., are they able to maintain posture in a specific set of circumstances) to judge progression. However, a generalized review of case studies involving locomotor training patients has shown that the more sessions of locomotor training a patient has performed generally the better the outcome (Harkema et al., 2011).

#### **2.4 LT translation to Pediatric Population**

Applying LT to the pediatric SCI patient population has shown remarkable results (Behrman et al., 2008; Fox et al., 2013; Howland et al., 2014). In a study examining neuromuscular control of reciprocal locomotor tasks in children with SCI as well as uninjured children, lower extremity electromyogram (EMG) recordings during locomotor type tasks (e.g., walking, pedaling, etc.) showed EMG data that was consistent with previous studies in animal and adults suggesting that interventions that activate the neuromuscular system to enhance walking also may influence the control of other locomotor tasks (Fox et al., 2013).

Adults who experience a spinal injury later in life have experience with all basic motor movements, however dependent upon a child's age at the time of injury, their central nervous system may not have developed various motor movements during childhood such as walking

(Howland et al., 2014). Research has shown that a lack of prior walking experience does not preclude development of walking after SCI (Howland et al., 2010; Howland et al., 2011).

Additional research has been conducted evaluating the effects of LT on a child with a chronic incomplete SCI and how neuroplasticity of an immature central nervous system responds to newer rehabilitation strategies (Behrman et al., 2008). A study on the evaluation of the effects of LT on a non-ambulatory 4 1/2-year-old boy with a low cervical SCI undergoing 76 sessions of locomotor-specific training, has produced an outcome of the child having no ability to use his legs at the beginning of training to community ambulation with a rolling walker suggesting that LT is a feasible strategy for promoting recovery of locomotion in children with chronic, severe SCI (Behrman et al., 2008).

## **2.5 Clinical Need**

Translation of LT into the clinical setting began around 2005 with the formation of the Christopher and Dana Reeve Foundation NeuroRecovery Network. Several aspects have supported this process e.g., standardized training and outcome measures, ongoing program evaluation and identifying patterns of recovery (Howland et al., 2014). This has provided a new neurorecovery-based approach to SCI rehabilitation and in addition, established a reimbursement mechanism as a clinical treatment using standardized codes (e.g., neuromuscular re-education) supporting translation of LT to clinical practice. This framework used with adults in the NeuroRecovery Network could provide a starting point for this approach with children (Howland et al., 2014).

To support this effort of applying locomotor training in a clinical setting, various types of training equipment have been developed such as the BWST discussed in 2.3. This system is the PowerStep System sold by PowerNeuroRecovery (<https://www.powerneurorecovery.com/thepowerstep>). The system is specifically designed to provide the necessary features and framework for performing LT including closed-looped force feedback and proper trainer seating, however, it was designed for use with adults weighing

upwards of 250 lbs. and lacks any consideration of needs of the pediatric population. Another partial body weight support treadmill, The Lokomat (Figure 2.5), sold by Hocoma (<https://www.hocoma.com/us/solutions/lokomat/>) is an investigative robotic rehabilitation device that provides repetitive physiological movement training.



Figure 2.5: Lokomat with pediatric add-on module

The Lokomat uses a robotic exoskeleton to provide control, support for patient trunk and legs during training which differs from LT-specific BWST and ultimately limits the ability of trainers to provide optimal sensorimotor experience crucial to the success of the therapy. A Pediatric add-on module is available, however there isn't proper closed-loop force feedback and the elimination of the trainer's interaction with the patient via the robotic exoskeleton eliminates the possibility to perform LT with the system.

Another gait therapy device, The ErgoTrainer (Figure 2.6) sold by Ergolet/WinnCare Group ([https://www.winnCare.com/fiche-produits-rehabilitation-ergo\\_trainer-12-630-int.htm](https://www.winnCare.com/fiche-produits-rehabilitation-ergo_trainer-12-630-int.htm)) is a gantry-type ceiling-mounted body weight support system. This system allows the clinic to provide body weight support over varying equipment or surfaces (e.g., floor/ground, treadmill, stationary bike, etc.). This system is designed for adults (max user weight 440 lbs.), lacks a

closed-looped force feedback system, and any trainer seating structure making it incompatible with pediatric locomotor training.



Figure 2.6: ErgoTrainer gantry system with treadmill

While considerations for using BWS systems with adults have been identified (Harkema et al., 1997), pediatric needs have not been described. Commercially available adult systems are neither suited to the needs of the pediatric population, nor to the needs of the trainers providing the therapy. Additionally, these systems have not been designed with an understanding of the science behind the therapeutic intervention of LT as applied with the use of a partial body weight support treadmill.

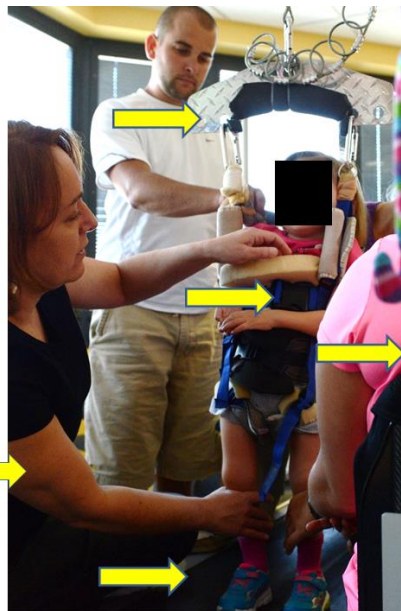
*This presents an unmet clinical need* to develop a pediatric BWST that will specifically meet the needs required to enable locomotor training with pediatric SCI patients. When performing LT with a child on an adult BWST many issues arise (Figure 2.7). The computer-controlled body weight support is not tuned to the weight and size of child instead it is optimized for an adult weighing greater than 100 pounds and is not easily modified to accommodate a lower, often much lower, weight range. The overall treadmill size is too long and wide for a child's gait causing a misfit and strain on the trainers, which ultimately limits the ability of the trainers to perform LT for an extended amount of time. In addition, the seating is not ergonomically designed for performing LT on a child thus causing poor positioning and strain on trainers. The trainers also

must lift the patient on and off the system. The design of the pediatric unit should address the aesthetics of an environment and product accepted and recognized as for children (e.g., color, design).

The currently used adult BWST for pediatric LT has many additional commercialization hurdles. Capital cost is significant at well over \$100,000 per system, long manufacturing lead times and limited design for manufacturability, a large overall footprint (9'10" H x 4' 9' W x 18' L), and often comes with a cumbersome install process with a workforce of 4 people needed over several days.

## Patient and Trainer Issues

- Child's view and potential for trainer interaction blocked by large crane structure
- Need ergonomic design
  - Keep trainers as close to neutral as possible
  - Eliminate trainer pain and reach



- Harness fit
- Body weight support
- Seating for trainers
- Treadmill width
- 4<sup>th</sup> trainer runs computer control
- Lifting child on/off system

Figure 2.7: Patient and Trainer Issues Experienced using an Adult BWST with a Pediatric Patient

This project outlines the development of a pediatric-system BWS and treadmill system that will specifically meet the needs relative to delivery of this therapy to children age 1-12 years. The product is innovative and consistent with an emerging paradigm shift in rehabilitation from compensation to recovery-based strategies whereby systems are meant to produce a therapeutic effect (i.e., change in neuromuscular capacity supporting new function or ability such as sitting, standing, or walking) as opposed to an end product (e.g., learn to and use a wheelchair to



compensate for loss of neuromuscular capacity). The overall development aims were distinguished based directly on end-user needs and developing a body weight support treadmill that better meets the clinical needs for performing locomotor training within the pediatric population.

## 2.6 Prior Work and System Limitations

An alpha (first iteration) version of a pediatric BWST based on system needs prototype was developed. Prior research and development spearheaded by the KSIRC, led to the development of a proof-of-concept system model (Figure 2.8) in the form of a scaled-down version of an existing adult BWST. This Alpha BWST was constructed from a commercial treadmill that was cannibalized and reconfigured into a custom frame using extruded aluminum (80/20 interchangeable structural aluminum framing). The system was assembled as a first step towards



Figure 2.8: Alpha Iteration Pediatric BWST CAD Model

a fully functional prototype. The structural framing allowed for modularity when making engineering adjustments, however, was not very practical for a commercialized system nor durability of the system over time. The alpha prototype design provided the initial feedback and framework needed to develop a more refined manufacturable design that better suits the intended design goals.



Figure 2.9: Fully Functional Prototype of Alpha Unit Pediatric BWST

### **III. MATERIALS & METHODS**

#### **3.1 Overview**

To meet project goals, a user-based iterative product development design approach was implemented to blend overall product goals, commercialization viability, design for manufacturing, user needs, and detailed engineering specs. User needs were defined from known predicate device limitations, direct trainer feedback, and design/project analysis. A quality function deployment (QFD) method was implemented to correlate the user needs to the technical requirements to meet these needs. This allowed for implementation of a ranking system to each of the customer needs that were most critical to the system. After establishing the critical features needed for the system, design output criteria were created based on these needs and general engineering evaluation. The output criteria were entered into a Design Failure Mode and Effects Analysis (DFMEA) to ensure risk was mitigated and a comprehensive verification testing plan was developed. Next, the design was modeled in computer-aided design (CAD) software and optimized to initially fit the design criteria. Finite element analysis (FEA) was used to simulate various load conditions to ensure device safety. Fabrication of system components was outsourced, verified with the manufacturer, then assembled to complete a fully functional prototype. Further verification and validation steps were taken to further evaluate the prototype against design criteria. Iterative redesigns were executed based on trainer feedback and operational results. This thesis presents this previously described iterative product development process described for each sub-assembly of the complete BWST.

## 3.2 User Needs Evaluation and Design Criteria Development

### 3.2.1 User Needs

User needs were determined through understanding of prior BWST work and its limitations and various discussions with researchers, and engineers from the University of Louisville Bioengineering Department and Kentucky Spinal Cord Injury Research Center.

Developing the overall system design goals and user needs, focus was concentrated in three principal areas. The system must:

- 1) Provide consistent BWS for the pediatric population using closed-loop force feedback during typical vertical gait oscillations
- 2) Promote appropriate pediatric patient body mechanics/gait training and
- 3) Provide ergonomic seating/positioning for sustained and repetitive delivery of this intense therapy to small patient sizes by the trainers.

These basic principles were expanded upon based on interviews and discussions with trainers and researchers of the cross-disciplinary project team. Table 3.1 lists all required user needs needed for the pediatric body weight support treadmill.

**Table 3.1 - Established BWST User Needs**

Number	User Need
1	Need ergonomic seating design, keep trainers as close to neutral as possible, Eliminate trainer pain and reach, Ease for trainer
2	Modular design. Design for Manufacturability, easier assembly, more affordable for clinics
3	Smaller footprint to integrate in clinic - to transport, allow easier install - reduce installation costs, symmetrical to fit in any space
4	Pediatric SCI patient
5	Integration of dynamic force-feedback BWS

Number	User Need
6	Lift system for placing child on/off treadmill and partial BWS, Drastic reduction of system footprint Elimination of need for ramp, safer HIPAA compliant solution, potential for additional training scenarios
7	Customized treadmill e.g., size motor control, etc. for pediatric size, Ergonomic access for trainers
8	Overall system safety, integrate structural factor of safety
9	Kid friendly and less intimidating and open floor plan for multiple trainer interaction

These collected user needs were evaluated within a quality function deployment (QFD) to better understand the critical user needs and establish corresponding technical parameters needed to meet these user requirements.

### 3.2.2 Quality Function Deployment

Quality Function Deployment (QFD; Figure 3.1) is a methodology that associates a set of customer/user requirements or needs with a set of technical requirements quantifying them with a priority level (Taylor & Ranganathan, 2013). A QFD methodology was used to determine which requirements of the pediatric BWST were “critical” to the success of the overall project.

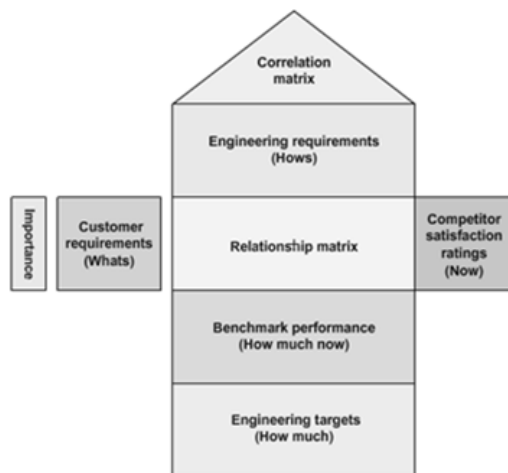


Figure 3.1: QFD Format (adapted from REF)

The QFD is setup with the customer requirements or user needs outlined in the rows on the left and the engineering/technical requirements to achieve these user needs are outlined in the columns at the top. The customer requirements are ranked from 1 (least required) to 5 (most required) on importance to the overall goals of the project. The correlation matrix at the top of the QFD indicates how each technical requirement is correlated with the rest of the technical requirements providing an idea of the design tradeoffs (Taylor & Ranganathan, 2013).

The relationship matrix in the middle is the key piece of the QFD correlating how much impact each technical requirement should be given to satisfy the customer requirement being analyzed. The entries in the matrix are strong (3), medium (2), weak (1), or none (0). After each cell in the relationship matrix is filled out, the sum of the product of each cell with the customer requirement priority is computed resulting in the scoring totals recorded at the bottom. Thus, the outcome of the QFD is the ranked and prioritized technical parameters of the device or system (Taylor & Ranganathan, 2013).

The QFD is used to bridge the gap between the user needs of the BWST as discussed with trainers and researchers and the technical requirements and priorities when designing the system to meet these user needs. The QFD results and technical requirements priorities are discussed and can be seen in section 4.1

### **3.2.3 Design Ideation and Design Criteria Creation**

The BWST technical aspects prioritized through the QFD process were evaluated along with current pediatric SCI patient metrics (APPENDIX XI: Pediatric SCI Patient Metrics Reference), prior completed work on the alpha BWST, and observations of LT training sessions to develop the refined design criteria. Evaluation of the alpha BWST prototype (Figure 2.9) showed several limitations. The system was constructed using 80/20 aluminum extrudes for the overall structure creating significant cost increase and raised questions about durability and strength. Wooden stairs and back deck of the alpha BWST added additional footprint space and unneeded complexity. The aluminum extrudes were flexible and could potentially affect BWS force

readings. The crane was located directly in front of the patient making it very difficult for the trainers to interact with the child and creating a large structure right in front of them. There was no ramp and the patient had to be manually lifted out of their wheelchairs to be placed on the system. The treadmill was a reconstructed version of an off-the-shelf pediatric treadmill model with 17 in. by 46 in. exposed belt width and length, respectively. Dimensionally the treadmill and seating were not a perfect fit for the patient and trainers. It was too wide and long for the trainers to gain proper access to the patient. Design for manufacturability was not considered and commercialization of the design was determined to be difficult.

Update treadmill dimension were determined from analysis of the alpha BWST dimensions (17 in. W x 46 in. L), discussions with researchers, and prior scientific journal research on pediatric gait analysis. One study analyzed the gait of 33 children ages 3 to 6 years old. Highest step length, step width, and time mean value seen was 19.69 in., 6.10 in., and 0.39 s respectively. Updated treadmill design criteria and additional system design criteria were determined and can be seen in Table 3.2.

**Table 3.2 – Further Refined Design Criteria Based on Established BWST User Needs**

<b>Number</b>	<b>User Need</b>	<b>Design Criteria</b>
<b>1</b>	Need ergonomic seating design, keep trainers as close to neutral as possible, eliminate trainer pain and reach, ease for trainer	Integrated seating design with fore/aft and up/down adjustability - ease of adjustability, alignment to patient and ability to support varying trainer sizes
<b>2</b>	Design for Manufacturability, easier assembly, more affordable for clinics	Modular design, symmetric front and back decks, multiple sub-assemblies, state-of-the-art manufacturing techniques to reduce cost, fewer components
<b>3</b>	Smaller footprint to integrate in clinic - to transport, allow easier install - reduce installation costs, symmetrical to fit in any space	Overall floor space 4'3" W x 6'3" L x 8'6"H
<b>4</b>	Adapt system to pediatric SCI patient metrics	Pediatric SCI patient metrics 1-12 years, 20-120 lbs., 1' 8" - 5'6"
<b>5</b>	Integration of dynamic force-feedback BWS	Pneumatic small cylinder for fine movement and electric actuator for gross control

<b>Number</b>	<b>User Need</b>	<b>Design Criteria</b>
<b>6</b>	Lift system for placing child on/off treadmill and partial BWS, Drastic reduction of system footprint Elimination of need for ramp, safer HIPAA compliant solution, potential for additional training scenarios	Crane (< 9 ft. tall to find in standard ceiling height), moved to rear of system, integration of slew ring and slew ring control
<b>7</b>	Customized treadmill e.g., size motor control, etc. for pediatric size, Ergonomic access for trainers	Treadmill specs, 40" L x 14.75" W, 0-6 mph with 0.1 mph increments
<b>8</b>	Overall system safety, integrate structural factor of safety	Max patient 120 lb. need factor of safety of 1.5, No sharp corners
<b>9</b>	Kid friendly and less intimidating and open floor plan for multiple trainer interaction	Bright colors, Storage for toys etc., Platforms for trainer-patient interaction, move crane behind patient which becomes less intimidating

Concept drawings (Figure 3.2 and Figure 3.3) for the beta iteration BWST were developed to further conceptualize the design with updated dimensions and features to further satisfy the established design criteria. This iteration was a fundamental redesign developed in conjunction with a professional industrial design firm (Adams-Kinkade Design). The primary goal for this beta iteration was to develop overall design aspects and integrate them in a way that will meet both the human ergonomic needs and the patient needs, i.e., the crane was moved behind the patient with integrated rotation feature, treadmill dimensions and specifications altered to better suit a pediatric stride length and composed out of a steel tubing skeleton for added strength. This concept drawing led the high-level concepts and features that a pediatric BWST should include, and ultimately refined the product roadmap.





Figure 3.2: Concept Solid Model Renderings of Beta Prototype



Figure 3.3: Concept Rendering of Beta Prototype Showing Modularity and Symmetry

When designing the pediatric BWST, design for manufacturability (DFM) was a key consideration throughout the designing process. DFM is an important part of the product

development process with an aim of not only creating a design that meets the design requirements but also is easily and economically manufactured. There are a multitude of industry standard ways to ensure DFM is integrated into the design of a product. Reducing the number of parts in a product's bill of materials (BOM) leads to reduced overall costs. Using state of the art manufacturing techniques reducing assembly and manufacturing cost while keeping component quality high. Creating multi-functional components that reduce the number of needed parts for assembly or even creating components that serve two purposes for the end user. Also, creating a modular design is a common DFM practice that breaks a larger system in multiple modular sub-assemblies that can be manufactured independently, replaced, or modified on the final system, and in turn simplifying the assembly process. By breaking down the system into sub-assemblies, a specialized manufacturer can be engaged based on the requirements of each sub-system. Engaging specialized manufacturers to suit your products needs early in the product development process is the best and most efficient way to ensure DFM is integrated into the product. Resulting in less design iterations, improved timelines, and saving time and money supporting the goal of commercialization of the pediatric BWST.

#### **3.2.4 Design Failure Mode and Effects Analysis (DFMEA)**

When designing the pediatric BWST, great care was taken to ensure patient safety and minimize patient risk. Risk management is a critical element to medical device design where patient safety and mitigating potential risk to patient safety is of utmost importance.

To further help analyze this potential risk, the established user needs were further refined into individual design inputs and outputs that could be verified through testing by use of A Design Failure Mode and Effects Analysis (DFMEA). Failure Mode and effect analysis (FMEA) is a tool to evaluate potential failure modes for processes and their effect on outcomes and/or product performance (Services & Administration, 2006). A DFMEA focuses on the product development and design process to eliminate, contain, reduce, or control the potential introduced failures of the system design ultimately reducing patient risk. The output/results of FMEA can be used as a basis

for design or further analysis (Services & Administration, 2006). It ensures design risks are mitigated by breaking down the entire designed system into more manageable criteria that can be tested and verified based on potential failure modes and the likely effects of these failures on the patient/user. The DFMEA that was developed identified a testing method for each of the design criteria or system components and associated risks.

This document was considered “active” throughout the iterative prototype development process. Periodically design inputs and outputs were refined as needs changed and further design needs were uncovered. Ultimately, this document served two purposes: it set up portions of our design verification testing ensuring risk reduction and secondly it organized very detailed design specifications to ensure we were meeting the established design requirements. The full DFMEA can be seen in APPENDIX I: DFMEA and is separated into individual design criteria and verification testing for each sub assembly (overall system criteria, treadmill criteria, seating criteria, deck criteria, crane criteria, and BWS and control system criteria) which are explained further in this thesis.

### **3.3 Engineering Methods for Initial Design Evaluation**

Various engineering simulation methods were used to provide a preliminary analysis of system design aspects and individual components prior to fabrication and testing of the device. This provided a “sanity check” for many design aspects and ensured components were properly design and suited for the potential environmental conditions the BWST would be subjected to. In addition, simulation can potentially reveal failure modes before money or resources are spent on manufacturing of the components.

The Finite Element Method (FEM) is a technique to enable numerical solutions to engineering problems such as heat transfer or stress analysis of a structure (Cook et al., 2002). Application of this method to investigate these structural and physical phenomena is referred to as Finite Element Analysis (FEA). Material properties, geometry fixtures, boundary conditions, and magnitude and direction of forces can be specified to further define the model and simulation

(boundary) conditions. A model of the system is created that is subdivided into thousands of individual finite “elements” that can be visualized as small pieces that make up the larger structure. Elements are connected at points called “nodes” and the arrangement of these elements is called a “mesh”. Numerically speaking, the mesh within an FEA simulation is represented by a system of algebraic equations to be solved for unknowns at the nodes (Cook et al., 2002). An FEA solution is not exact, however, increasing the number of elements or “mesh density” will improve accuracy as more elements are used to represent the overall structure (Cook et al., 2002). Some form of physical verification testing typically follows FEA and must be completed to ensure design and system results are appropriate with the systems intended use or conditions seen.

When analyzing FEA simulations of the BWST, von Mises stress (used to predict yield of ductile material) and overall factor of safety (FOS) will be used to determine component/system safety and performance. The BWST structure will be made from mild steel which is a ductile material leading to von Mises stress to be the preferred metric of analysis. A FOS of 1.5 (industry standard for highly reliable materials where loading is not severe) or in other words the max von Mises stress is 1.5 times the yield stress (minimum stress where a solid will undergo permanent deformation) of the material being analyzed (Maria, 2016).

Various types of FEA analysis modes exist depending on certain loading or environmental situations required for analysis. Static linear analysis looks at an applied load not in relation to time and acts proportionally to as the load increases the stresses increase as well. It means that there is a proportional relationship between the load applied and the amount of stress seen. A linear dynamic study shows the stress in relation to time and allows for a varying cyclical force to be applied with respect to time. Frequency analysis is used to analysis the natural modes of a structure to determine any potential resonant frequencies of an applied load or environmental condition - will the component or system resonate under a commonly or expected applied operating load frequency? Additionally, a motion analysis will incorporate how the components

are mated within the entire system and use a physics-based solver to determine the physical movements of the system under load.

### **3.4 Beta Prototype – Re-design for Manufacturability**

#### **3.4.1 Overall System Design Requirements and Layout Development**

The body weight support treadmill includes five main sub-assemblies – treadmill, integrated seating/footrests, stabilizing decks, crane, and body weight support control system as shown in Figure 3.4. The system features a custom central treadmill that provides a large central anchoring mass improving safety during loading and unloading of a patient. The treadmill also doubles as a mounting base for the front and back stabilizing decks as well as the side seating system. The front and rear stabilizing decks were added to act as supporting extensions of the treadmill by extending outward to further ensure system stability. The entire system was designed and modeled using computer aided design (CAD) software SolidWorks (Dassault Systèmes). A full list of design criteria for the overall BWST can be seen in APPENDIX II: Overall BWST Design Criteria.

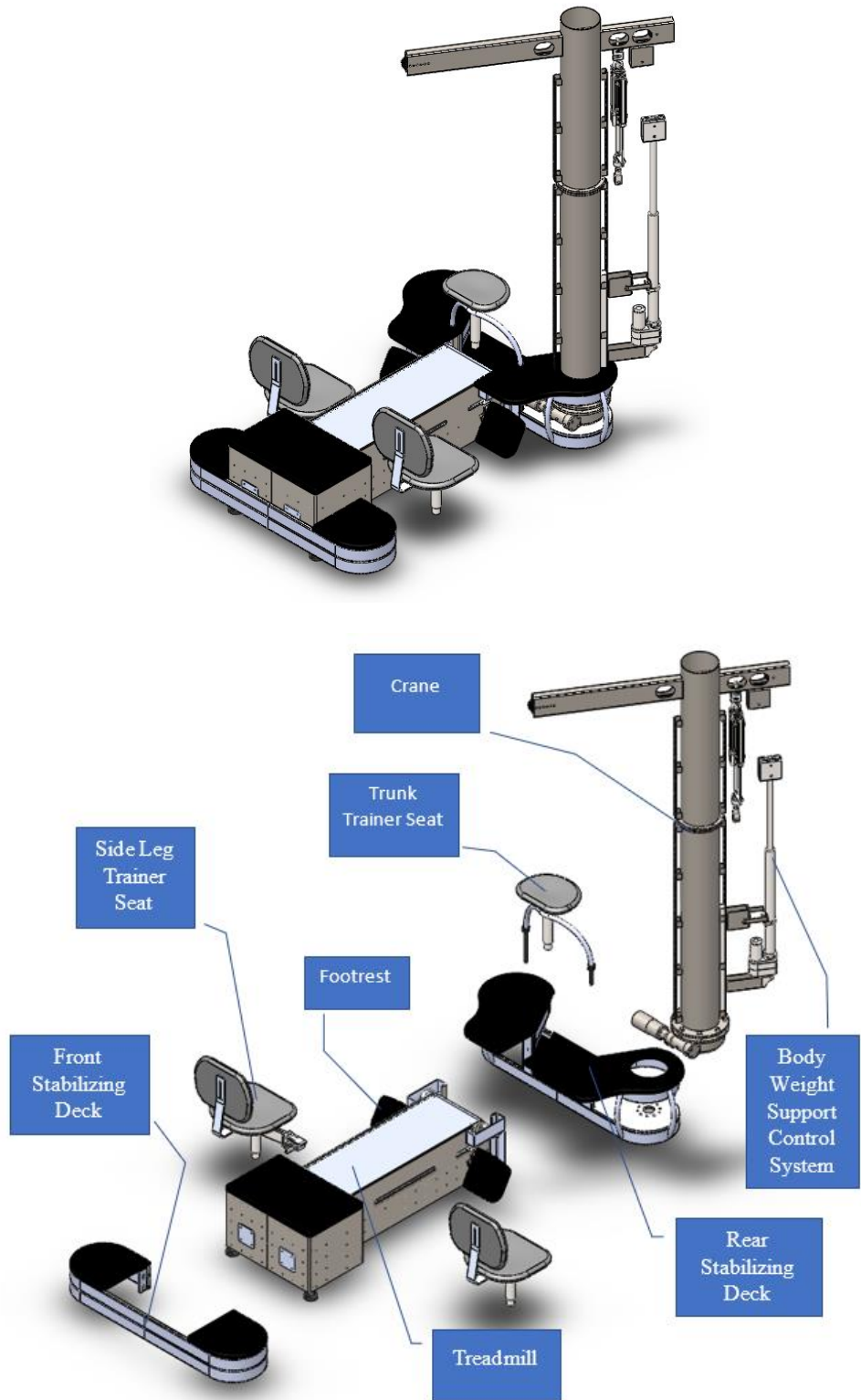


Figure 3.4: Full system (top), Full system exploded view with each sub assembly labeled (bottom)

The overall system was designed in a symmetrical modular sub-assembly format including a two-piece crane design to allow for simplified installation satisfying a main design criterion. The symmetry along the midline of the treadmill allows for potentially two configurations of the crane – right or left side - which allows for added flexibility when fitting the system within the often-tight clinical space. In addition, the modularity allows for ease of assembly and transportation to the clinic for installation. Figure 3.5 shows the top view of the complete system showing the symmetry along the midline of the treadmill.

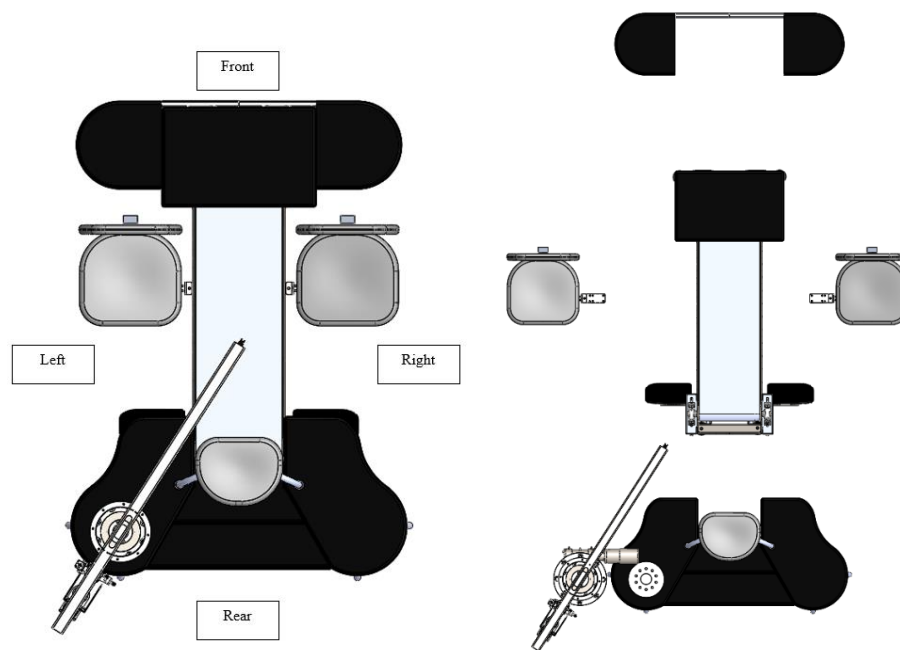


Figure 3.5: Top view of system showing orientation (left) and exploded view (right)

The lifting crane was moved to the rear of the system allowing for an ergonomic design with the front end completely open as the patient is facing away from the lifting crane. Figure 3.6 shows patient orientation in relation to the crane. This design feature allowed the system to become less imposing/non-threatening to the young patients and would allow for improved patient-trainer interaction promoting more engaged productive therapy sessions. This

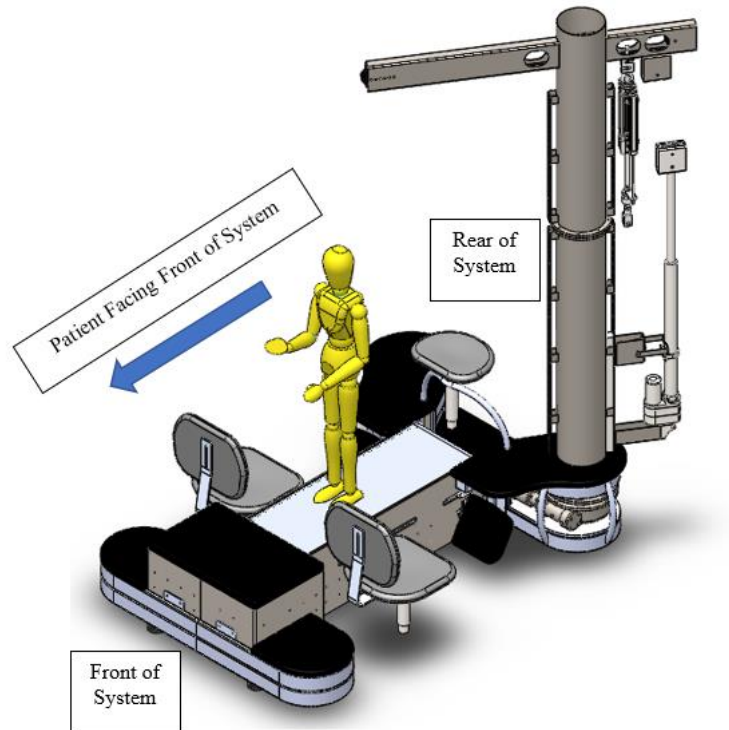


Figure 3.6: Full System with Patient Showing Patient Orientation

fundamental re-positioning of the crane also allowed for the integration of crane rotation as well. This rotation creates a safer loading and unloading of the pediatric patient since they could be harnessed and lifted directly from a seated position. In addition, crane rotation removes the need for a sizable ramp to be installed on the rear of the crane for patient wheelchair access ultimately saving valuable footprint space. To further reduce the overall footprint, a unique cantilevered seating system was designed and incorporated into the treadmill chassis to provide a more simplistic design allowing for easier assembly and reduction of overall system footprint. The BWST footprint was additionally reduced with a “floating” seating system explained further in section 3.6 and updated overall dimension more acceptable for the pediatric population (1-12 years, 20-120 lbs., 5’6” max)



### 3.4.2 Motion Analysis Tipping Scenario

To evaluate overall system risk of tipping or instability, a simplified model for motion analysis was made and subsequently solved establishing the amount of force needed to create tipping of the system. To show a tipping scenario was unlikely, the system was required to hold the max patient size (120 lbs.) with a factor of safety of 1.5 (180 lbs.) with the crane in the most cantilevered position to simulate picking up a patient.

First, the center of mass was found using the mass properties functionality with SolidWorks. The treadmill motor was determined to weigh approximately 60 lbs. (motor specification sheet), as well as the rotating slew ring and slew ring motor (56.96 lbs. as outlined from the spec sheet). Within the 3D model, material properties were assigned to each component of the frame of the treadmill. Using mostly plain carbon steel for the frame, 1060 Aluminum alloy for the rollers, and designating the motor as a fixed mass of 60 lbs. Using the SolidWorks mass properties function, the entire system mass and center of mass location (Figure 3.7) along with each individual modular sub-assembly mass was determined and can be seen in Table 3.3.

**Table 3.3 - Simulated System Sub-Assembly Weights in Pounds**

<b>Sub-assembly</b>	<b>Simulated Weight (lbs.)</b>
<b>Front Stabilizing Deck</b>	50.81
<b>Back Stabilizing Deck</b>	106.93
<b>Treadmill</b>	409.87
<b>Crane</b>	104.96
<b>Slew Ring</b>	56.96
<b>Trunk Trainer Seat</b>	11.04
<b>Left Side Leg Trainer Seat</b>	14.23
<b>Right Side Leg Trainer Seat</b>	14.23
<b>Left Footrest</b>	4.26
<b>Right Footrest</b>	4.26
<b>Total</b>	777.55

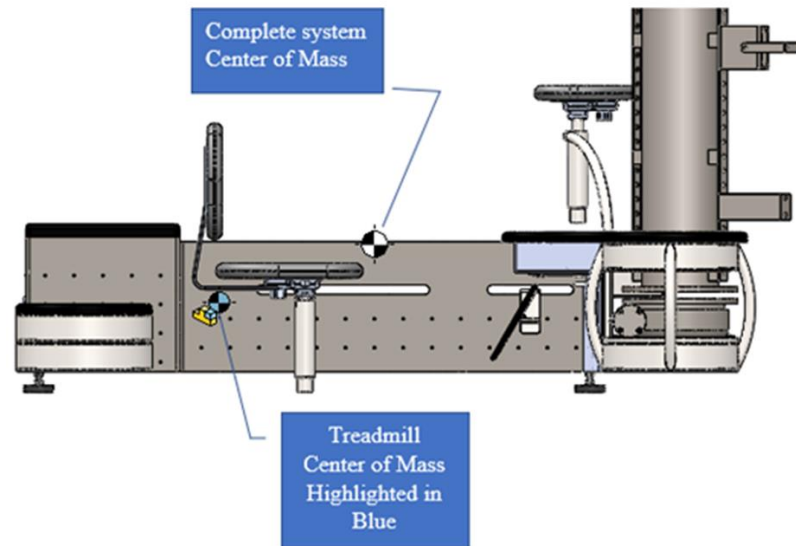


Figure 3.7: Treadmill and Complete BWST Center of Mass

A simplified CAD model was created (Figure 3.8) to conserve computer resources during simulation with a center of mass at the same location as seen in Figure 3.7. The crane position within the model was fully rotated simulating picking up a patient from their wheelchair in a worst case “most cantilevered” scenario.

The simplified CAD model was imported into SolidWorks Motion Analysis. A 300” x 100” x 0.5” thick plain carbon steel component was added to simulate the floor during the motion analysis (Figure 3.9). This component was specified as an “envelope” component so the mass would affect the BWST previously determined center of mass. A coincident mate was made at the bottom edge of the aft deck feet. A solid body contact was added on all components including the floor component. The body contact was simulated as steel-to-steel contact with a coefficient of friction of 0.25. Gravity ( $32.2 \text{ ft/s}^2$ ) was added to the model. A force was applied at time  $t=0$  seconds to the end face of the crane boom arm and the study was running for a total of 5 seconds ( $t=5$ ).

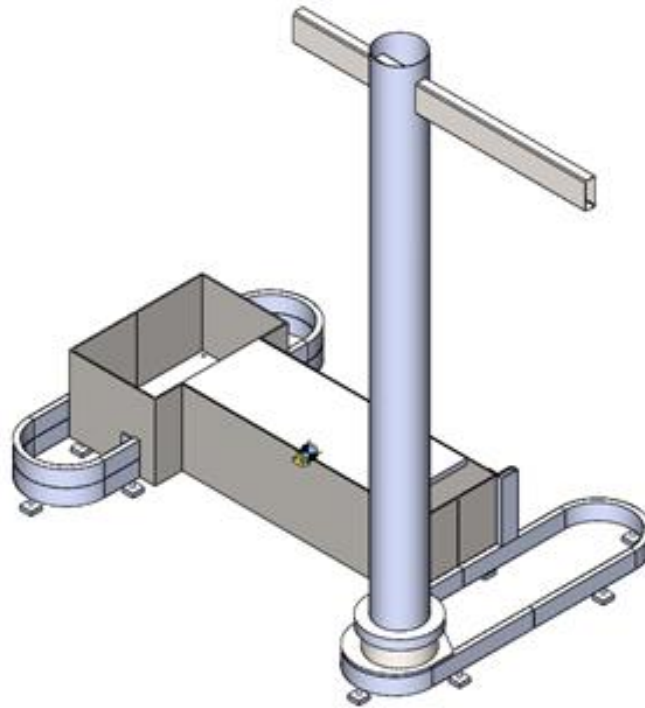


Figure 3.8: Simplified CAD Model Showing Center of Mass for Motion Analysis

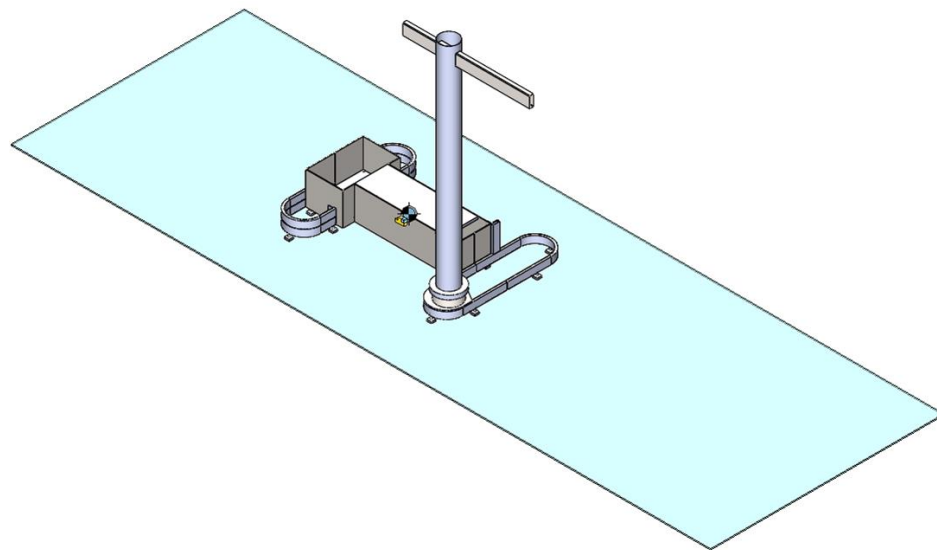


Figure 3.9: Motion Analysis BWST with Floor Setup

### **3.4.3 Fabrication and Assembly**

The sub-assemblies were produced by three independent contract manufacturers based on the requirements of each sub-assembly. Once detailed CAD drawings were created of the system, the designs were further refined in tandem with the specified contract manufacturer based on DFM and manufacturing capabilities/limitations. The central treadmill was designed in cooperation with Tuff Tread, Inc., a custom treadmill company in Conroe, Texas. Tuff Tread is known for building tough and durable treadmills with the lowest cost of operation for very high-use applications and industries. The front and back decks and seating cantilevers were developed with the support of Winston Industries, Inc. (Louisville, KY), a contract manufacturer specializing in machined and fabricated metal components – including sheet metal laser cutting, welding, bending, secondary processing/assembly, and forming. The crane system was developed with Hafendorfer Machine, Inc. based in Louisville, KY. Hafendorfer Machine is a metal machining and fabrication shop with the capability of large steel tube laser cutting. Design cooperation with each end manufacturer allowed for an improved and optimized manufacturable design. With the DFM considered, it allowed for a cost reduction in the final product ultimately making it more affordable for clinics to purchase and implement the LT.

The manufactured sub-assemblies were assembled and tested at Frazier Rehabilitation Institute in Louisville, KY.

### **3.4.4 Verification Testing**

Weight testing of the final system prototype was utilized to test the potential tipping scenario during loading/unloading of the patient. The crane was maneuvered to the most extended cantilever position (150 degrees from neutral/default position) to simulate picking up a patient. Standard free weights were acquired and weighed using a scale to get exact known weight. Table 3.4 shows the weights used for this testing as well as their actual measured weights. 325.24 lbs. (small chain + large chain + yoke and carabiner + parts F, G, H, I, J, K, L) was used to provide a

factor of safety at least 2.5 of the maximum patient load (120lb). This weight was lifted and held for 15 minutes simulating an extended period lifting the patient out of their wheelchair.

**Table 3.4 - Free Weights Used for Weight testing**

<b>Item</b>	<b>Labeled Weight (lbs.)</b>	<b>Measured Weight (lbs.)</b>
<b>Small Chain</b>	N/A	1.10
<b>Large Chain</b>	N/A	2.90
<b>Yoke and Carabiner</b>	N/A	2.00
<b>A</b>	10	10.13
<b>B</b>	10	10.24
<b>C</b>	5	5.08
<b>D</b>	5	5.13
<b>E</b>	30	30.02
<b>F</b>	45	48.15
<b>G</b>	45	46.79
<b>H</b>	45	45.20
<b>I</b>	45	47.50
<b>J</b>	45	45.30
<b>K</b>	45	47.00
<b>L</b>	45	45.30

An additional design criterion was determined that the device should support up to 600 lbs. to account for the patient and all trainers as seen during a standard training session. To test, the crane was loaded with 130.31 lbs. of free weights (G + I + E + Yoke and Carabiner + Small Chain + Large Chain) while one trainer stood on the motor housing and one trainer sat on each seat (two side seats and trunk trainer seat). Total weight was approximately 620 lbs. and was held for 10 minutes ensuring the system remained stable.

## 3.5 Treadmill

### 3.5.1 Treadmill Design Requirements and Development

The treadmill is a completely custom design specifically tuned to the needs of a pediatric patient, as well as the needs of the trainers performing therapy, and essentially is the anchor of the system. The custom treadmill features a motor housing, a central treadmill belt dimensionally optimized to a pediatric population, and rear attachment flanges for rear deck/ crane secure points.

Adjustable leveling feet were integrated as shown in Figure 3.10 to provide adjustability in the clinical space ensuring the treadmill deck was level for stability of installation and gait performance of the patient. To ensure stability, the treadmill featured a robust symmetrical design configured mainly from two  $\frac{1}{4}$  inch steel plates welded together to form the shell of the treadmill. As the crane is rotating picking up a patient, at various points a large cantilever is created. This is counterbalanced by the robust central treadmill acting as the central counterweight to the entire system. The steel frame treadmill as designed weighs 409.87 lbs. which is greater than the specified design criteria of at least 350 lbs.

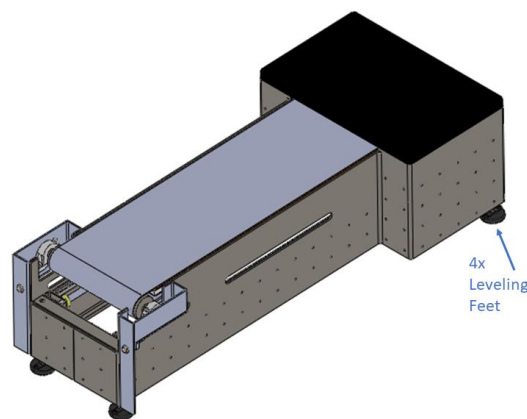


Figure 3.10: Isometric View of Treadmill Showing Rear Flanges and Leveling Feet

Modularity, where each subsection could be manufactured separately, was a central theme throughout the design development of the body weight support treadmill. Modularity will allow for quicker assembly and implementation of the entire system into the clinical floor space.

The frame of the treadmill incorporates  $\frac{1}{4}$  inch mounting holes through out to allow for easy modifications, assembly, and mounting of system components throughout the prototyping process. To ensure proper strength and rigidity,  $\frac{3}{16}$ " x 13.5" x 2.25" steel flanges were added on the back of the treadmill to provide a secure mounting location for the back deck which attaches the lifting crane to the entire system.  $\frac{3}{8}$ " mounting holes provide easy mounting options for the fore and aft support decks that will be explained further in this thesis.

These decks will act as "out riggers" further strengthening the treadmill and system from movement or tipping. These flanges provide additional strength and support for the rotating crane.

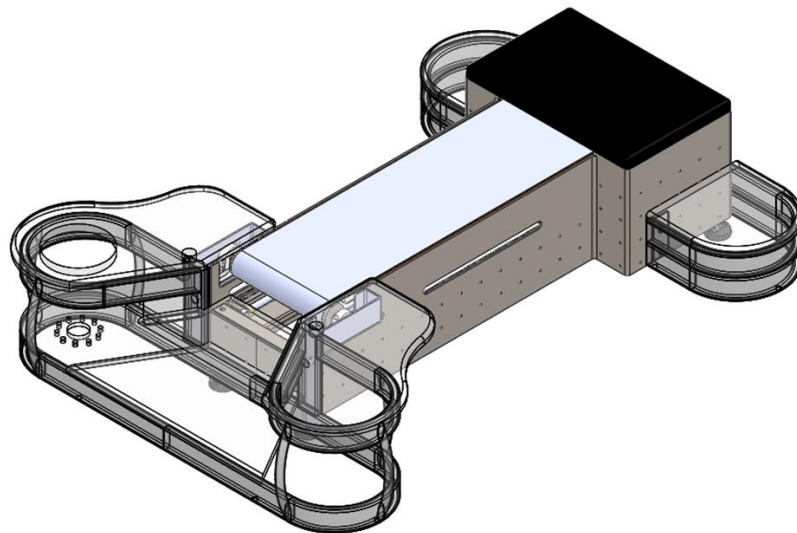


Figure 3.11: Central Treadmill Highlighted and Translucent Front and Back Stabilizing Decks

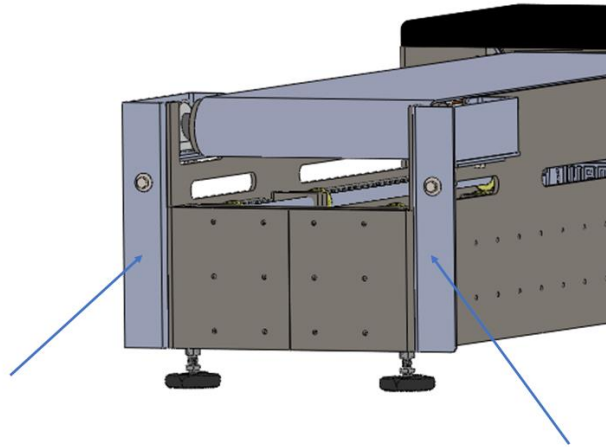


Figure 3.12: Rear Flanges for Rear Stabilizing Deck Attachment

Towards the front of the treadmill, a front motor housing was added to contain all electrical and mechanical components for control and operation of the treadmill (motor, motor control unit, electrical control box, etc.). Two options were considered for motor placement on the treadmill ultimately determining if it will drive the front or rear treadmill roller. When the motor drives the rear roller, it will allow the patient to walk on the “tension” side of the belt. This allows for lower drive belt tensions that could potentially increase motor life and allow for a smaller motor to be selected. Ultimately, placing the motor in the front driving the front roller was chosen as the added counterweight to offset the crane located in the rear of the BWST outweighed the benefits of a rear mounted motor. Additionally, moving the motor to the front of the treadmill, which is comparative to many standard, on-the-market treadmills allowed ample room in the rear of the treadmill for integrating stairs and mounting the crane.



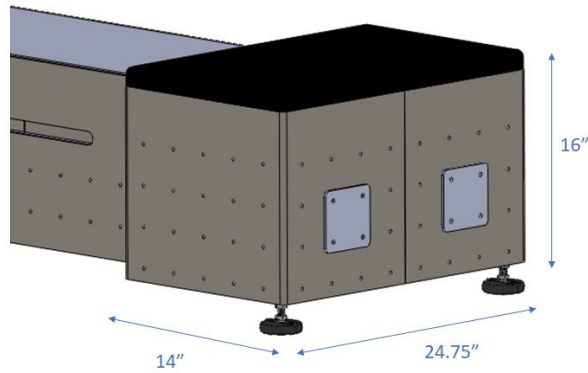


Figure 3.13: Treadmill Motor Housing

The entire motor housing measured 24.75" x 16" x 14" totaling 5,544 in<sup>3</sup> or 3.21 ft<sup>3</sup> surpassing the design criteria of at least 2 ft<sup>3</sup> to contain all necessary components. The housing also features a platform to provide a standing surface for a trainer during training. The platform was designed to be 24.75" x 16" in providing ample room for one trainer to stand facing the patient allowing them to provide training feedback or patient interaction. To provide enough structural support for a trainer to stand on the motor housing, the housing cover was made from TRESPA material - high-pressure laminate (HPL) plate. TRESPA material is made by compressing impregnated paper or wood fibers and epoxy resin at high pressure and high temperature. This is easily machined to shape and exhibits an extremely high flexural strength with reduced weight.

The entire system power was integrated into the front platform of the treadmill as shown in Figure 3.14. The power in is a 220 volt plug that is inserted into the breaker box that splits the power to the various sub-components of the system. One outlet and breaker combo take 220-volt power to the treadmill motor. The other is a 110-volt outlet that takes power to the slew ring motor and the final 110 outlet takes power to the computer/control box. This integrated breaker box helps simplify install/repairs, allows the need for only one external 220-volt plug and with the addition of the breakers helps ensure patient and trainer safety.

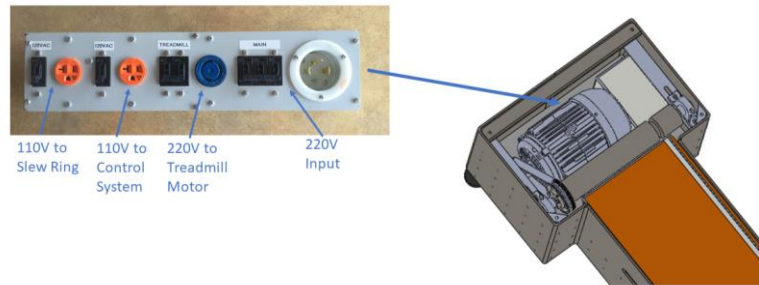


Figure 3.14: Treadmill Motor Location (Right) and BWST Power Breaker Box (Left)

The treadmill features a three-phase induction motor (WEG W22 2 HP) that produces output power to the shaft from a magnetic field produced by a rotor. This is a very rugged and reliable industrial motor with minimal servicing needed. The motor is controlled using a variable frequency drive (VFD) controller (Yaskawa V1000) that varies motor input frequency and voltage to give the user fine control over the speed of the motor. This allows for speed control in 0.1 mph increments and up to 6 mph. This gives the trainers the ability to control the gait progression training gradually and more accurately with the patient ultimately providing enough speed variability increasing the therapy capabilities of the system. This VFD comes equipped with an RS-485 serial port that allows for a simplified computer-controlled interface to the motor. An incline motor/feature was determined to not be needed and subsequently was not integrated into the treadmill control design.

The VFD also allows for active braking to be implemented with the induction motor. Standard treadmills use the weight of the patient and friction to slow down the belt and cause the belt and rotor attached to the motor to stop turning. With active braking, the VFD will switch the stator field of the motor causing a reversing of the electromagnetic field bringing the motor to a stop very quickly. This will allow the treadmill belt to a stop very quickly thus saving valuable time when trainers rotate, and training regiments are changed. The treadmill was designed to stop in under two seconds.

The treadmill deck was designed using 1” laminate veneer lumber. This is an engineered wood product assembled with 11 plies crisscrossed and glued together. The manufacturing of laminated veneer lumber allows it to be stronger, straighter, and exhibit more uniform material properties than traditional wood or plywood. This also allows for less warping over time. Laminated veneer lumber minimizes the effects of grain anisotropy and allow for a higher mechanical stress. The deck is supported using 4 3/16<sup>th</sup> inch thick steel flange brackets. FEA structural analysis was done to ensure the deck could handle the desired patient weight ranges with a factor of safety of at least 1.5. This is explained later in the design evaluation section of the treadmill.

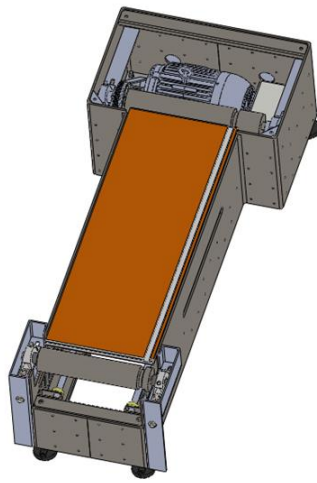


Figure 3.15: Treadmill with Exposed Treadmill Deck Highlighted in Orange

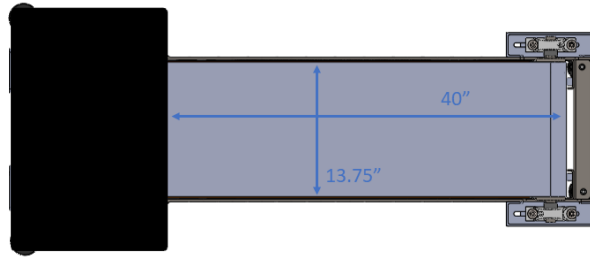


Figure 3.16: Treadmill Top View of Belt

The treadmill belt dimensions were designed to fit a pediatric populations gait/ stride length and was required to have a minimum of 40” exposed length and 12.5”-14” exposed width. The designed exposed belt length measured 40 inches and the exposed belt width measured 13.75 inches.

The treadmill incorporated a slim thin-walled design to allow the trainers to gain up close access to the patient’s legs during therapy. The entire treadmill width is 14.75 inches which provides a sufficiently narrow platform as to not restrict the trainer’s ability to reach the patient and fits within the specified design criteria of 13.5”-15”.

The treadmill uses a custom 3-inch diameter by 14.5-inch-long back roller and a 3” by 17.5” front roller to provide room for the belt pulley and to fit within the motor housing. This is an oversized roller when compared to typical treadmills of this size. This was done because larger rollers can run the treadmill belt with less tension reducing slippage. Less tension will increase the longevity of the belt and the larger diameter allows the roller to turn slower reducing bearing wear.

The roller also features a “v” groove that is mirrored on the belt to fit a “v” flange allowing for minimal “walking” or “sliding” of the treadmill belt. This keeps the belt center in the

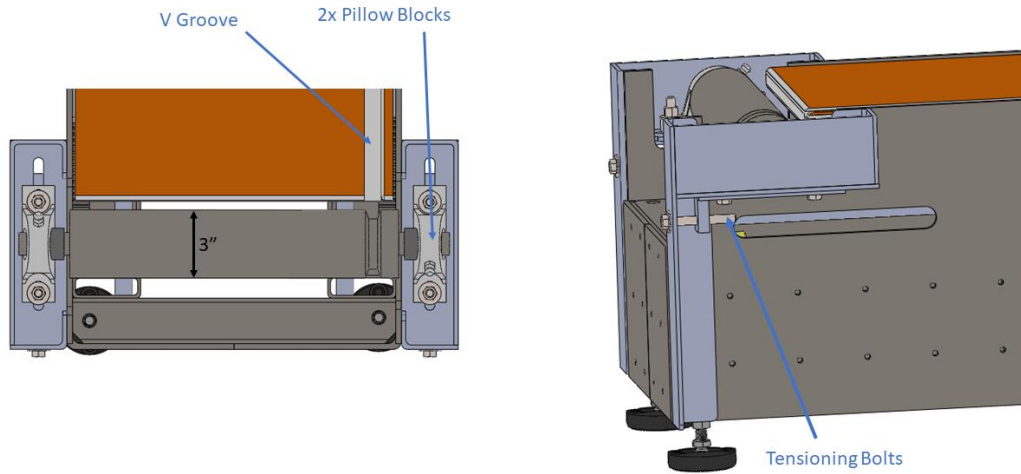


Figure 3.17: Treadmill Rear Roller (Left) Without the Belt Showing "V" Groove and Rear Pillow Blocks (Right)

treadmill reducing belt wear. In addition, to keep the belt tensioned the rear roller is integrated into adjustable “pillow blocks.” These pillow blocks can be tightened or loosened with the two tensioning bolts seen at the rear of the treadmill. The treadmill belt is made from a 2-ply belt with a Polyvinyl Chloride (PVC) top layer and a reinforced cotton and polyester underside. This provides durability without adding additional resistance to the motor.

The treadmill frame features an integrated seating design that allowed for the leg trainers seats to be cantilevered off the side of the treadmill. To ensure the proper amount of adjustability was achieved, two slots on each side of the treadmill were incorporated. One 17” slot is for the fore and aft movement of the seat and one 8” slot is for the fore and aft movement of the footrest. This will allow for seating adjustment based on trainer height and patient gait length. The development of the design feature will be explained in greater detail further in this thesis.

Safety of the system was of utmost concern. Rounded edges were integrated. The back side of the treadmill was left open to ensure patient safety. If the patient were to slip backwards the open ensured the patient would not get his or her foot stuck between the roller and frame.

The overall design was optimized for trainer body mechanics, patient positioning, and the repetitive delivery of intense locomotor therapy.

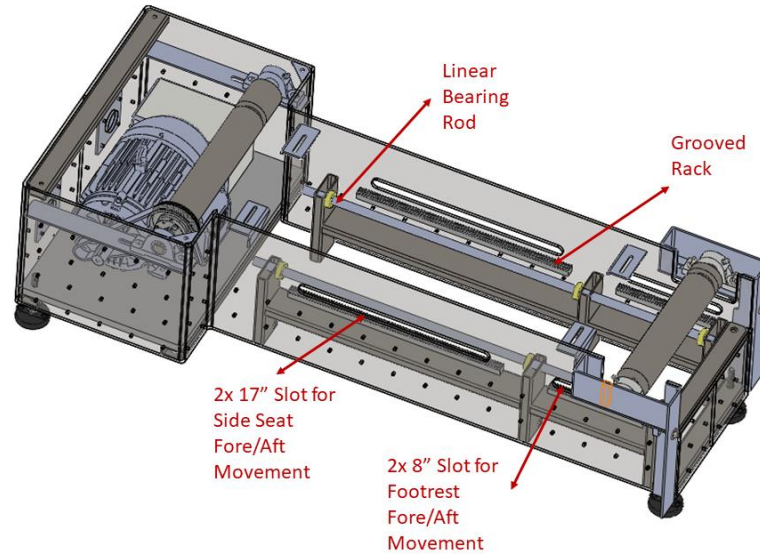


Figure 3.18: Isometric Treadmill View with Exposed Internal Seating Adjustment Components

### 3.5.2 Treadmill Deck FEA Simulation

After completion of the treadmill design, FEA was used to ensure strength and safety within the desired patient weight range for the treadmill deck. The criteria used to determine safety was a 1.5 factor of safety for the max patient size the system was designed for – 120 lbs. To simplify the simulation geometry, only the treadmill deck and four mounting brackets were used during the simulation as seen in Figure 3.19.

The simulation was based on a scenario if the max patient weight (120 lbs.) was standing on the weakest point, a 10" x 10" rectangle in the center of the treadmill deck. The 120 lb. force was evenly distributed across a 10" x 10" surface as seen in Figure 3.19. Each edge of the four mounting brackets were fixed as if welded to the side frame of the treadmill. A 5/16" bolt and nut

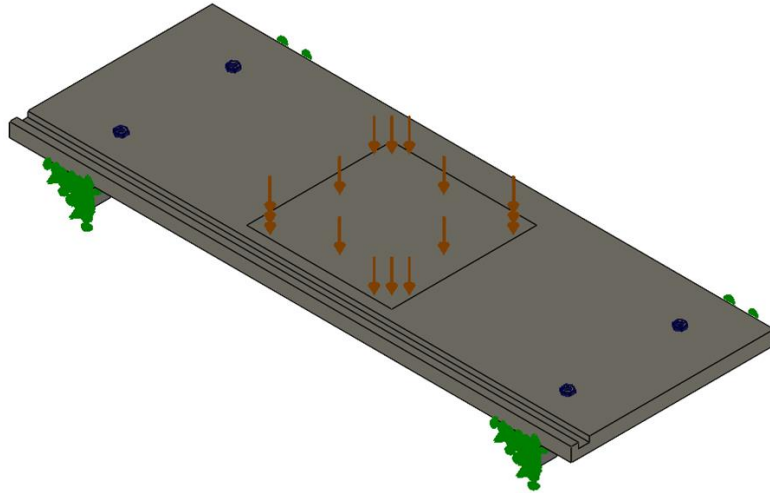


Figure 3.19: FEA of Treadmill Deck Showing Load and Fixture Locations

connector was added to each of the four mounting bracket treadmill deck connection points. A 10 lbf-in preload torque was added to each connector to simulate the deck being bolted to the mounting brackets. The model had four no-penetration component contact sets added between each of the tops of the four metal brackets and the bottom side of the treadmill deck.

The specified treadmill deck material was a 1-inch thick 11-ply laminated veneer lumber with a top and bottom composite fiberboard layer. Laminated veneer construction uses multiple plies crisscrossed called cross graining and glued together to provide uniform material properties that are comparable to solid wood lumber. The layer structure leads to more uniform properties than solid wood since the effects of grain anisotropy are minimized. Therefore, it was safe to assume the deck could be modeled as a linear elastic isotropic material. In addition, loading conditions are predicted to be small deformations and limit strain and not yield therefore linear elastic can be assumed. A good test is to visualize the part in the real world and significant displacement is observed, then there is potential for large deformation and a need to apply non-linear analysis. The mounting bracket material used was plain carbon steel, and the bolt material used was AISI 316 stainless steel. A more detailed list of material and simulation properties is listed in detail in Table 3.5.

**Table 3.5 - Treadmill Deck FEA Properties**

<b>FEA Properties - Treadmill Deck</b>			
<b>Laminated Veneer Lumber Material Properties</b>		<b>Plain Carbon Steel Material Properties</b>	
<b>Property</b>	<b>Value</b>	<b>Property</b>	<b>Value</b>
<b>Elastic Modulus</b>	1.30534x10 <sup>6</sup> psi	<b>Elastic Modulus</b>	3.04579x10 <sup>7</sup> psi
<b>Poisson's Ratio</b>	0.3	<b>Poisson's Ratio</b>	0.28
<b>Mass Density</b>	0.0227602 lb/in <sup>3</sup>	<b>Mass Density</b>	0.281793 lb/in <sup>3</sup>
<b>Tensile Strength</b>	3,016.78 psi	<b>Tensile Strength</b>	57,989.85 psi
<b>Compressive Strength</b>	4,496.17 psi	<b>Yield Strength</b>	31,994.45 psi
<b>Yield Strength</b>	4,902.28 psi		
<b>Component Contact</b>		Bonded Compatible Mesh, No-Penetration at bracket surface	
<b>Mesh Type</b>		Solid, blended curvature-based mesh	
<b>Max Element Size, Min Element Size</b>		1.25", 0.25"	
<b>Total Elements</b>		28591	
<b>Max Aspect Ratio</b>		97.1% of elements < 3	
<b>Analysis Type</b>		Static	
<b>Large Displacement</b>		Off	
<b>Laminated Veneer Lumber</b>		linear elastic isotropic	
<b>Plain carbon Steel</b>		linear elastic isotropic	

A solid element blended curvature-based mesh was used to further refine the mesh density around high stress areas and connection points as seen in Figure 3.20. Specifically, around the bolt holes and mounting bracket slots. The simulation produced stress, displacement, and factor of safety results plots.



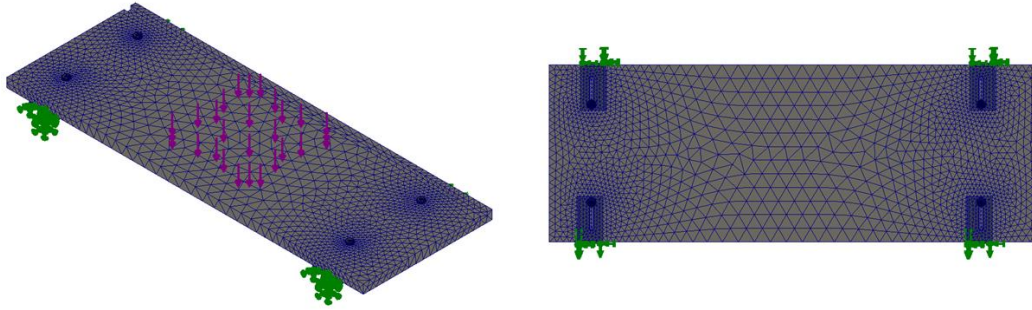


Figure 3.20: Treadmill Deck Mesh

### 3.5.3 Fabrication and Assembly

Manufacture of the treadmill was performed at Tuff Tread, Inc. using multiple metal fabrication techniques and processes – MIG and TIG welding, large press break bending for sheet metal bending, milling, etc.

Preliminary testing during manufacturing showed slightly more flex than anticipated in the side panel walls of the treadmill when force was placed on the integrating seating components. Three 3" x 1" x 14.25" - .125" thick ( $\frac{1}{8}$  inch thick or 11 gauge) rectangular steel tubing cross beams were added to reinforce the main left and right treadmill steel sheet side panels. Each crossbeam was welded to the left and right internal face of the side of the treadmill just under the integrated seating support beam. This is shown in the Figure 3.21.

To increase surface durability and protection of the treadmill, a two-coat powder coat process was used to cover the entire fabricated metal frame of the treadmill. Powder coating creates a tougher, more durable finish compared to traditional paint. The powder coat base was CARDINAL C209-GN411 Tractor Green color, and a clear low flat sheen topcoat (CARDINAL



Figure 3.21: Treadmill bottom view – note internal crossbeam supports

T002-CL02 Clearcoat) was added to cut sheen and increase durability. Cutting sheen ensured there was limited interference with gait camera analysis equipment. This powder coat process, color, and topcoat finish was completed on the entire system for durability and a uniform kid-friendly look.

The overall treadmill was designed to not require servicing for a period of three years. Every design aspect of the treadmill was designed with durability in mind. The rigorous nature of locomotor training puts a lot of wear and tear on a standard treadmill. Flip the deck every 3 years,

change the belt every 3-5 years, and change the motor brushes every 3-8 years. Check the drive belt tension and belt walking monthly for safety and proper function. The unit was received fully assembled ready to be integrated in the overall system upon arrival.

### **3.5.4 Verification Testing**

Dimensional verification of the treadmill was completed using a 25 ft SAE measuring tape. Motor housing (LxWxH), exposed belt surface (LxW), chassis width, and side seat/footrest fore/aft movement slots will all be measured.

To determine the weight of the treadmill, the mass properties within SolidWorks will be analyzed to determine treadmill weight. This was further verified to be a sufficient amount of weight during the tipping weight testing described in section 3.4.4

A 4 ft. level was placed across the motor housing shell as well as the two side panels of the treadmill to check for any unevenness of the treadmill. The treadmill leveling feet were adjusted to ensure treadmill was level.

Visual inspection was completed to ensure integrated linear bearing, steel rod, and rack system was stable, rear flanges and deck mounting holes were seen, the treadmill had no sharp corners or jagged edges, motor and no treadmill incline feature was integrated. Additionally, the motor, VFD, and electrical panel were inspected to ensure it fit comfortably within the motor housing and included all necessary power outlets.

Weight testing of the assembled treadmill deck was tested with a volunteer (195 lbs.) standing on the treadmill for 10 minutes and subsequently checking the system for any obvious failures or excessive deformation.

To weight test the motor housing, 309.96 lbs. (E, F, G, H, I, J, K) was placed on the motor housing deck for 10 mins and observed for any obvious failures or excessive deformation.

To ensure proper functionality of the treadmill operation, 220 V power was connected to the power input of the electric panel and then the treadmill motor and VFD were connected as well.

A computer with BWS control software installed was connected via serial port to the VFD. The treadmill was ramped up to 6 mph via software control using increments of 0.1 mph. Stopping time of the treadmill belt after a stop command was observed.

To check for any treadmill belt slippage or side to side movement, the treadmill belt was tensioned using the two tension bolts on the aft side of the treadmill. To ensure each bolt was properly tensioned, the number of wrench rotations was counted and double checked by measuring the distance from the “pillow blocks” to the bolt head. This procedure was documented for use during install and maintenance during commercialization efforts. Next, the student (195 lbs.) walked on the belt for 10 minutes to make certain no slippage was observed.

Preliminary durability testing was conducted by running the treadmill for 45 minutes at a 4-mph speed and checking for any failures or issues. Complete validation of treadmill maintenance life was out of scope of this thesis and should be conducted over time from clinical feedback.

### **3.6 Integrated Seating and Footrest System**

#### **3.6.1 Seating/Footrest Design Requirements and Development**

To meet the needs of locomotor training, the BWST is required to have two seats for the right and left leg trainers with corresponding footrests and an additional seat on the top of the treadmill for the trunk trainer. Figure 3.22 shows the three trainer seats installed on the central treadmill. The treadmill seating was designed to provide optimal space for three adult trainers of varying size and was optimized to allow for ergonomic body mechanics conducive to the intense hands-on locomotor training.

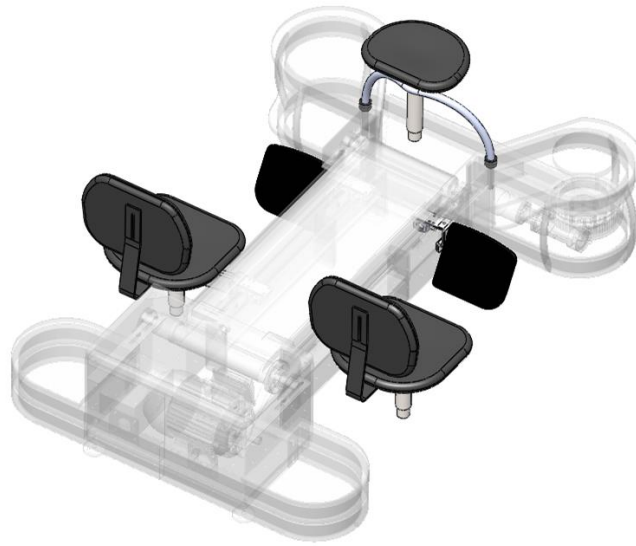


Figure 3.22: Highlighted Right/Left Trunk Trainer Seats and Right/Left Footrests

The two side trainer seats and footrests as seen in Figure 3.23 were integrated within the right and left side of the treadmill via a cantilever arm and linear bearing system allowing for the seats to be “floating” above the floor. This helps to reduce the system’s overall footprint and allow for an easier install reducing shipment size.

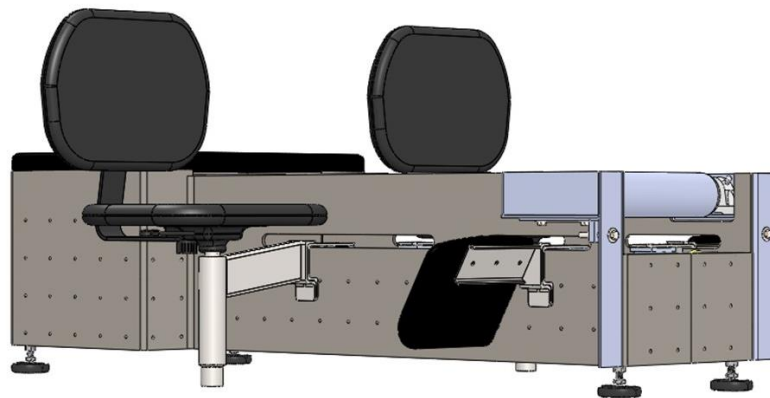


Figure 3.23: Side View of “Floating” Side Seat and Footrest Design

Figure 3.24 shows the design of each side trainer seat which consists of an off-the-shelf office chair, gas cylinder for adjustability, cantilever mounting arm, attachment bracket, and a linear bearing. The cantilever arm was designed out of 3x1 steel tubing with a welded off-the-shelf gas cylinder that would allow for varying standardized seating to be installed. The side seat was

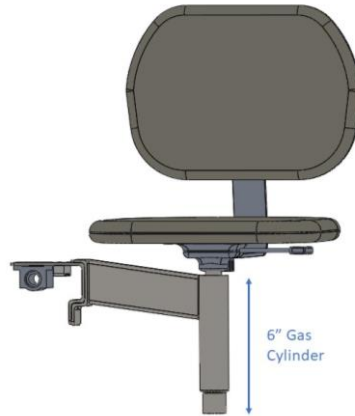


Figure 3.24: Side Leg Trainer Seat and Cantilever Mounting Arm

positioned 17.37" from seat base center to midline of the treadmill as seen in Figure 3.25 meeting the design specification of 17"  $\pm$  1". A 6" gas cylinder was used to give the proper amount of vertical adjustability as established with in the design requirements (5"  $\pm$  1"). Total vertical adjustable range of the seat base was 2" below the treadmill belt to 4" above. To meet the side

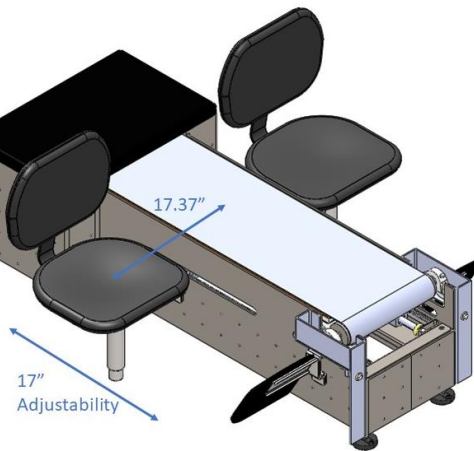


Figure 3.25: Side Seat Positioning and Adjustability Range

seat horizontal adjustment design requirement, a 17” slot was designed into the side panel of the treadmill allowing access to the linear bearing system.

Both the side leg trainer seats and corresponding footrests (Figure 3.28) used a linear bearing and grooved rack configuration (Figure 3.26) hidden within the central treadmill to provide the necessary horizontal adjustability and locking features required by the design specifications. The linear bearing system was designed using a 38” long by 3/4” diameter steel rod along each right and left side of the treadmill providing the horizontal distance and strength needed to support the side seats. The linear bearing was a 2” by 2” off-the-shelf aluminum linear bearing from McMaster Carr (6374k133). A grooved rack section was used to provide a firm grip and set once the correct seating and footrest position was found as shown in Figure 3.27. Horizontal seat and footrest adjustability is achieved by slightly lifting the side seat or footrest to disengage the teeth of the grooved rack allowing it to freely slide along the steel rod as shown in Figure 3.27.

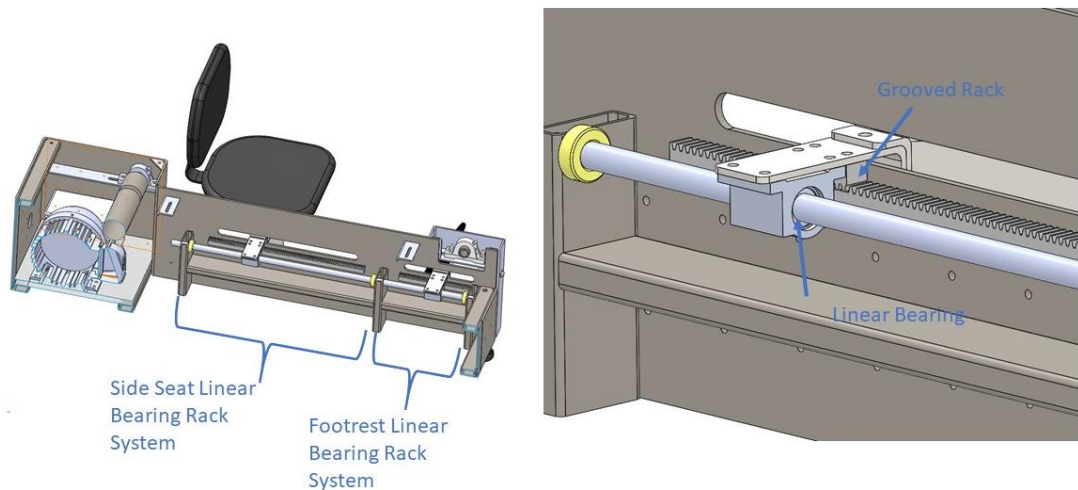


Figure 3.26: Seating and Footrest Linear Bearing and Rack System

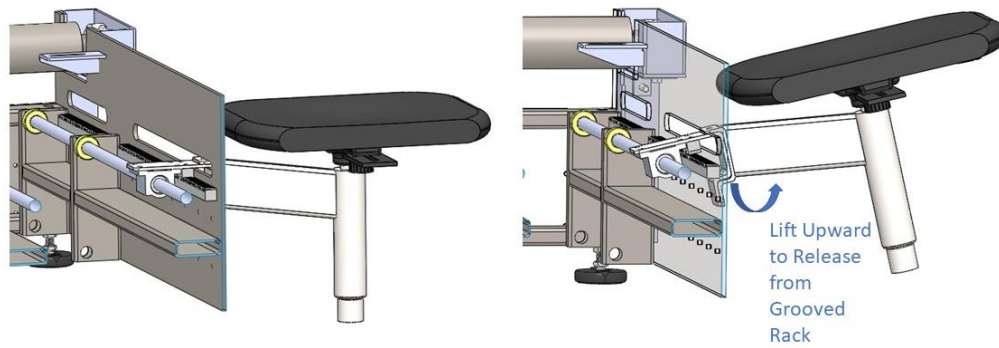


Figure 3.27: Side Seating Rotational Movement to Disengage Rack for Fore and Aft Movement

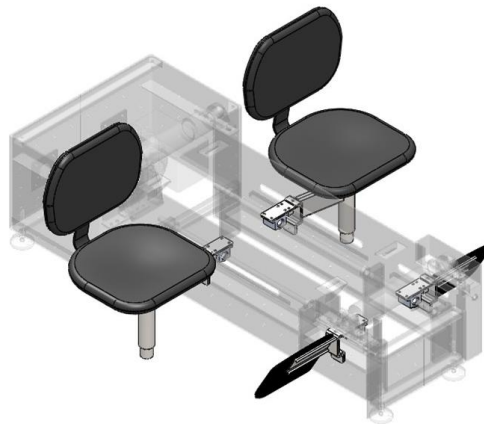


Figure 3.28: Highlighted Seating and Footrest Cantilever Arms Mounted to Linear Bearing and Rack/Pinion Adjustability System

In addition to trainers manipulating the legs of the patient, locomotor training calls for a trainer supporting the waist/trunk stabilizing and maneuvering the patient of the trunk throughout the training session. The trunk trainer seat was designed as a semi-circle base made from 1” diameter bent steel tube that vertically slides into the back deck of the BWST allowing for easy removal during loading and unloading of the patient. This placement of the trunk trainer seat is shown in Figure 3.29. The semi-circle base used a similar design as the side seats with a welded gas cylinder to allow for proper up and down movement of the seat. A 6” standard gas cylinder



was used to give the proper amount of vertical adjustability as established with in the design requirements (3" +/- 1"). In addition, this allowed for a standard off-the-shelf seat base to be used. Total vertical adjustable range of the trunk trainer seat base was 15.75" – 21.75" above the treadmill belt. The trunk trainer seat was not required to have horizontal adjustment since the trainer can easily sit more forward or backward on the seat as needed. The trunk trainer seat was positioned 22.07" from the central axis of where the patient will be standing on the treadmill meeting the required design specification of 24" +/- 1".

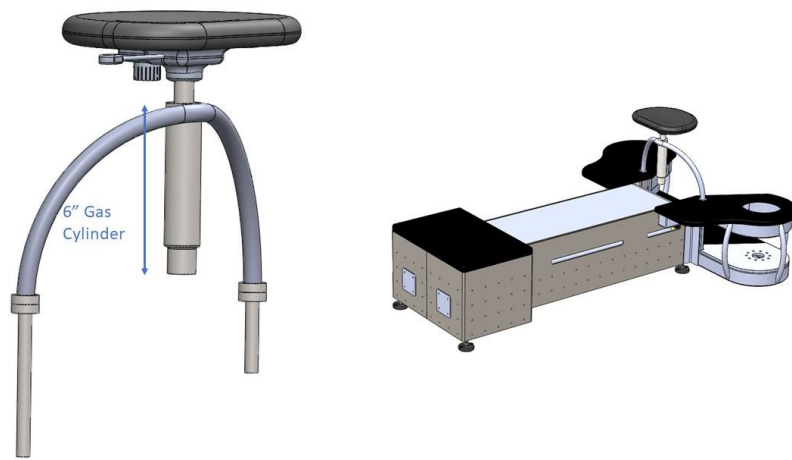


Figure 3.29: Trunk Trainer Seat (Left) and Trunk Trainer Seat Installed Location (Right)

Another requirement of the trunk trainer seat was it needed to be removable to allow for the loading and unloading of the patient. This was achieved by a very simple design incorporating one 4" by 3/4" diameter rod and one 8" by 3/4" diameter rod attached to each end of the semi-circle trunk trainer seat base. These rods slide into the open end of 3" x 1" steel tubing incorporated into the back deck as shown in Figure 3.30. The design allows for easy slide in and out maneuverability for complete trunk trainer seat removal and an ability to swing the seat out of the way as shown in Figure 3.31. The swing motion is achieved by pulling the smaller 4" rod out of the steel tubing without removing the longer 8" rod creating a pivot point to maneuver the trunk

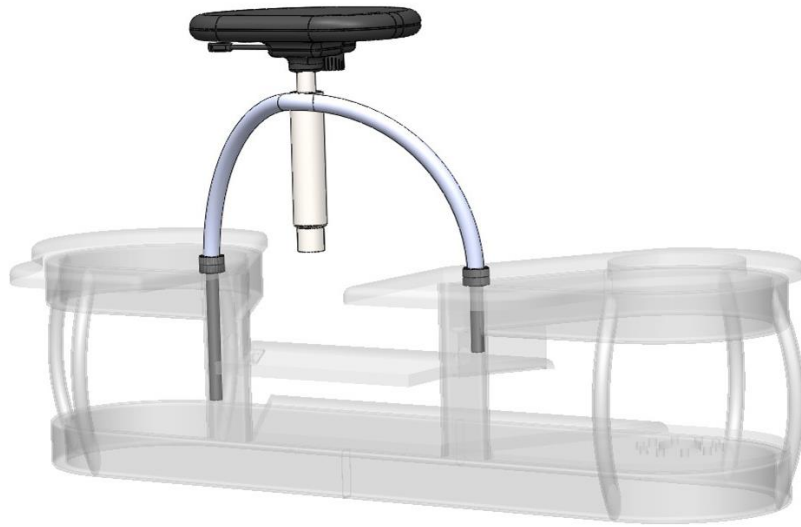


Figure 3.30: Trunk Trainer Seat Attachment points

trainer seat away from the rear of the treadmill creating additional space to become open when loading and unloading the patient.

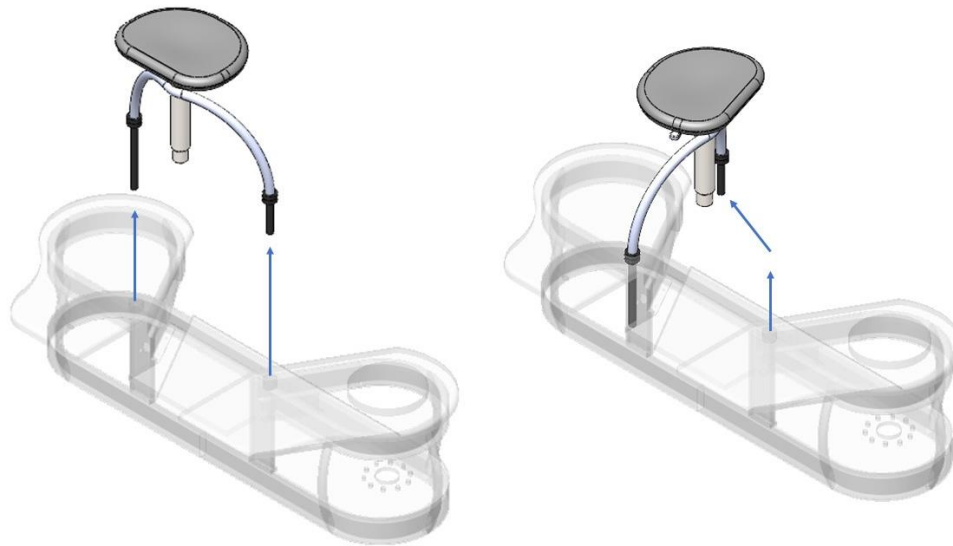


Figure 3.31: Trunk Trainer Seat Swivel Movement and Modularity

The corresponding side seat footrests were integrated using the same linear bearing system and mounting bracket as discussed earlier in this section. The cantilever arm was a 3" wide by 7" long steel plate with three 5/16" mounting holes as shown in Figure 3.32.

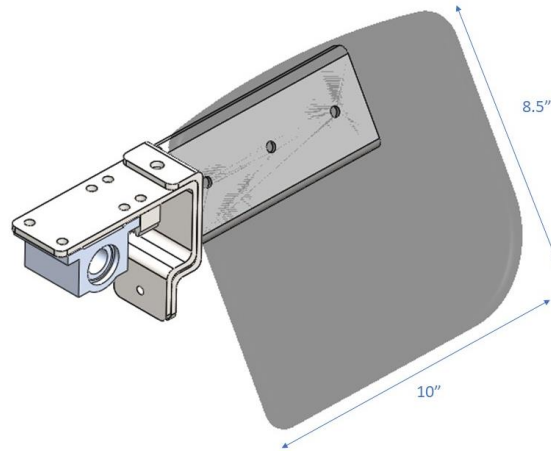


Figure 3.32: Side Leg Trainer Footrest

A 10"x 8.5" piece of TRESPA board was used as the footrest surface to easily meet the design specification of at least 6" by 2" and providing an extremely strong and durable footrest. This allowed for a very stable place to push off against during rigorous training sessions. Fore and aft adjustment was designed to be 8" surpassing design specification of 4" to 6" as seen in Figure 3.33. Movement of the footrests is done in the same way as the side leg trainer seats discussed previously.

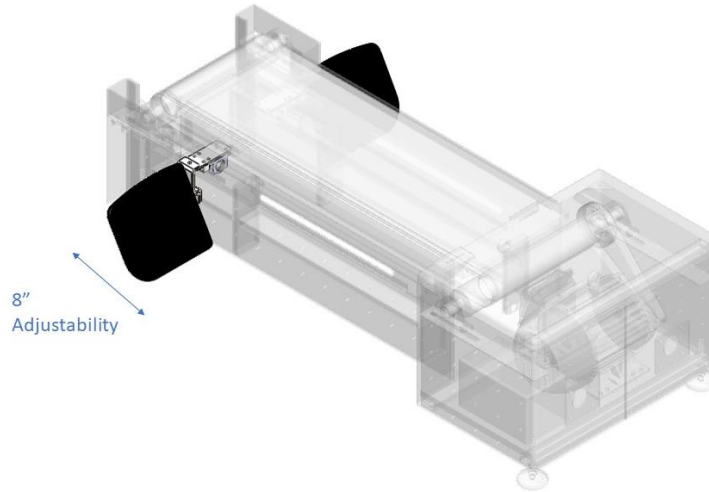


Figure 3.33: Footrest Adjustability Range

### 3.6.2 Safety FEA Evaluation of Trunk and Side Seating

After completion of the seating and footrest design, FEA was performed on the side seating cantilever arm to ensure strength and safety within the desired trainer weight range. The criteria used to determine proper safety of the design was a 1.5 factor of safety of the proposed design criteria force. The load requirement for the side seating is a minimum of 250 pounds which was chosen as a conservative amount significantly above the average male weight of 197.8 lbs. (Fryar et al., 2018).

A simplified model of the side seat cantilever arm, bracketry, and linear bearing was created (Figure 3.34). Plain carbon steel was used to simulate all components with material properties listed in Table 3.6. The bottom face of both the treadmill side panel and the two vertical steel tubing treadmill supports were fixed. The 250 lbs. force was applied to the outermost surface of the cantilevered seating arm where the gas cylinder will be welded (Left picture in Figure 3.34). A universal bonded contact was applied with specific no-penetration contact types at the rack-to-rack surface, rack to treadmill side panel surface, and at the seating arm mounting bracket to treadmill side panel surface.

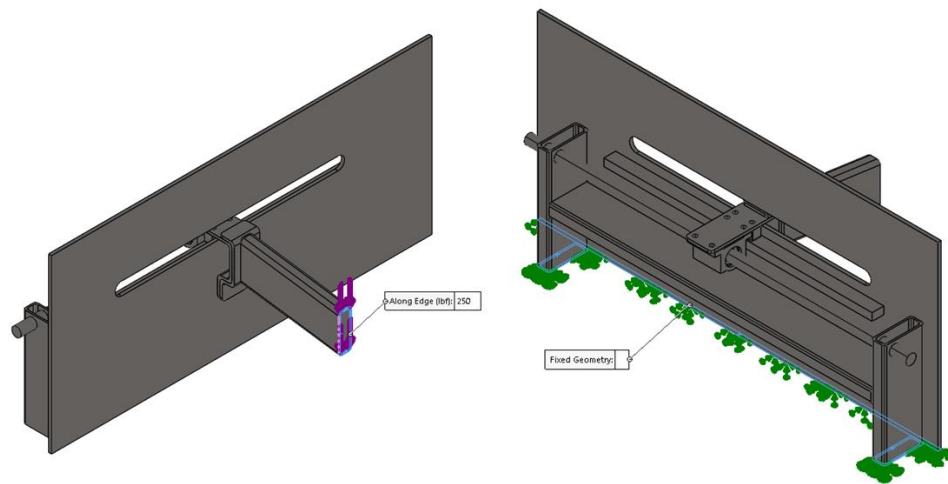


Figure 3.34: Force Location (Left) and Fixed Geometry Location (Right) of Seating Cantilever Arm FEA Simulation

**Table 3.6 – Side Seat Cantilever Arm FEA Properties**

<b>FEA Properties – Cantilever Seating Arm</b>	
<b>Plain Carbon Steel Material Properties</b>	
<b>Property</b>	Value
<b>Elastic Modulus</b>	3.04579x10 <sup>7</sup> psi
<b>Poisson’s Ratio</b>	0.28
<b>Mass Density</b>	0.281793 lb/in <sup>3</sup>
<b>Tensile Strength</b>	57,989.85 psi
<b>Yield Strength</b>	31,994.45 psi
<b>Component Contact</b>	Bonded Compatible Mesh, No-Penetration at rack-to-rack surface, No-Penetration at rack to treadmill side panel surface, No-Penetration at seating arm mounting bracket to treadmill side panel surface,
<b>Mesh Type</b>	Solid, blended curvature-based mesh
<b>Max Element Size, Min Element Size</b>	1.0”, 0.15”
<b>Total Elements</b>	121141
<b>Max Aspect Ratio</b>	94.0% of elements < 3
<b>Analysis Type</b>	Static
<b>Large Displacement</b>	Off
<b>Plain carbon Steel</b>	linear elastic isotropic

A solid element blended curvature-based mesh was used to further refine the mesh density around high stress areas and connection points (Figure 3.35), with emphasis around the bracketry connecting the cantilever arm to the linear bearing. The mesh density formed a total of 121411 elements with 94% of elements less than an aspect ratio of 3. The simulation produced stress, displacement, and factor of safety results plots.

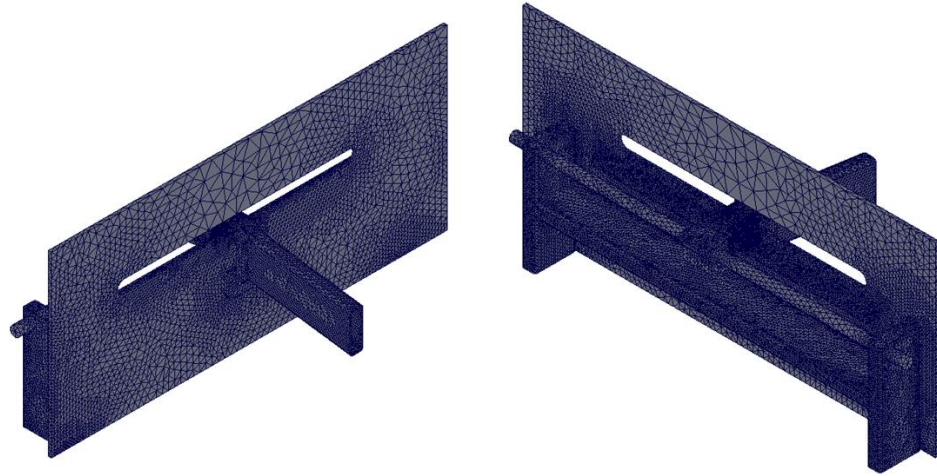


Figure 3.35: Mesh Density of Seating Cantilever Arm FEA

Each footrest needed to be able to support up to 125 lbs. with a factor of safety of 1.5. Due to the footrest support bracketry being the same as the seating, it was justified that the seating FEA evaluation would suffice for evaluation of the footrests as well. This is explained further in the results and discussion section.

Similarly, as the side seat cantilever arm, a static FEA was performed on the trunk trainer seat to ensure strength and safety within the desired trainer weight range. The criteria used to determine proper safety of the design was a 1.5 factor of safety of the proposed design criteria force. The design criteria listed for the trunk trainer seat was the same as previously discussed for the side seats - a requirement to support at least 250 lbs.

A simplified model of the trunk trainer seat with removal of the seating surface as seen in Figure 3.36 was created. Plain carbon steel was used to simulate all components with material properties listed in Table 3.7. The bottom face of both the left and right spacer rings were fixed simulating placement within the rear treadmill deck. The 250 lbs. force was applied to the top surface of the gas cylinder (left picture in Figure 3.36). A universal bonded contact was applied to the entire model.

A solid element curvature-based mesh was used to further refine the mesh density around high stress areas and connection points as seen in Figure 3.37. The mesh density formed a total of 104869 elements with 99.6% of elements less than an aspect ratio of 3. The simulation produced stress, displacement, and factor of safety results plots.

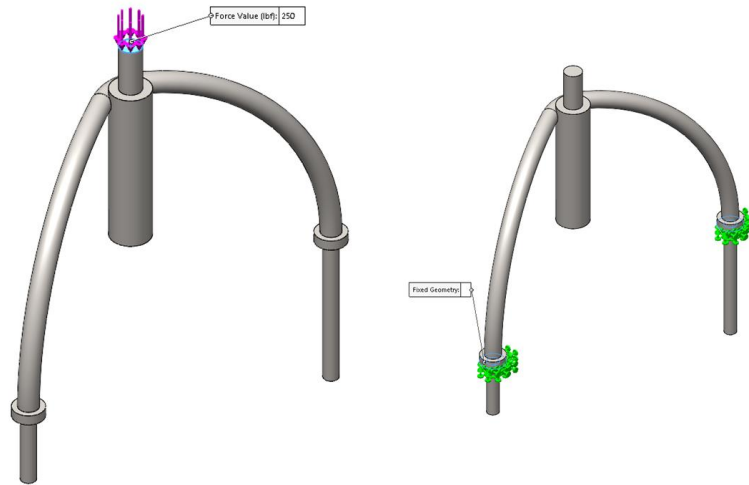


Figure 3.36: Force Location (Left) and Fixed Geometry Location (Right) of Trunk Trainer Seat FEA Simulation



Figure 3.37: Mesh Density of Trunk Trainer Seat FEA



**Table 3.7 - Trunk Trainer Seat FEA Properties**

<b>FEA Properties – Trunk Trainer Seat</b>	
<b>Plain Carbon Steel Material Properties</b>	
<b>Property</b>	Value
<b>Elastic Modulus</b>	3.04579x10 <sup>7</sup> psi
<b>Poisson’s Ratio</b>	0.28
<b>Mass Density</b>	0.281793 lb/in <sup>3</sup>
<b>Tensile Strength</b>	57,989.85 psi
<b>Yield Strength</b>	31,994.45 psi
<b>Component Contact</b>	Bonded Compatible Mesh
<b>Mesh Type</b>	Solid, curvature-based mesh
<b>Max Element Size, Min Element Size</b>	0.15”, 0.05”
<b>Total Elements</b>	104869
<b>Max Aspect Ratio</b>	99.6% of elements < 3
<b>Analysis Type</b>	Static
<b>Large Displacement</b>	Off
<b>Plain carbon Steel</b>	linear elastic isotropic

### **3.6.3 Fabrication and Assembly**

Manufacturing took place at Winston Industries, Inc. using multiple metal fabrication techniques, machines, and processes – MIG and TIG welding, Salvagnini laser cutter press break for bending sheet metal, milling, turret punch presses, and metal finishing techniques. These manufacturing methods along with six sigma lean manufacturing principles employed at Winston Industries, Inc. allowed for increased part consistency and improved quality ensuring every component meets the desired specification. Certified onsite welders completed the assembly of components which were delivered ready to install in the main BWST.

### **3.6.4 Verification Testing**

Dimensional verification of the seating and footrest system was completed using a 25 ft SAE measuring tape. Center of right and left side seat to treadmill midline, right and left side seat vertical gas cylinder adjustment, right and left side seat fore/aft adjustment, trunk trainer seat vertical adjustment, right and left footrest fore/aft adjustment, and right and left footrest platform (L x W) will be measured. Additionally, to verify the design requirement of the trunk trainer seat should be within  $24 \pm 2$  in. from patient position, a plumb bob will be hung from the end of the crane boom and the measurement from the center of the trunk trainer seat to the plumb bob will be taken.

Functionality testing was completed on the trunk trainer seat and both side leg trainer seats by repeatedly moving the side seats fore and after engaging and disengaging the linear bearing rack system. The trunk trainer seat was repeatedly removed and rotated ensuring proper functionality.

Weight testing of the assembled right and left side trainer seats as well as the trunk trainer seat was completed by the student (195 lbs.) holding weights, B + F, while sitting on each seat for 10 minutes. Total weight used for testing was 253.39 lbs. Each seat was checked for any failures or deformation.

The design criteria for the footrests states they need to be able to support up to 125 lbs. with a factor of safety of 1.5. Because the footrests use the same bracketry as the side seats, static FEA and weight testing of the side seats will be used to show the footrests meet design requirements.

## **3.7 Stabilizing Decks**

### **3.7.1 Fore and Aft Deck Design Requirements and Development**

To further stabilize the system, front and rear stabilizing decks were designed as modular attachments to the central treadmill (Figure 3.38). The design intent was to create easily installed decks to attach to the central treadmill that would stabilize the entire system from oscillation of the system during training and loading/unloading of a patient.

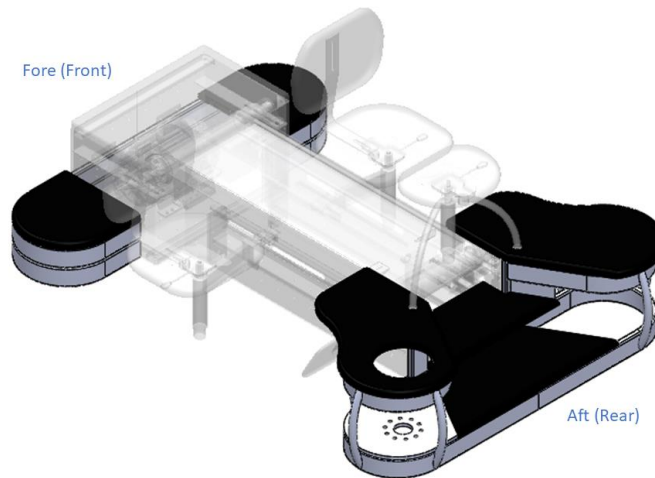


Figure 3.38: Front and Rear Stabilizing Decks Highlighted

The add-on of the front and rear decks provided lateral stabilization from the midline of the central treadmill creating increased safety of the entire system (Figure 3.39). In addition, the symmetric design of the front and rear decks provided modularity and versatility to the entire system (Figure 3.40). The entire system layout provides a more open floorplan allowing easier access to the patient from all sides. Trainers can easily climb onto the motor housing in front of the patient via the left or right step of the front deck and the ability of the crane to be mounted to either the right or left side provided the necessary adaptability of the system to varying clinical spaces.

The front deck is designed in a way that provides a socket to fit around the front platform of the treadmill (Figure 3.41). The deck forms a step on each side of the front treadmill platform allowing the trainers to easily make their way atop the front platform in front of the patient. Leveling feet (McMaster Carr, 2531K410) were added on both the right and left side to ensure the system can be properly leveled during installation as required by the design criteria.

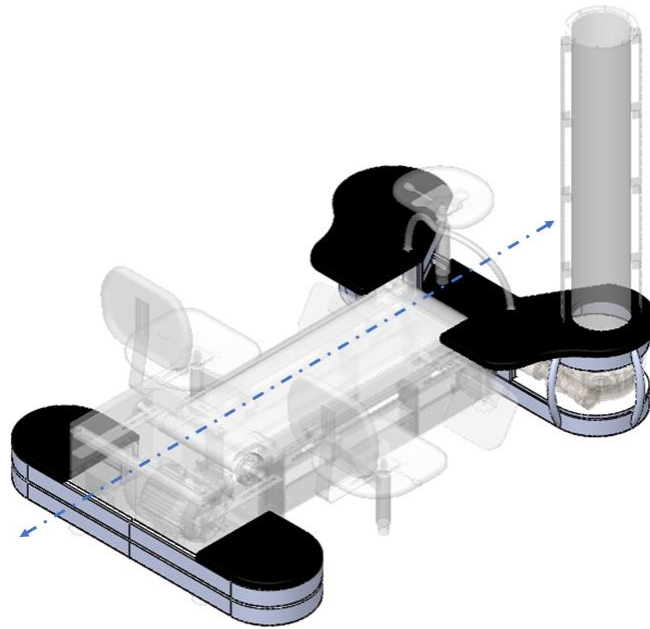


Figure 3.39: Isometric View of Front and Rear Decks Including a Center Axis Line Showing Symmetry.

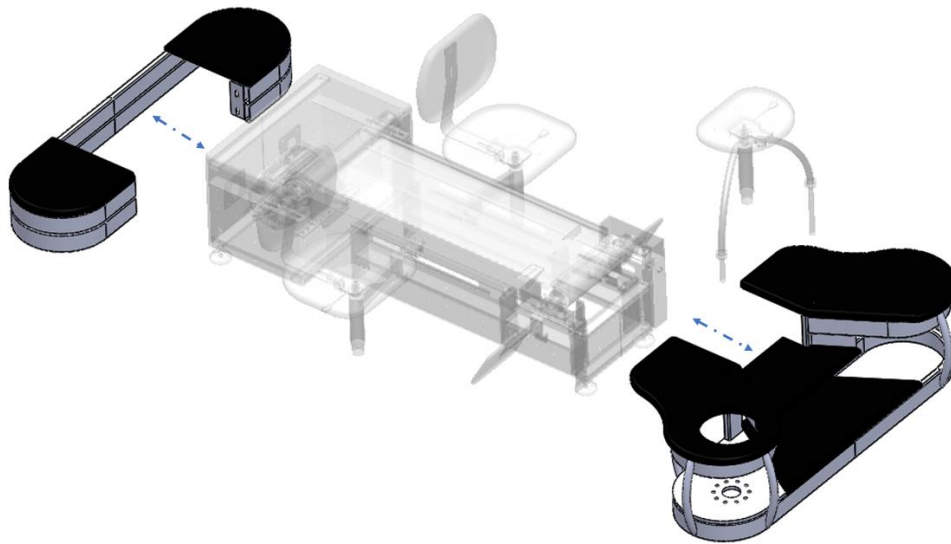


Figure 3.40: Front and Rear Stabilizing Decks Exploded View Showing Modularity

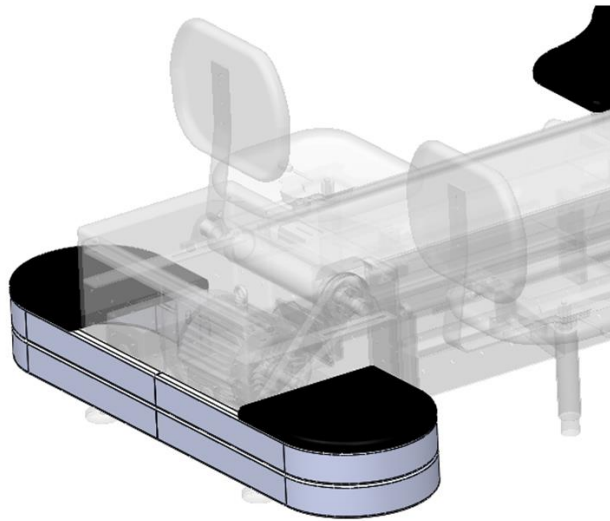


Figure 3.41: Front Stabilizing Deck with Steps to Treadmill Motor Housing Platform

The overall length of the front deck was designed at 52” which surpasses the design criteria of greater than or equal to 50” as shown in Figure 3.42. The height of the deck structure was 7” and an additional 2” for leveling feet for an overall height totaling 9”. The structure was designed from a 12 gauge (.109”) thick 3” x 1” rectangular steel tubing that has been bent to form providing rounded edges and increased safety for the patient and trainers.

Mounting brackets were added for attachment of the right and left sides of the motor housing located towards the front of the central treadmill as shown in Figure 3.43. The mounting brackets are 7 gauge (.179”) thick steel with dimensions of 2.25” x 5.5”.

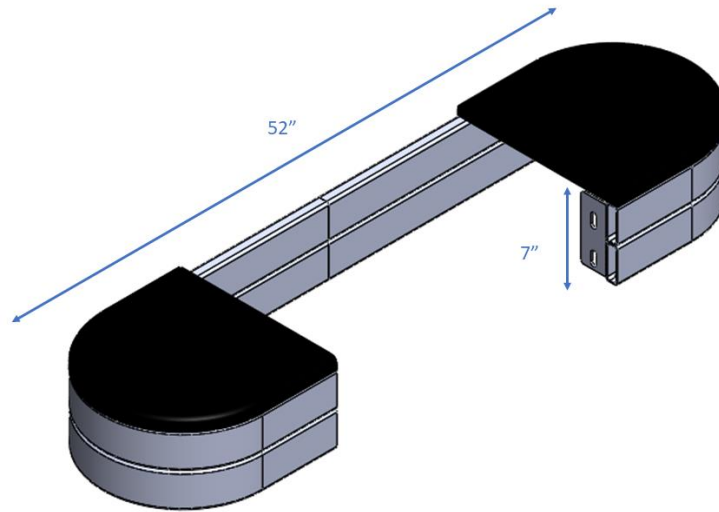


Figure 3.42: Front Deck Dimensions

Each step/deck was made from a  $\frac{3}{4}$ " inch thick TRESPA Toplab material (Figure 3.43) which is a high-pressure compact laminate that is reinforced with wood-based fibers under high pressure and temperature. This durable material will ensure the strength, lifespan, and hygiene needed for clinical use of the BWST. The TRESPA Toplab sheets are attached via ball and sockets (Snaploc by Bollhoff) to allow them to easily be removed for access to storage and installation purposes.

The rear deck attaches to the two mounting flanges located on the end of the treadmill described previously in treadmill design section via two vertical 10.5" long 12 gauge (.109") thick 3" x 1" rectangular steel tubing.

Similarly, to the front deck, the overall length of the rear deck was designed at 52" which surpasses the design criteria of greater than or equal to 50" (Figure 3.44). The overall height of the rear deck structure was 14.48" with an additional 2" for leveling feet for an overall height totaling 16.48". The structure was designed from a 12 gauge (.109") thick 3" x 1" rectangular steel tubing that has been bent to form providing rounded edges and increased safety for the

patient and trainers. Bent 1" diameter steel tubes were added connecting the top and bottom rear deck structure providing additional strength and support.

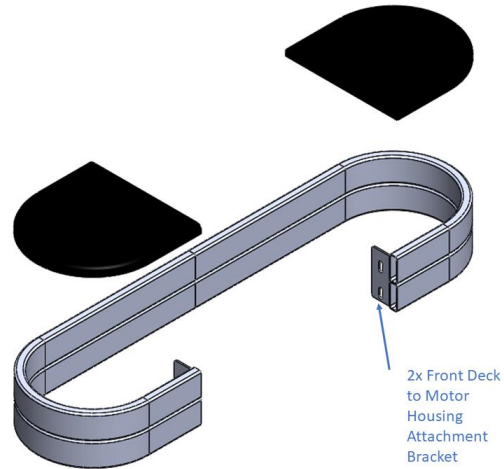


Figure 3.43: Front Deck Exploded View Showing Mounting Brackets

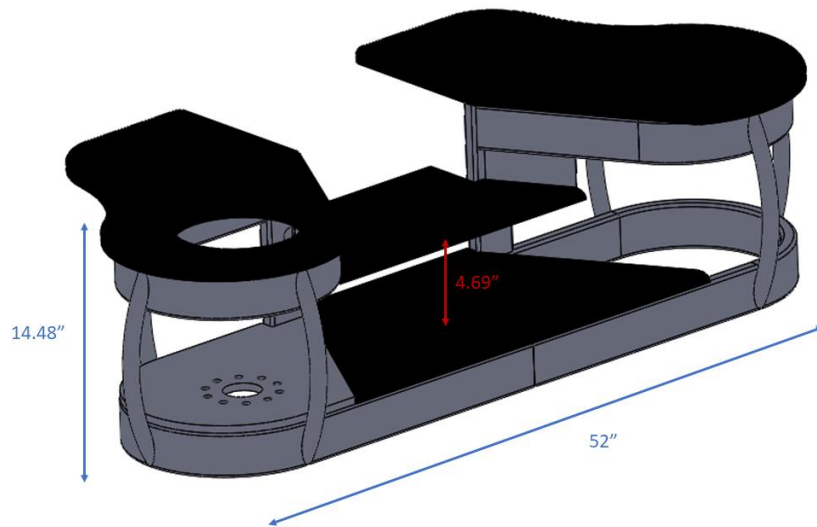


Figure 3.44: Rear Stabilizing Deck Dimensions

An additional design criterion for the rear deck required the integration of stairs to provide potential additional training opportunities for the patient and easy access for the trunk trainer getting on and off the trunk trainer seat. The steps were designed at 4.69” (Figure 3.44). This meets the stair height design criteria of 5” +/- 1”. Two Mounting brackets were added for attachment of the patient step at the rear of the central treadmill as seen in Figure 3.45. The mounting brackets are 11 gauge (.120”) thick steel with dimensions of 2.75” x 6”.

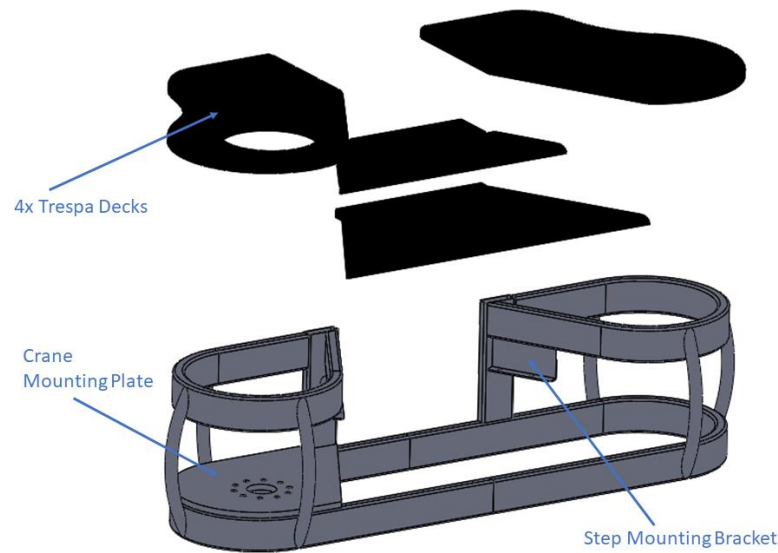


Figure 3.45: Exploded Rear Deck View

The rear deck contains a 0.5 in. steel mounting plate including 11 - 0.5in mounting holes equal spaced in circular pattern that provides a strong base for the attachment of the slew ring and subsequently the crane. It incorporates a symmetrical design allowing the crane to be mounted on the right or left side (Figure 3.46) depending on the clinical space the system is being installed within.

The rear deck top surfaces and stairs are made from 0.75” thick TRESPA TopLab material. The top TRESPA decks feature a rounded form for patient safety and a 7.5” x 10” extension on



the right and left side to provide a strong sturdy platform for trainers to stand and ample space for the trunk trainers feet.

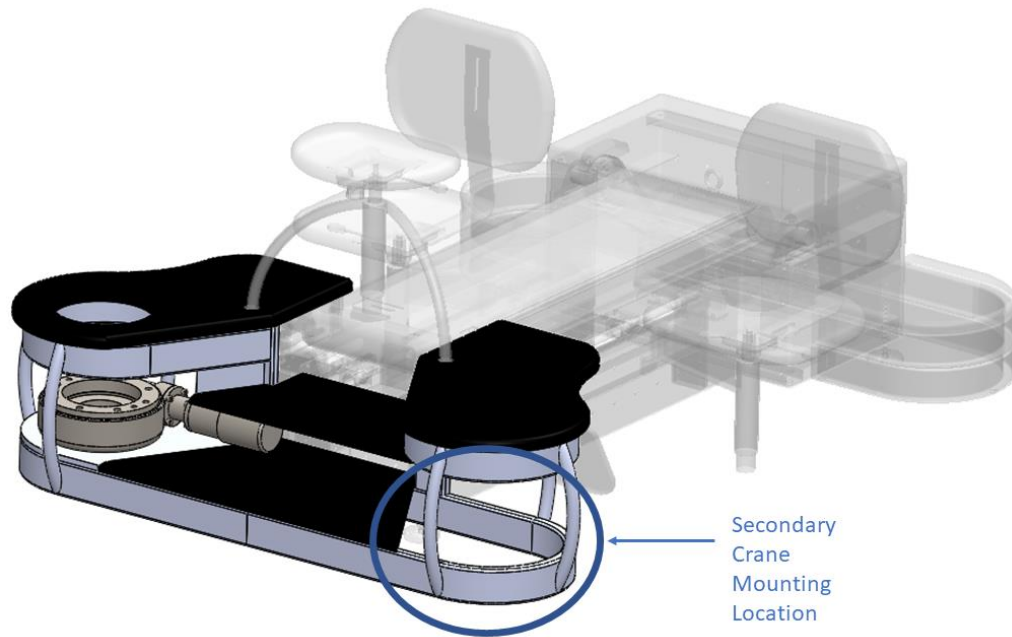


Figure 3.46: Rear Stabilizing Deck Showing Crane Mounting Locations.

### 3.7.2 Fabrication and Assembly

Manufacturing took place at Winston Industries, Inc. using multiple metal fabrication and tubing techniques/processes including MIG and TIG welding and tube bending machines. The rectangular tubing was bent to shape using a tube bending machine and bending die (Figure 3.47 and Figure 3.48, respectively) and the round tubing support struts were formed using the machine in Figure 3.49. The front and rear deck TRESPA surface cut to shape using a CNC router. The fore and aft decks were delivered completely assembled without the TRESPA attached.



Figure 3.47: Beatty Tube Bending Machine at Winston Industries



Figure 3.48: Tube Bending Die for 1"x3" Steel Tube



Figure 3.49: Tube Bender for Support Struts on Rear Deck

### 3.7.3 Verification Testing

Dimensional verification of the front and back decks was completed using a 25 ft SAE measuring tape. Dimensions measured are below:

- Overall front deck length
- Overall back deck length
- Patient stair height
- Slew ring mounting plate and mounting holes

A 4 ft. level was placed across the front deck and back deck to check for level after installation. The front and back deck leveling feet were adjusted as necessary to ensure both decks were level

Visual inspection was completed after installation of the front and back decks to the central treadmill ensuring all design requirements were met. Visual Inspection results will be discussed

in 4.6.1 and results listed in APPENDIX V: Front/Rear Decks Design Criteria and Verification Results.

To weight test the back deck stairs, right and left front deck platforms, 309.96 lbs. (E, F, G, H, I, J, K) was placed on surface being tested for 10 mins and observed for any failures or deformation.

### 3.8 Crane

#### 3.8.1 Rotating Crane Design Requirements and Development

The BWST incorporates a support crane that allows for body weight support of the patient during training and rotation for loading/unloading of the patient as seen in the left panel of Figure 3.50.

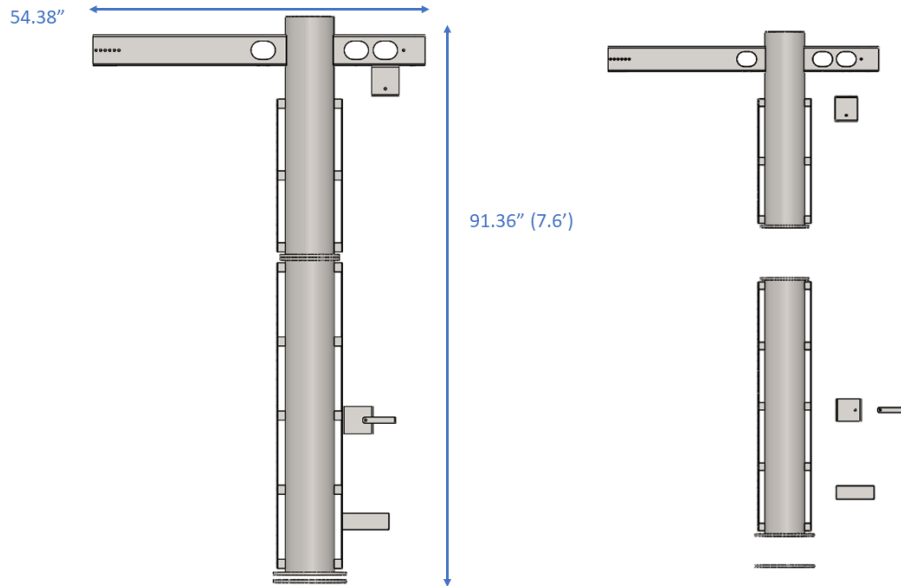


Figure 3.50: Profile View of Two-Piece Support Crane (Left) and Exploded View Including BWS Bracketry (Right)

The crane features two sections, a top mast, and a bottom mast, fastened together via two circular flange plates. In addition, two pulley brackets and a body weight support attachment bracket were integrated to hold the necessary body weight support components discussed in a

later section 3.9.1. The bottom mast is 51.98” long and made from 8” diameter 16-gauge (0.0625”, 1/16” thick) circular mild steel tube. A 0.5” thick 12” diameter steel flange plate with 8 x .5” holes was added to the bottom of the mast for attachment to a slew ring that will be described in detail later in this section. The top mast is 39.38” long and made from 8” diameter 16-gauge (0.0625”, 1/16” thick) circular mild steel tube. A 0.5” thick 9.75” diameter steel flange plate with 8 x 0.3126” (5/16”) holes was added to the bottom of the top mast and the top of the bottom mast for attachment during installation of the crane.

The top mast of the crane incorporates a .125” thick (1/8 inch thick, 11 gauge) boom arm which is designed as a single cantilever 5” x 2” mild steel rectangular tube. The boom fully seats into the circular tower penetrating both the front and back of the top crane mast allowing for increased strength. The total boom length is 54.38” with a 37” cantilever measured from the central mast to the end of the boom.

A design requirement was established that the crane height should be less than standard ceiling height of 9’ or 108” providing enough clearance to assemble and install the BWST in any clinical setting. The total height of the crane from the floor to the top of the central crane mast as designed measures 101.85” (8.49’).

Included on both the top and bottom mast was a .125” thick (1/8 inch thick, 11 gauge) sheet metal bracket welded to the outer surface of the top and bottom crane mast sections, shown in Figure 3.52. A series of 0.5” holes were laser cut into the bracket to provide attachment points for attaching the pneumatic and electric cylinders as well as the pulley brackets. The bracket spanned both the front and back of the bottom and top masts.

The crane mounting location was implemented on the back side of the treadmill with the patient facing away from the crane mast seen in Figure 3.52. With the patient facing away from the crane, it provides a more kid-friendly and less intimidating experience for the pediatric patient, as well as providing easier access for loading and unloading of the patient.

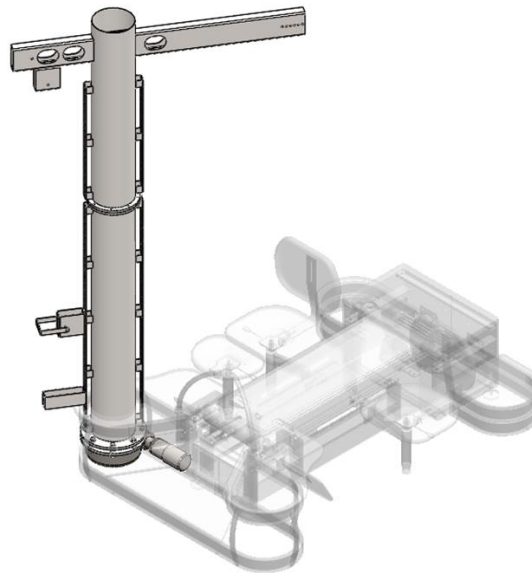


Figure 3.52: Crane Mounting Location on Aft/Rear Deck

Reduction of overall system footprint was one of the primary design criteria for the entire system. A large part of this was achieved by integrating crane rotation using a slew ring (Figure 3.51) attached to the base flange on the bottom mast. This eliminated the need for a lengthy ramp to be utilized for maneuvering a patient's wheelchair on to the treadmill. In addition, this provided a safer compliant solution to the Health Insurance Portability and Accountability Act (HIPAA) by eliminating the need for the trainers to have to lift the patient out of the wheelchair

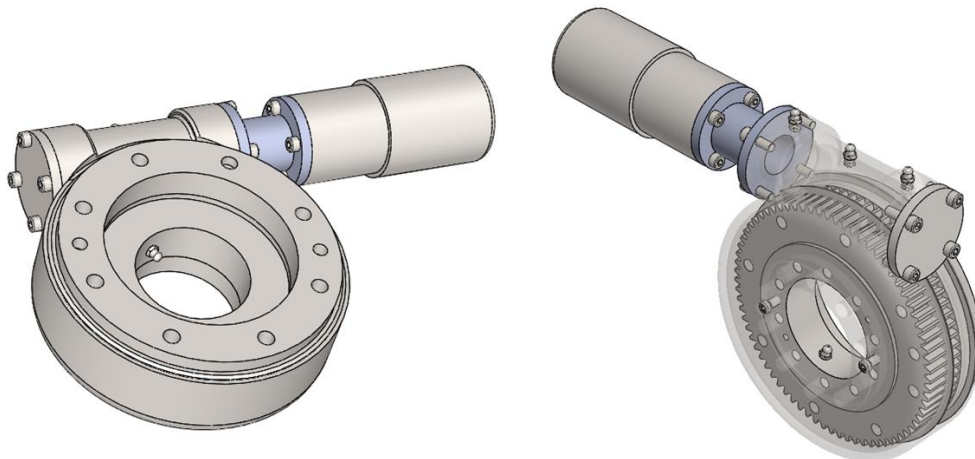


Figure 3.51: Slew Ring (Left) and Transport Slew ring Casing Showing Internal Gear (Right)

to harness them into the body weight support treadmill. Rotation of the patient for loading and unloading will also increase training time and reducing the amount of time per session spent loading and unloading the patient.

The slew ring (SE7C-73MHC-2410-RC) from Kinematics Manufacturing is a worm gear driven motorized slew ring to provide crane rotation for loading and unloading the patients. It features a minimal maintenance durable design common in industrial applications. In addition, the gear motor can be flipped to any side of the slew ring allowing for installation on either the right or left of the back deck. The slew ring allowed for a crane rotation of 150 degrees (Figure 3.53) to allow for reaching the patient within a wheelchair at the aft/rear side of the BWST. It features a 7" mounting base, 1 rpm to allow safe slow rotation, and 566 ft\*lbs. of normal output torque providing enough torque to adequately rotate the max patient size. It features an electrical gear motor that can also be manually driven with a socket wrench during malfunction or power failure to unload the patient. The slew ring is powered by a high current 24V power supply described in section 3.9.1. Slew ring foot pedal control was implemented to allow the trainer to have hands free forward and reverse control of the slew ring.

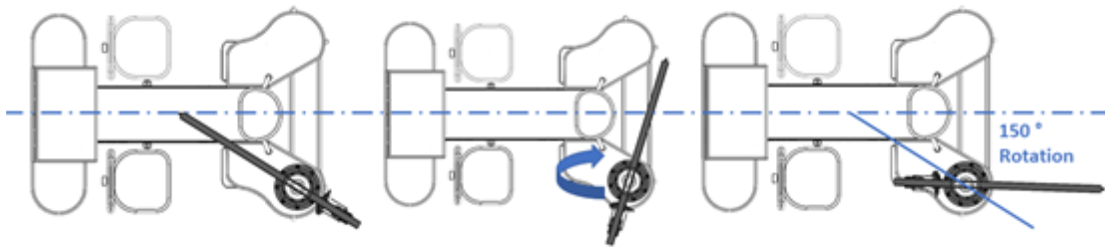


Figure 3.53: Top View Showing Clockwise Crane Rotation of 150 Degrees

### 3.8.2 Gusset/Non-gusset Design Comparison and Crane Safety FEA Evaluation

Before the final crane design was confirmed, two options were developed and evaluated – gusseted (left panel in Figure 3.54) vs non-gusseted (right panel in Figure 3.54). These options were evaluated using FEA in SolidWorks to ensure strength and safety within the desired trainer weight range. For each design, a static stress analysis was performed. The design criterion for ensuring safety of the crane design was a FOS of 1.5 when the max patient size load (120 lbs.) was applied.

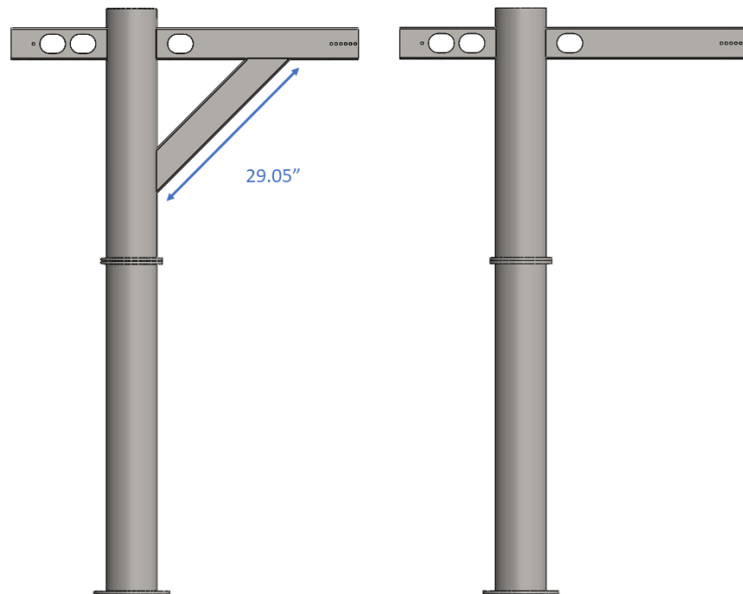


Figure 3.54: Gusseted Solid Static FEA Model (Left) and Non-Gusset Solid Static FEA Model (Right)

The gusset for the gusset crane design was designed as a 0.125” thick (1/8 inch thick, 11 gauge) 5” x 2” mild steel rectangular tube. The gusset is 29.05” long with 45-degree cuts at each end for attachment to the middle of the cantilever boom arm as seen in the left picture in Figure 3.54.

For the gusset crane simulation, plain carbon steel was used to simulate all components with material properties listed in Table 3.8. All eight of the mounting holes on the circular base flange of the crane were fixed in the simulation study shown in the right picture of Figure 3.55. The



patient simulating force was applied to the outer most right and left pulley mounting holes of the cantilevered crane boom totaling 120 lbs. as shown in the left picture of Figure 3.55. A universal bonded contact was applied to all components simulating welded joints.

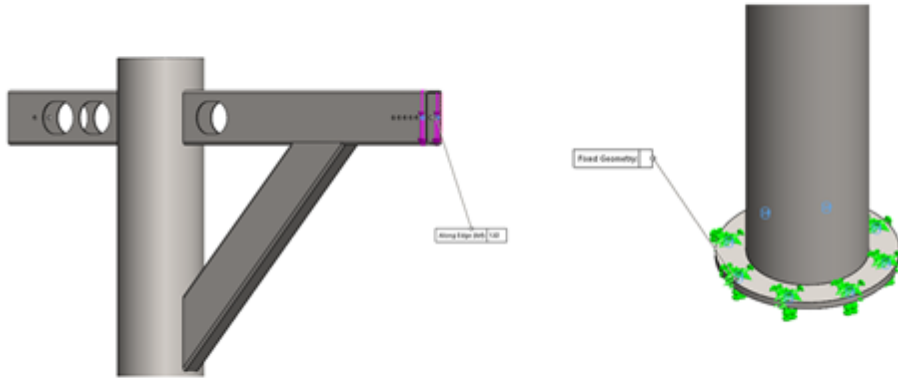


Figure 3.55: Crane FEA Force placement (Left) and Crane FEA Fixed Geometry (Right)

A solid element blended curvature-based mesh was used to further refine the mesh density around high stress areas and connection points as shown in Figure 3.56. Specifically, around the gusset connections to the top central crane mast and the cantilever boom arm. The

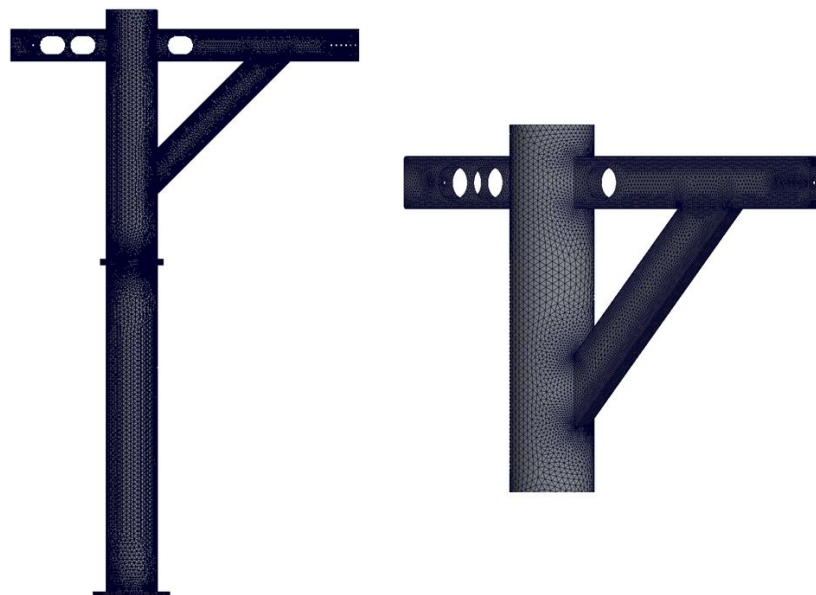


Figure 3.56: Mesh Density of Gusset Crane for Static FEA Analysis

mesh density formed a total of 504504 elements with 91% of elements less than an aspect ratio of 3 as listed in Table 3.8. The simulation produced stress, displacement, and factor of safety results plots.

**Table 3.8 - Gusset Crane Static FEA Properties**

<b>FEA Properties – Gusset Crane Static Analysis</b>	
<b>Plain Carbon Steel Material Properties</b>	
<b>Property</b>	Value
<b>Elastic Modulus</b>	3.04579x10 <sup>7</sup> psi
<b>Poisson’s Ratio</b>	0.28
<b>Mass Density</b>	0.281793 lb/in <sup>3</sup>
<b>Tensile Strength</b>	57,989.85 psi
<b>Yield Strength</b>	31,994.45 psi
<b>Component Contact</b>	Bonded Compatible Mesh
<b>Mesh Type</b>	Solid, blended curvature-based mesh
<b>Max Element Size, Min Element Size</b>	0.7”, 0.05”
<b>Total Elements</b>	504504
<b>Max Aspect Ratio</b>	91.0% of elements < 3
<b>Analysis Type</b>	Static
<b>Large Displacement</b>	Off
<b>Plain carbon Steel</b>	linear elastic isotropic

For the non-gusset crane simulation, plain carbon steel was used to simulate all components with material properties listed in Table 3.9. The fixed geometry and application of the force was done the same as previously discussed with the gusset FEA analysis and shown in Figure 3.55. A universal bonded contact was applied to all components simulating welded joints.

**Table 3.9 – Non-Gusset Crane Static FEA Properties**

<b>FEA Properties – Non-Gusset Crane Static Analysis</b>	
<b>Plain Carbon Steel Material Properties</b>	
<b>Property</b>	Value
<b>Elastic Modulus</b>	3.04579x10 <sup>7</sup> psi
<b>Poisson’s Ratio</b>	0.28
<b>Mass Density</b>	0.281793 lb/in <sup>3</sup>
<b>Tensile Strength</b>	57,989.85 psi
<b>Yield Strength</b>	31,994.45 psi
<b>Component Contact</b>	Bonded Compatible Mesh
<b>Mesh Type</b>	Solid, blended curvature-based mesh
<b>Max Element Size, Min Element Size</b>	0.7”, 0.05”
<b>Total Elements</b>	282899
<b>Max Aspect Ratio</b>	88.2% of elements < 3
<b>Analysis Type</b>	Static
<b>Large Displacement</b>	Off
<b>Plain carbon Steel</b>	linear elastic isotropic

A solid element blended curvature-based mesh was used to create the mesh with maximum/minimum element sizes listed in Table 3.9. the created mesh density can be seen in Figure 3.57. The mesh density formed a total of 282899 elements with 88.2% of elements less than an aspect ratio of 3 as shown in Table 3.9. The simulation produced stress, displacement, and factor of safety results plots.

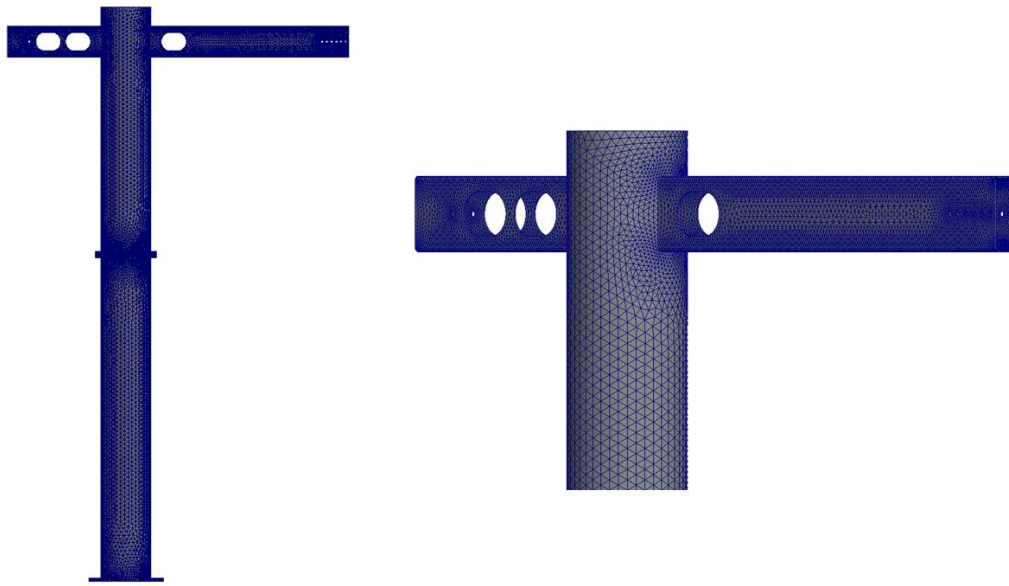


Figure 3.57: Mesh Density of Non-Gusset Crane for Static FEA Analysis

To better characterize the crane design under a cyclical walking load, a frequency-based and linear dynamic modal time history analysis was performed on the non-gusset crane design in SolidWorks. A linear dynamic modal time history analysis was chosen as it shows a resulting stress as it relates to time of an applied cyclical load.

To assure there were no possibilities of mechanical resonance, a frequency analysis was performed to ensure the typical walking frequency of a child did not resonate with any natural frequencies of the crane. Mechanical resonance occurs when a structural or mechanical system responds (bends) at a greater amplitude when the frequency of oscillation matches the natural frequency of vibration of the system (call the resonance frequency or resonant frequency). This condition may lead to violent swaying motions and potentially catastrophic failure of the support structure (Zahid et al., 2020). The modal frequency analysis was performed using the same model seen in the left panel of Figure 3.54 using the same material and mesh properties found in Table 3.9 to find the natural frequencies of the system. A stepping frequency of 2.5 Hz - ambulatory

preschooler (6-year-old), step speed 0.40 s, 2.8 mph treadmill (Verbecque et al., 2017) - was used as the typical cyclic frequency seen on the crane.

To conserve computer resources when solving the linear dynamic study, the non-gusset crane model as seen in the left panel of Figure 3.54 was modified from a solid model to a surface model allowing for simulation using shell elements. A mid-surface was taken of each crane structure component and the solid body subsequently deleted resulting in the non-gusset surface model shown in Figure 3.58. Within the shell manager of the linear dynamic study, the thickness of each surface was specified for simulation – all flange plates (0.5”), cantilever boom (0.125”), top and bottom mast (0.0625”).

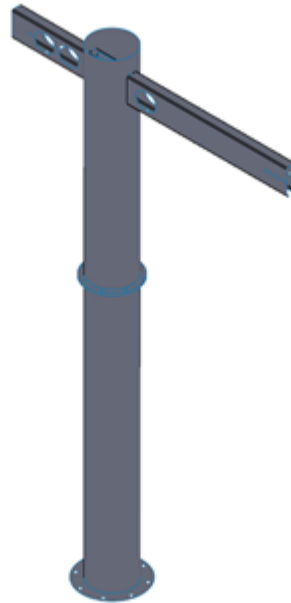


Figure 3.58: Non-Gusset Shell Linear FEA Model

To develop the necessary cyclical force data for the linear dynamic study, data, as seen in APPENDIX VIII: Original Patient Force Data for FEA Dynamic Analysis, was retrieved from a pediatric patient undergoing LT using a body weight support treadmill at the Kosair Charities Center for Pediatric NeuroRecovery. This patient was a 14-year-old male weighing 116.85 lbs. with a height of 5’ 4.5”. This was chosen because the weight and height are towards the high side

of the design specifications presenting a more conservative case analysis. 30s of force data was collected every 0.0005s at 50% body weight support and treadmill speed of 2.4 mph. The first 5 seconds of data was extracted and then averaged every 100<sup>th</sup> (.01 sec) of a second. Within in this subset of data, it was found to have a max force value of 120.94 lbs. Next, every 0.01 seconds of force data was divided by the max force value to convert each force reading to a percentage of the max force. This data is shown in Figure 3.59.

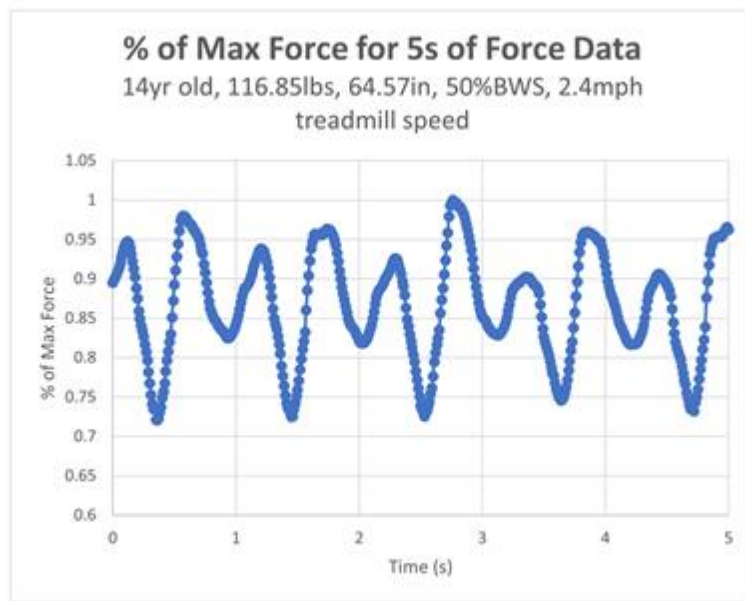


Figure 3.59: Crane FEA Force placement (Left) and Crane FEA Fixed Geometry (Right)

Plain carbon steel was used to simulate all components with material properties listed in Table 3.10. A modal damping ratio of 0.02 was applied as a conservative estimate. The fixed geometry and the max force of 120.94 was applied at the same location of the force previously discussed with the non-gusset static FEA analysis and seen in Figure 3.55. A universal bonded contact was applied to all components simulating welded joints. In addition to the application of a max force, the previously established force curve data was entered over a 5 second period.

**Table 3.10 - Non-Gusset Crane Linear Dynamic FEA Properties**

<b>FEA Properties – Dynamic Crane Analysis</b>	
<b>Plain Carbon Steel Material Properties</b>	
<b>Property</b>	Value
<b>Elastic Modulus</b>	3.04579x10 <sup>7</sup> psi
<b>Poisson’s Ratio</b>	0.28
<b>Mass Density</b>	0.281793 lb/in <sup>3</sup>
<b>Tensile Strength</b>	57,989.9 psi
<b>Yield Strength</b>	31,994.5 psi
<b>Component Contact</b>	Bonded Compatible Mesh
<b>Mesh Type</b>	Mid surface shell, Blended Curvature Mesh
<b>Max Element Size, Min Element Size</b>	0.7”, 0.05”
<b>Total Elements</b>	62,992
<b>Max Aspect Ratio</b>	3.31
<b>Analysis Type</b>	Linear Dynamic (Modal Time History), 24 Frequencies, 0-5.11s, Modal Damping – Ratio 0.02
<b>Large Displacement</b>	Off
<b>Plain carbon Steel</b>	Linear Elastic Isotropic

A mid-surface shell element curvature-based mesh was used to create the mesh with maximum/minimum element sizes listed in Table 3.10. The created mesh density is shown in Figure 3.60. The mesh density formed a total of 62,992 elements with a max aspect ratio of 3.31; other simulation parameters are listed in Table 3.10.

Von Mises stress plots (psi) were taken of the five second period at each of the nodes listed in Figure 3.61 – cantilever end (Node 13108), cantilever mast joint (Node 111750), crane mast joining flange plate (Node 95003), and crane mounting plate (Node 103353).

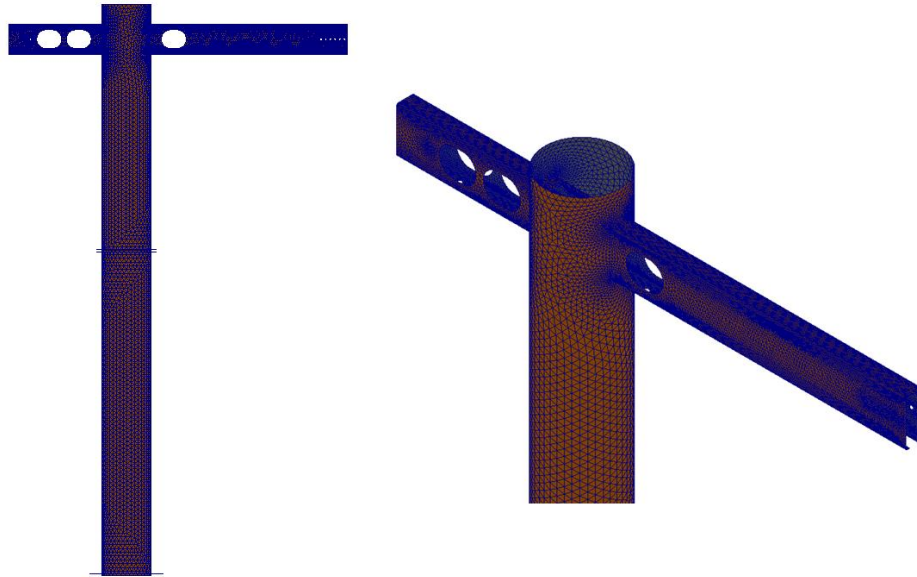


Figure 3.60: Mesh Density of Non-Gusset Crane for Linear Dynamic FEA Analysis

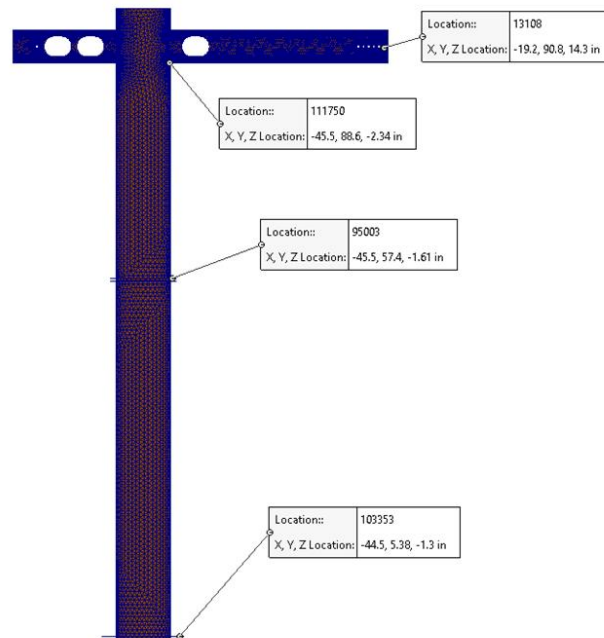


Figure 3.61: Node Location for von Mises Stress Data Analysis from Modal Time History Analysis



### 3.8.3 Fabrication and Assembly

The quality management system used by Hafendorfer Machine, Inc. is certified ISO 9001:2015 and AS9100D for the design and manufacture of machined and fabricated components. This allowed for increased part consistency and improved quality ensuring every component meets the desired specification. The top and bottom crane masts were fabricated using a Trumpf TruLaser 7000 Tube multi-axis laser cutter (Figure 3.62) allowing for precision cutting, including chamfering and diagonal cuts. This state-of-the-art machine allowed for the laser-cut slot for the crane boom on the top mast. This permitted the rectangular boom tube to be fully captured around the rectangular perimeter, positioned at the appropriate length, and welded on both sides of the top crane mast ultimately providing maximum strength and durability. Certified onsite welders completed the assembly of components which were delivered ready to install in the main BWST.



Figure 3.62: Trumpf Trulaser Tube 7000 Steel Tube Laser Cutter at Hafendorfer Machine, Inc.

### **3.8.4 Verification Testing**

Dimensional verification of the crane was completed using a 25 ft SAE measuring tape. Crane height will be measured from the floor to the highest point of the top mast. Additionally, to verify the design requirement of the crane must center the patient on the treadmill, a plumb bob was hung from the end of the crane boom and the measurement from the motor housing to the plumb bob was taken (20 in.  $\pm$  1 in.) and the measurement of the side of the treadmill belt to the plumb bob will be taken (7 in.  $\pm$  1 in.).

Functionality testing was completed on the slew ring to determine if the crane could properly rotate clockwise 150 degrees to be able to reach a patient in a wheelchair at the rear the BWST and to assure the crane rotation speed was not more than 20 deg/sec. Neutral position of the crane over the treadmill was used as a starting point. 150 degrees clockwise rotation was determined and marked. Crane rotation was initiated along with a stopwatch. Time and degrees travelled was recorded.

Weight testing of the assembled crane with BWS components was completed by attaching the yoke subsequent weights (small chain + large chain + carabiner + parts F, G, H, I, J, K, L) to the crane cable and testing for 10 minutes. Total weight used for testing was 325.24 pounds. The crane was checked for any observable failures or excessive deformation.

All crane dimensional verification, functionality testing, visual inspection, and weight testing criteria can be as seen in APPENDIX VI: Crane Design Criteria and Verification Results.

## **3.9 Body Weight Support and Control System**

### **3.9.1 BWS and Control System Design Requirements and Development**

The primary design criteria for the pediatric BWST control and BWS system was properly integrating a previous established control system taken from the adult body weight support treadmills previously being used during feasibility studies of locomotor training on pediatric patients. However, to properly integrate this system changes needed to be implemented to adapt

the system for use with the pediatric population. Integrated body weight support was achieved by the addition of a specialized pneumatic and electric actuator system attached to the back of the support crane. The actuator system and control system design, as shown in Figure 3.63, were modified from the Alpha prototype previously discussed and designed by the Frazier Rehab Engineering core. The control system software and algorithm used were adapted from previous adult body weight support treadmills and enabled by another team member.

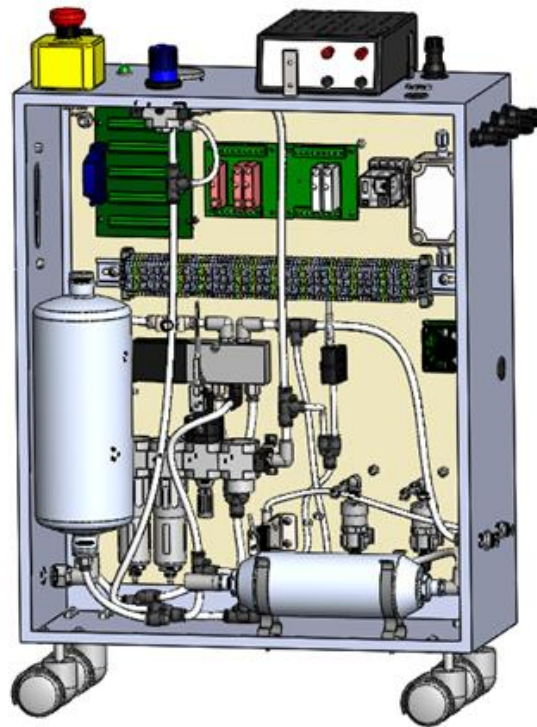


Figure 3.63: Electric and pneumatic control system

Modifications were needed to optimize the body weight support and control system to the pediatric BWST. A smaller load cell (Omega LC101-200 S-Beam) rated at 200 lbf was selected to ensure the tension force readings were in a tighter range more apt to measuring the smaller forces seen in the pediatric weight range (< 120 lb.).

A Festo pneumatic cylinder (DNC-50-150-P-A-S11-KP) with 150mm (5.9”) stroke, as shown in Figure 3.64, length was used to provide the necessary speed of the minute adjustments needed during gait locomotor training of the patient.

Due to the reduced specified weight capacity of the BWST, it was decided to use an electric actuator instead of a pneumatic actuator to reduce cost, overall system complexity, and reduction of the operating air pressure needed ultimately allowing for a smaller air compressor. The electric cylinder was a 12-volt electric liner actuator (Servo City SDA24-263) with a 24” stoke length. The thrust rating for this actuator is 560 pounds with a max load rating of 1574 lbs. providing

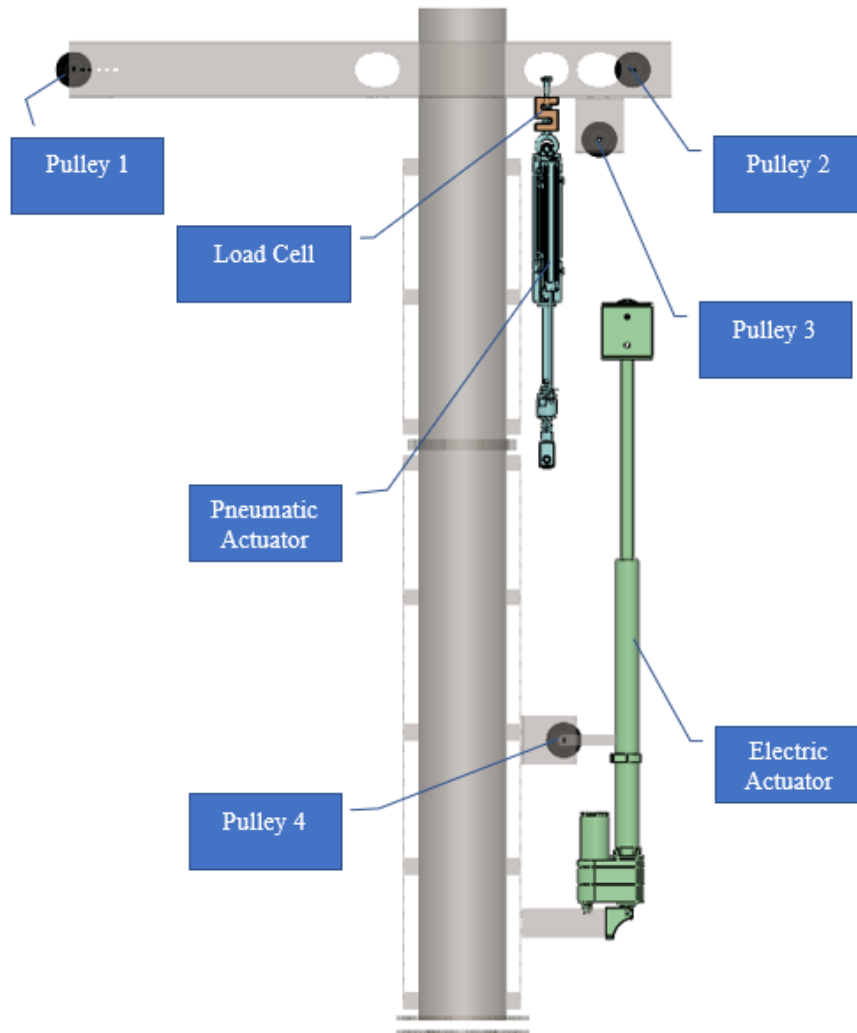


Figure 3.64: BWS Pulley System and BWS Labeled Components

enough power with adequate factor of safety when lifting the patient out of their wheelchair on to the treadmill.

A pulley system was added to gain the necessary distance of travel needed for varying patient heights and loading/unloading of the patients. To achieve this functionality, a five-pulley system was designed with one cable end terminating at the yoke above the patient's head while the opposite end terminates at the pneumatic cylinder. Figure 3.64 shows the pulley system design with forces showing travel path of the cable. The large electric cylinder is in a 1:2 pulley ratio, while the smaller pneumatic cylinder controlled by the proprietary body weight support algorithm is setup as a 1:1 pulley ratio. The 1:2 electric cylinder pulley ratio allows for twice the travel on the cable end with the tradeoff of double the workload on the electric cylinder. This allowed for sufficient travel distance of the cable when loading and unloading patients while providing enough factor of safety over the load experienced by the electric actuator. The 1:1 pneumatic cylinder pulley ratio allowed for no needed changes to the BWS algorithm allowing for the load cell to experience a 1:1 ratio of the patient's actual weight. With the max patient weight of 120, the electric actuator will experience a max of 240 lb. load from the pulley system design. The 560 lb. thrust rating of the electric actuator gives a 2.33 factor of safety which ensures durability over time. With the double increase in travel range of a cable the yoke can be manipulated a total of 48" ensuring max and min patients heights of the design will be achieved.

The cable used was a 3/16" by 300" maxibraid from John Sakach Company to reduce stretch and fatigue while providing adequate strength. This was the same type of cable as previously used and verified with the Alpha BWST unit. Additionally, the same yoke design and safety cable will be used within the Beta BWST. Because the yoke, cable, and safety cable were verified with the previous Alpha BWST prototype no testing or additional design verification was performed on those components.

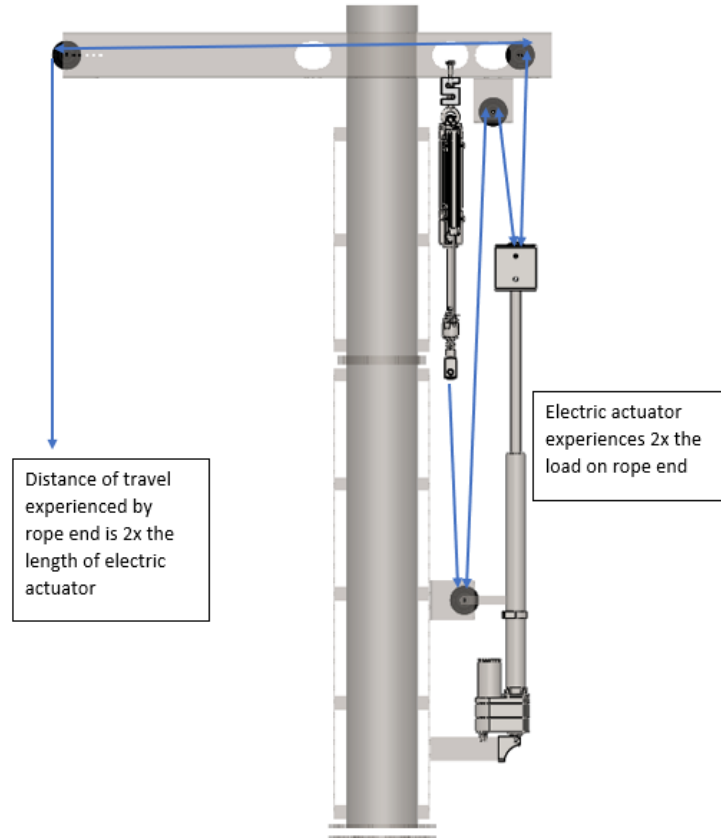


Figure 3.65: BWS Pulley System Setup

The slew ring motion control circuit board layout is shown in Figure 3.66. Included in the circuitry was a high-current commercial motor driver (SyRen 25A, Dimension Engineering, Hudson, Ohio) acting as an H-bridge that provided the ability to switch the polarity of the 24V power supply (Mean Well SDR-480-24, 20 A rated, 110V, 20A) to enable forward and reverse motion of the slew ring. An Atmega328P microcontroller (5V 16MHz Pro Trinket, Adafruit, New York, NY) 5V was used to control the logic to read the input from the foot pedal, activate the H-bridge and rotate the crane.

Two whisker type limit switches (Honeywell SZL-VL-F) were installed to signal at the maximum limit of rotation in both clockwise and counterclockwise rotations ensuring the electric

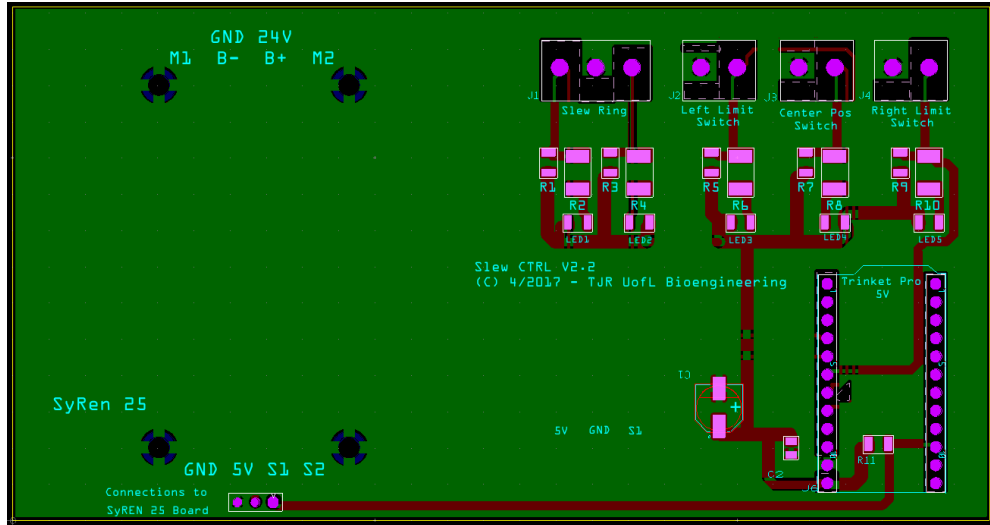


Figure 3.66: PCB layout for slew ring control

cylinder did not collide with the rear deck. A magnetic centering proximity sensor (Littlefuse 59065-010) was used to center the slew ring and crane over the center line of the treadmill providing accurate positioning of the patient on the treadmill. A heavy-duty two-channel foot pedal switch (ConTrol International Series 220) provided control the manipulation of the slew ring for the trainers (Figure 3.67). programming of the foot pedal switch required the user to hold the switch down with their foot to activate the slew ring rotation. When the user lifts their foot after activation of the slew ring, the rotation would instantly stop with negligible backlash adding an additional layer of safety.



Figure 3.67: Slew Ring Control Switch

### **3.9.2 Fabrication and Assembly**

Parts were sourced from several vendors McMaster Carr, Servo City, Digi-key, Mouser, Festo, Grainger, Novotechnik, National Instruments, Omega Engineering, OPTO22, and Allied Electronics. Parts were received and assembled at Frazier Rehab Institute, Louisville, KY.

The PCB board was produced by (Seed Studio Fusion PCB) and the circuit was assembled using standard soldering techniques.

The magnetic centering sensor installation was done by first centering the crane on the treadmill using a plumb bob extended from the crane ensuring crane alignment 20 inches from the motor housing and 7 in. from the side of treadmill belt. Next, the sensor was installed on the front crane mounting bar ensuring alignment with the corresponding actuator.



### 3.9.3 Verification Testing

Dimensional verification of the BWS and Control System was completed using a 25 ft SAE measuring tape. To obtain the patient height range that is capable with the system, the electric actuator was moved to its lowest position resulting in the highest yoke position. Measurement was taken from the highest position underneath the yoke where the patient's head would be to the treadmill belt and recorded. Next, the electric actuator was moved to its highest position resulting in the lowest yoke position. Measurement was taken from the highest position underneath the yoke where the patient's head would be to the treadmill belt and recorded. With the electric actuator still in the highest position, the slew ring was activated to move the crane clockwise simulating the picking up of a patient from their wheelchair. A measurement was taken from the floor to the highest point underneath the yoke and recorded.

Upon installation of the BWS and control system, the load cell will be calibrated and subsequently incrementally weight tested to ensure proper calibration and reading of weights within the desired patient weight range (up to 120 lbs.). To calibrate the load cell, a reading was taken without any weight and set within the BWS software as the zero point. Next, 120.66 lbs. (A+G+I+B+Yoke+Small Chain+Large Chain) was hung from the cable and entered the BWS software as the max weight. The BWS software produces a calibration of the load cell base on these readings (Table 3.11).

**Table 3.11 - Load Cell Calibration Min/Max Weight Used**

Load Cell Calibration		
Equipment and Weights Used	Calculated Weight (lbs.)	
Nothing Free Hanging Rope	0.20	Min
A+G+I+B+Yoke+Small Chain+Large Chain	120.66	Max

Load cell calibration verification and functionality testing was conducted by incrementally applying weight to the crane yoke representing 7 increments – 0, 20, 40, 60, 80, 100, and 120

pounds. Next, the actual load cell force reading was recorded at each increment as displayed on the BWS software. Weights used are listed in Table 3.12. A load cell force graph comparing actual weight vs. weight registered by the load was created and analyzed for linearity.

**Table 3.12 - Load Cell Linearity Testing Weights**

<b>Load Cell Linearity Test</b>		
<b>Testing Increments (lbs.)</b>	<b>Equipment and Weights Used</b>	<b>Actual Weight (lbs.)</b>
0	Nothing Free Hanging Cable	0.00
20	A+B+Yoke+Small Chain	23.47
40	E+B+Yoke+Small Chain	44.26
60	A+B+C+D+E+Yoke+Small Chain	63.70
80	G+A+E+Yoke+Small Chain+Large Chain	92.94
100	G+I+A+Yoke+Small Chain+Large Chain	110.42
120	G+I+E+Yoke+Small Chain+Large Chain	130.31

Functionality testing was completed by attaching a 45-pound weight to the yoke activating the BWST and setting treadmill speed to 1 mph while the BWS is set to 20%. The emergency stop button will be engaged and the BWS behavior was recorded. With the Emergency stop button engaged, an attempt was made to rotate the crane 90 +/-5 degrees clockwise, and then returned to the starting position with system behavior recorded.

The next functionality test involved attaching the same 45-pound weight to the yoke with treadmill speed set to 1 mph and BWS set to 20%. The emergency stop button was engaged to observe the display of computer screen which should indicate that the emergency stop button is activated. The operator then attempted to reactivate the machine while the emergency button is engaged. Emergency button was then disengaged, and the operator attempted to resume normal system use.

To ensure proper functionality of the limit switches, the centering switch was first deactivated then the crane was rotated until fully cantilever on the aft end of the BWST activating the whisker

limit switch on the clockwise rotation. The crane was then rotated counterclockwise until activation of the second whisker switch. Next, the center switch was reactivated, and the slew ring rotation initiated to observe a full stop with the center switch aligned and cantilever suspended in the appropriate position over the treadmill.

The control system and slew ring motor 24 V power supply and the electric actuator 12 V power supply will be measured with a digital multimeter to ensure proper voltage is achieved.

## IV. RESULTS & DISCUSSION

### 4.1 QFD Results

Figure 4.1 shows the completed QFD for the overall pediatric BWST user needs and technical requirements.

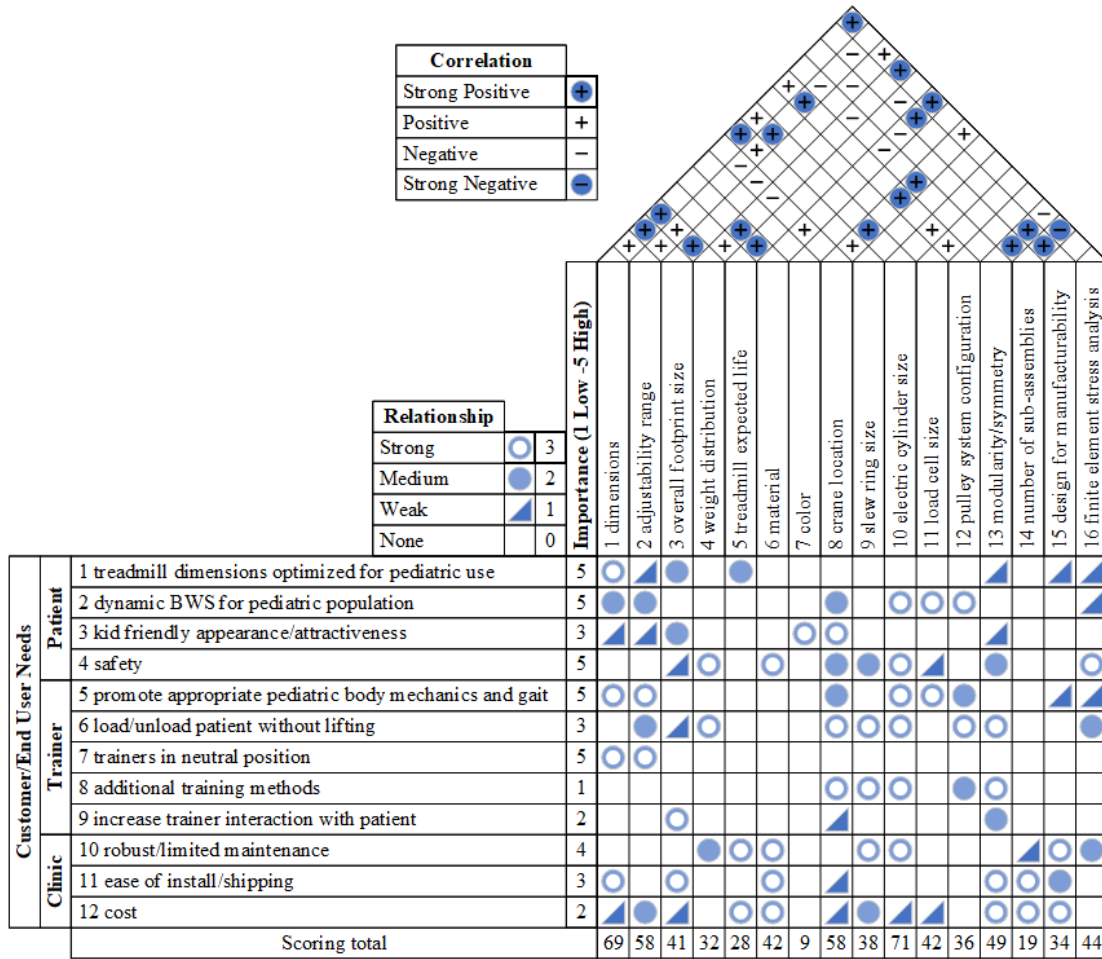


Figure 4.1: QFD for complete BWST

Figure 4.2 shows each technical requirement's score as a percentage of the total points calculated in the relationship matrix of the QFD analysis. There were 6 technical design requirements that received above 6.5% of total points calculated – dimensions, adjustability range, crane location, electric cylinder size, symmetry/modularity, and FEA stress analysis. These were determined to have the most impact on ensuring user need requirements were met with the design.

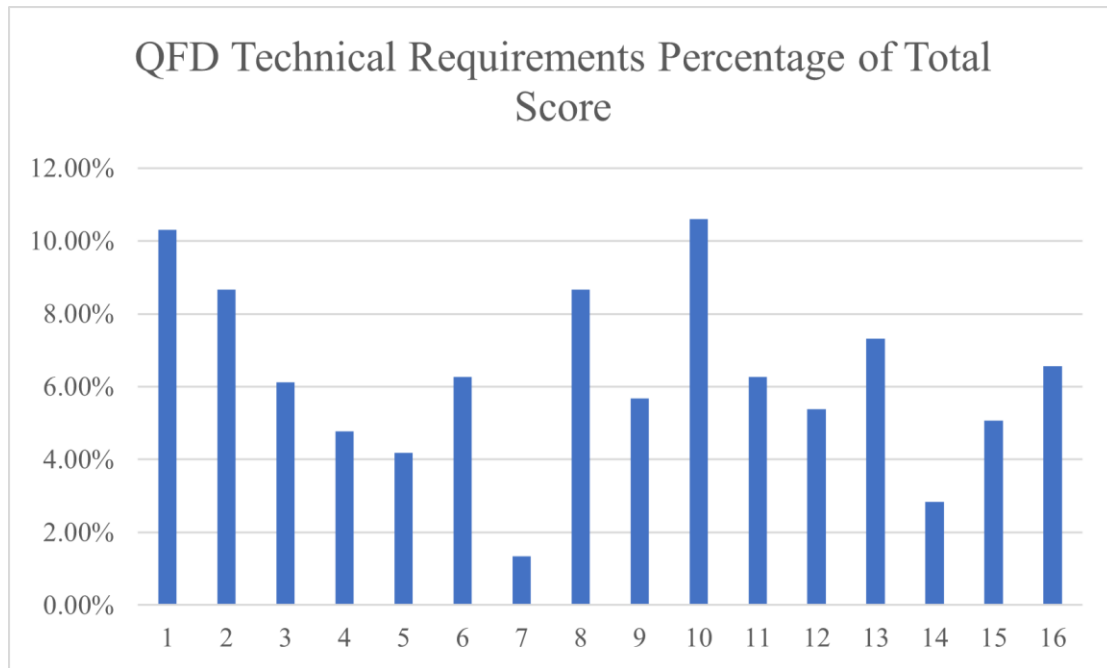


Figure 4.2: QFD technical requirements prioritized as percentage of total points

## 4.2 DFMEA Results

The complete DFMEA is seen in APPENDIX I: DFMEA and each sub assembly design criteria, verification test, and result are broken out from the full DFMEA and can be seen in APPENDIX II to APPENDIX VII.

The DFMEA was structured with the user needs stated and each need divided into multiple design inputs or design criteria needed to satisfy each need. Each design input was analyzed to

determine potential failure modes and the cause of the failure mode associated with not meeting the design input. An attribute (pass/fail) or variable (measured value) test method was created to ensure the design input was achieved, thus reducing the potential risk level for the failure mode. The design output of the DFMEA is the verification testing results.

### **4.3 Overall System**

#### **4.3.1 Modularity and Dimensional adjustment to Pediatric Population**

The fully functional and assembled BWST beta prototype is shown in Figure 4.3. All modular sub-assemblies (fore/aft decks, elevated seating/footrests, central treadmill, crane) were successfully integrated into the complete BWST.



Figure 4.3: Complete BWST Assembled for Testing

The resulting assembly was completely redesigned to fit the size requirement of the pediatric population. Figure 4.4 shows two pediatric manikins (heights of 3' 3" and 4' 9", respectively) simulating use by a pediatric patient in the redesigned BWST. When comparing the updated design with the issues and constricted cramped feel of the trainers and pediatric patients when using an adult BWST (Figure 2.7), it is apparent that the system design is more open and kid friendly. The rear lifting crane is less intimidating for the patient and the system is more ergonomic for the trainers, with easy access to the patient's trunk and legs as required by LT.

Figure 4.4 also show the crane relocated behind the patient which satisfies one of the system design requirements.



Figure 4.4: Complete BWST System with 3' 3" Child Manikin (Left) and 4' 9" Child Manikin (Right)

### 4.3.2 Tipping Scenario Verification and Motion Analysis Results

Motion analysis results of the tipping scenario simulated in SolidWorks resulted in an estimation of the minimal force requirement of 957 pounds to create a tipping moment of the entire system. This load was applied vertically down on the face of the cantilever crane boom. This result suggests a FOS of 7.98 for the max patient weight of 120 pounds which far exceeds the design criteria established at a FOS of 1.5. The motion analysis tipping result graphic is shown in Figure 4.6, where 957 pounds were required to tip the system around the rear deck support feet.



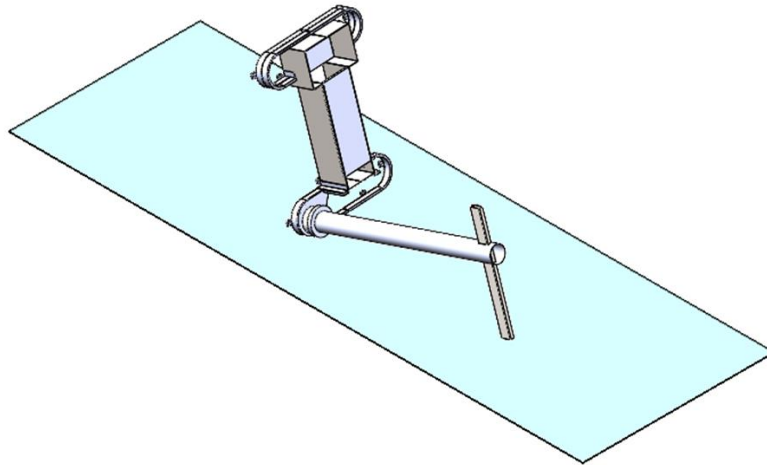


Figure 4.6: Complete BWST Tipping Motion Analysis Results

Physical weight testing of the assembled BWST is shown in Figure 4.5. With the 325.24 lbs. loaded on the crane in the 150-degree cantilevered position, no system instability, tipping moment, or mechanical failure was observed.



Figure 4.5: Crane Weight Testing

### 4.3.3 Footprint Reduction and Ease of Installation

With the removal of the wheelchair ramp and updated dimensions for the pediatric population, the overall square footage of the system totaled 27.06 ft<sup>2</sup> (6.25 ft x 4.33 ft) equaling a 315% reduction in square footage footprint when compared to on-the-market adult BWST (85.5 ft<sup>2</sup>, 4.75 ft x 18 ft). Overall system symmetry is shown in Figure 4.7 with the midline of the treadmill acting as the midline for the entire system.



Figure 4.7: Assembled Beta Prototype Showing Symmetry and System Footprint

With the reduction in overall footprint and added modularity, the BWST has improved efficiency during install and transportation to the clinic ultimately reducing cost and labor. Figure 4.8 shows one pallet containing the front/rear decks and the top/bottom crane components. The entire system can be shipped on 3 to 4 common wooden pallets.



Figure 4.8: Shipping Pallet Containing Top/bottom Crane Mast, Back Deck, Front Deck and Crane Plate

By using of state-of-the-art manufacturing techniques and design simplification, overall system cost was significantly by approximately 50% when compared to the adult BWST. A high-level cost breakdown can be seen in APPENDIX X: High-level Cost Structure.

#### **4.3.4 Overall System Stability Testing**

When simulating a typical load seen by the entire BWST during a typical training scenario (crane loaded with 130.31 lbs. with 4 trainers on system), no system instability or mechanical failure was observed which passes the design requirement.

All the testing results and design criteria for the complete BWST can be seen in APPENDIX II: Overall BWST Design Criteria and Verification Results.

## 4.4 Treadmill

### 4.4.1 Dimensional and Visual Analysis of Central Treadmill

Figure 4.9 show the fully assembled treadmill as received from Tuff Tread, Inc. Dimensional verification was completed using a 25 ft SAE measuring tape. The treadmill passed all dimensional verifications and weight requirements as seen in APPENDIX III: Treadmill Design Criteria and Verification Results. Additionally, a 4 ft. level was placed across the motor housing shell as well as the two side panels of the treadmill to check for any unevenness of the treadmill. The treadmill was determined to be sufficiently level, with minor adjustments enabled via the included leveling feet.



Figure 4.9: Assembled Central Treadmill



Visual inspection of the motor housing (Figure 4.10) confirmed the electrical panel with necessary power outlets, motor, and VFD comfortably fit within the housing, again meeting the design criteria.



Figure 4.10: Treadmill Motor Housing Showing Motor, Electrical Panel, and VFD

Upon visual inspection, the integrated linear bearing, steel rod, and rack system seen in Figure 4.11 was determined to be sturdy and free from manufacturing defects. The side seat and footrest fore/aft slots were measured and determined to meet design criteria – 17” for side seats and 8” for footrests.

Rear flanges (Figure 4.16) for rear deck mounting and motor housing mounting holes were seen and measured allowing for mounting of the front and rear decks meeting design requirements.

The treadmill had no sharp corners or jagged edges ensuring safety for the patient and trainers, and no treadmill incline feature was integrated per the design criteria.



Figure 4.11: Integrated Linear Bearing and Rack System for Side Seat/Footrest within Central Treadmill

#### 4.4.2 Treadmill Deck Static FEA and Weight Testing Results

Figure 4.12 shows the von Mises stress results from the 120 lbs. treadmill deck static FEA simulation.

Most of the stress concentration occurs around the mounting brackets and bolts connectors with the treadmill deck (laminated veneer lumber) itself experiencing minimal stress. The max stress that was seen was 15,540 psi found on the bottom side of the mounting at the tensioned bolt connectors significantly below the yield stress of carbon steel - 31,994.45 psi. A close-up view of the mounting bracket stress concentration is shown in Figure 4.13.

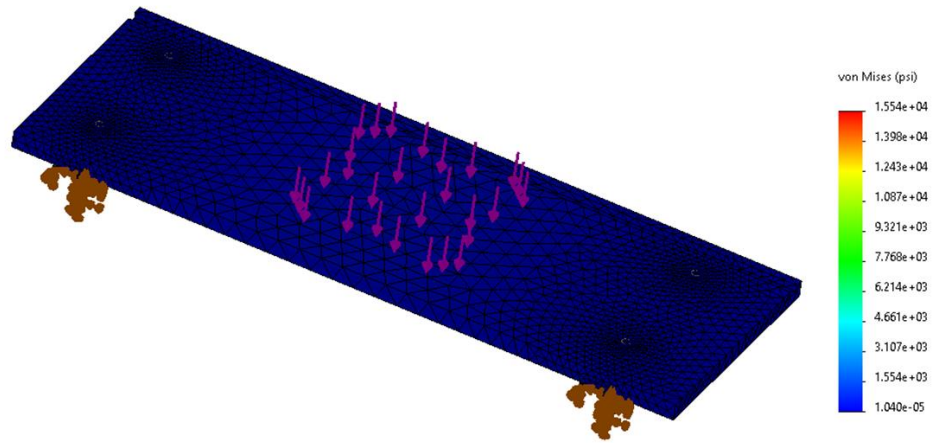


Figure 4.12: Treadmill Deck and Mounting Brackets von Mises Stress Plot (psi) – Zero Deformation Scale

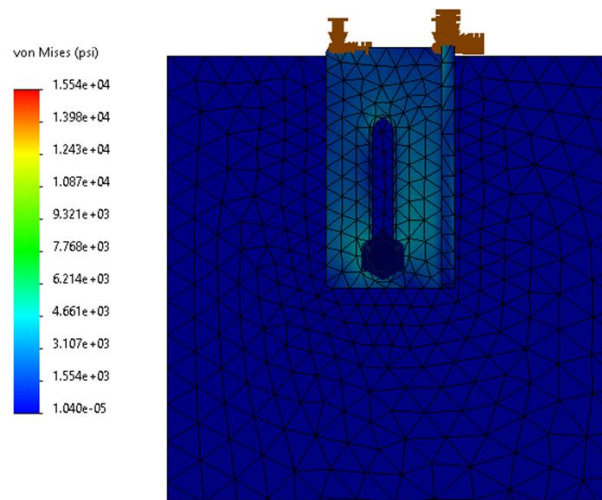


Figure 4.13: Treadmill Mounting Bracket von Mises Stress Plot (psi) – Zero Deformation Scale

Figure 4.14 shows the displacement of the treadmill deck from the 120 lbs. static FEA analysis. Note there is a deformation scaling factor set on the plot to better depict how the treadmill deck deforms (30x scaling factor). A max displacement of 0.03 in. is observed around the center of the deck where the force is being applied and the deformation depicts a curved concave deck shape. This deformation is representative of what is expected and presents no issues of concern.

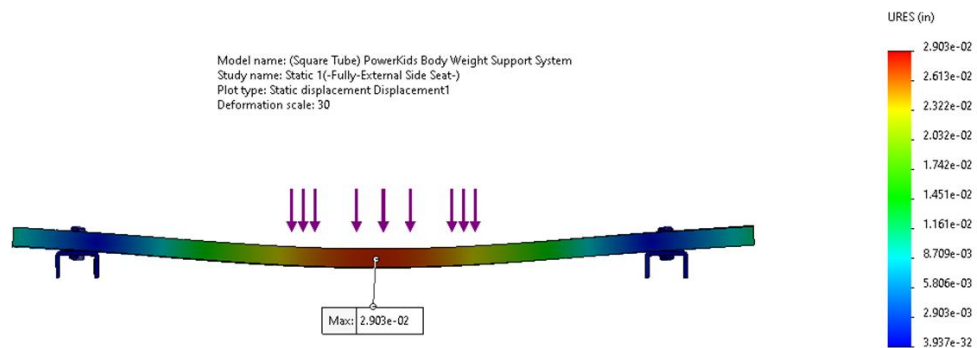


Figure 4.14: Treadmill Deck and Mounting Brackets Displacement Plot (in) – 30 Deformation Scale

A factor of safety plot of the treadmill deck and the four mounting brackets reveals an overall FOS of 2.1 with 120 lbs. applied. This exceeds the design criteria of the treadmill deck which requires support 120 lbs. with a FOS of 1.5

Weight testing (195 lbs. volunteer) of the assembled treadmill deck for 10 minutes presented no failures, unusual deformation, or permanent deformation.



Figure 4.15 shows the weight testing of the motor housing. No failures or deformation was observed therefore this configuration passes the design criteria where the motor housing should be able to support up to 300 pounds. as if a trainer was standing on it.



Figure 4.15: Weight Testing of Motor Housing - 309.96 lbs. (E, F, G, H, I, J, K) for 10 mins.

#### **4.4.3 Treadmill Functionality Testing Results**

Functionality of the treadmill operation was conducted to ensure a 6-mph belt speed could be reached with adjustability of speed at 0.1 mph and can stop in less than 2 seconds. The treadmill successfully powered up ensuring proper power from the electrical control panel and results are included in APPENDIX III: Treadmill Design Criteria and Verification Results.

A belt slippage test was conducted after properly tensioning the belt using the two tensioning bolts on the aft side of the treadmill as shown in Figure 4.16. The volunteer (195 lbs.) walked on the belt for 10 minutes without experiencing any slippage or side-to-side movement of the belt.

To ensure the design meets the requirement of reducing maintenance over time and is durable enough to use with minimal servicing use over time, a more complete analysis will need to happen as the system is used. Preliminary tests of running the treadmill consecutively for 45 mins showed no failures or issues. Complete validation was out of scope of this thesis and will be conducted overtime from clinical feedback.



Figure 4.16: Rear View of Treadmill Showing Open Back End and Roller Tensioning Bolts

## 4.5 Integrated Seating and Footrest System

### 4.5.1 Seating and Footrest Dimensional Verification and Visual Analysis Results

Figure 4.17 and Figure 4.18 show the fully assembled (Revision 1) side seating and (Revision 1) footrests as received from Winston Industries, Inc. Functionality testing showed the installed side seats and footrests properly disengaging from the grooved rack system upon a vertical lifting force and smoothly sliding fore/aft. Additionally, the side seats and footrests passed all dimensional verification and visual inspection as seen in APPENDIX IV: Seating/Footrest Design Criteria and Verification Results.

Figure 4.19 shows the fully assembled and installed trunk trainer seat as received from Winston Industries, Inc. Functionality testing showed that the trunk trainer seat could be easily lifted rotated or completely removed with minimal force. The trunk trainer seat passed all dimensional verification and visual inspection as seen in APPENDIX IV: Integrated Seating/Footrest Design Criteria and Verification Results.



Figure 4.17: Installed Rev. 1 Footrest Arm and Rev. 1 Side Seating Arms



Figure 4.18: Assembled Rev. 1 Right and Left Side Seats and Rev. 1 Footrests

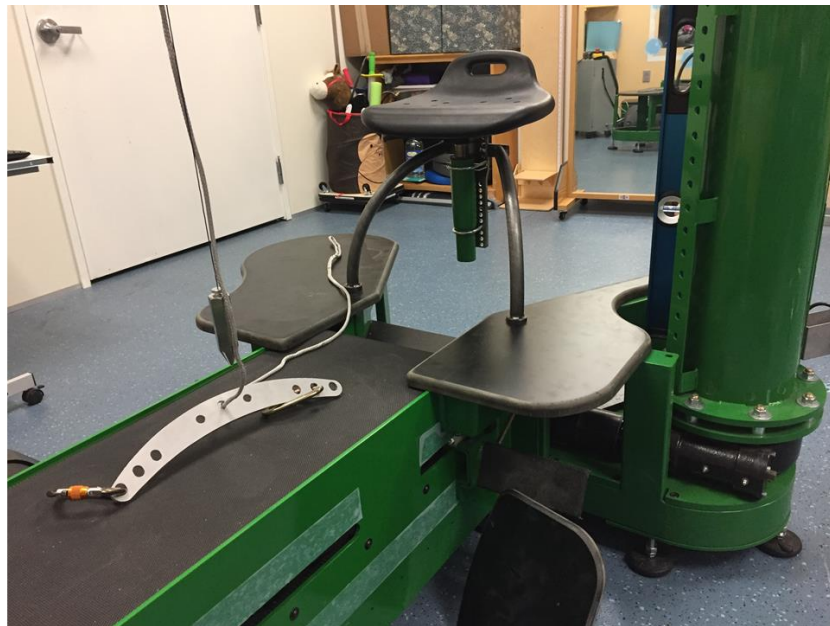


Figure 4.19: Trunk Trainer Seat Installation

#### 4.5.2 Trunk and Side Trainer Seating Static FEA Results and Weight Testing

Figure 4.20 shows the von Mises stress results from the 250 lbs. side seating cantilever arm static FEA simulation. The max stress that was seen was 14,010 psi found on the bottom side of the mounting bracket from the cantilever arm to the linear bearing attachment bracket significantly below the yield stress of carbon steel - 31,994.45 psi. Additionally, a stress concentration can be seen across the entire treadmill side panel face. This is as expected and designed as such helping to dissipate some of the stress across the entire panel face of the treadmill.

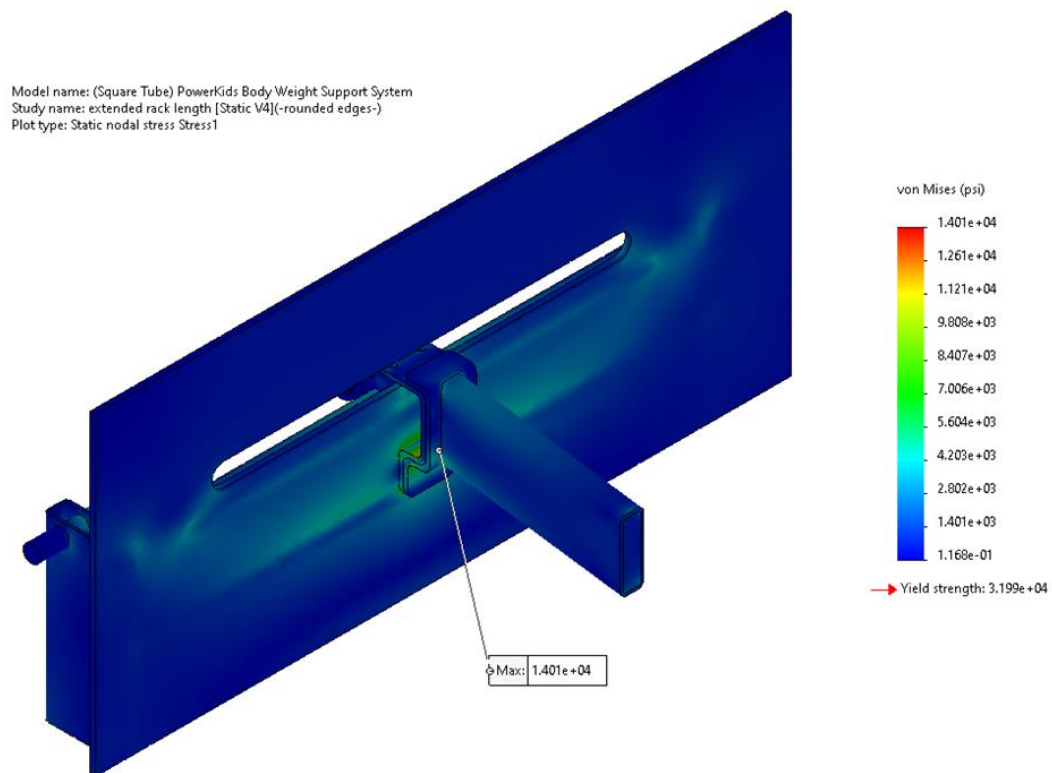


Figure 4.20: Side Seat Cantilever Arm and Treadmill Side Panel von Mises Stress Plot (psi) – Zero Deformation Scale



The left picture in Figure 4.21 shows a close-up view of the cantilever arm mounting bracket where the highest stress is seen. The right picture in Figure 4.21 shows the stress concentration of the linear bearing and rack system internally mounted within the treadmill. Stress was dissipated across the mounted rack helping to relieve stress on the actual linear bearing which should in turn increase longevity of the bearing and help with overall seat adjustability.

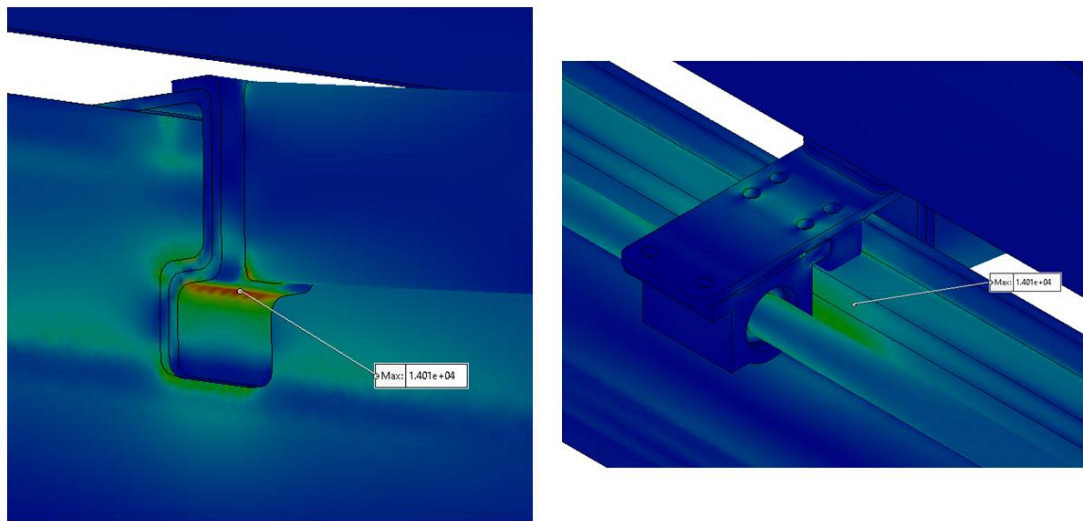


Figure 4.21: Close-up Side Seat Bracketry von Mises Stress Plot (psi) – Zero Deformation Scale

Figure 4.22 shows the displacement of the side seat cantilever arm from the 250 lbs. static FEA analysis. Note there is a deformation scaling factor of 50x applied on the plot to better depict how the side seat cantilever arm deforms. A max displacement of 0.03 in. is seen at the end of the cantilever arm. This is deformation is representative of what is expected and presents no issues of concern.

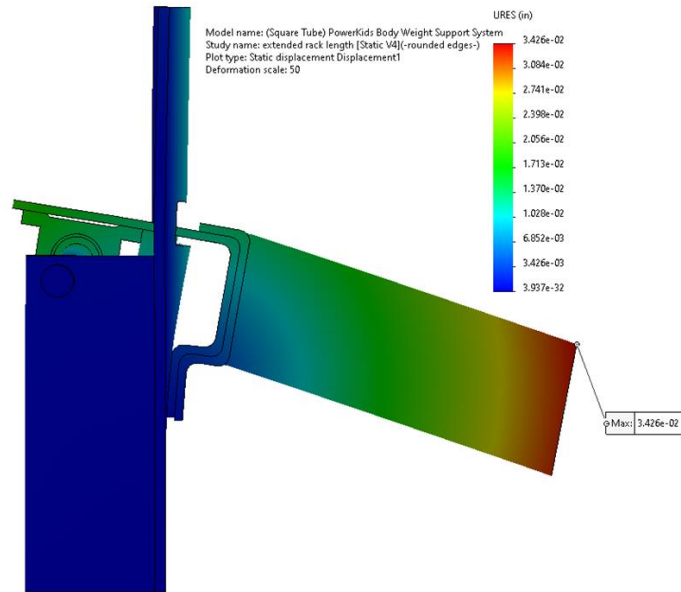


Figure 4.22: Profile View Side Seat Cantilever Arm Displacement Plot (in) – 50 Deformation Scale

Figure 4.23 shows the displacement of linear bearing and rack system from the 250 lbs. static FEA analysis. Note there is a deformation scaling factor of 50x applied to the plot to better depict how the linear bearing and side treadmill panel deforms. A displacement of 0.02 in. is observed around the linear bearing attachment bracket. This displacement is minimal but shows an outward bowing of the linear bearing system and treadmill side panel. The additionally rectangular crossbeams added during manufacturing of the treadmill (section 3.5.3) will elevate this outward bowing providing even less displacement and increasing longevity of the seating system.

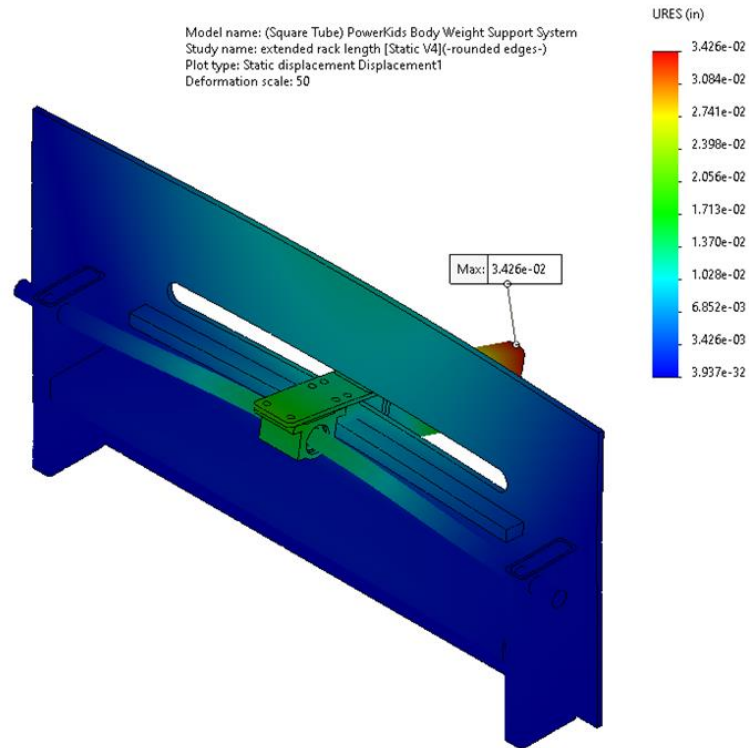


Figure 4.23: Side Seat Linear Bearing Displacement Plot (in) – 50 Deformation Scale

A factor of safety plot of the seating cantilever arm and linear bearing system showed an overall FOS of 1.9 with 250 lbs. applied. This exceeds the design criteria of the side seating arm being able to support 250 lbs. with a FOS of 1.5

Weight testing (195 lbs. volunteer + B + F) of the assembled right and left side seats for 10 minutes presented no failures, unusual deformation, or permanent deformation.

Figure 4.24 shows the von Mises stress results from the 250 lbs. trunk trainer seat static FEA simulation. The max stress that was seen was 12,960 psi found on the welded gas cylinder connection to the round tubing frame significantly below the yield stress of carbon steel - 31,994.45 psi. A higher stress concentration can be seen across the round tubing frame closer to the attachment points to the back deck.



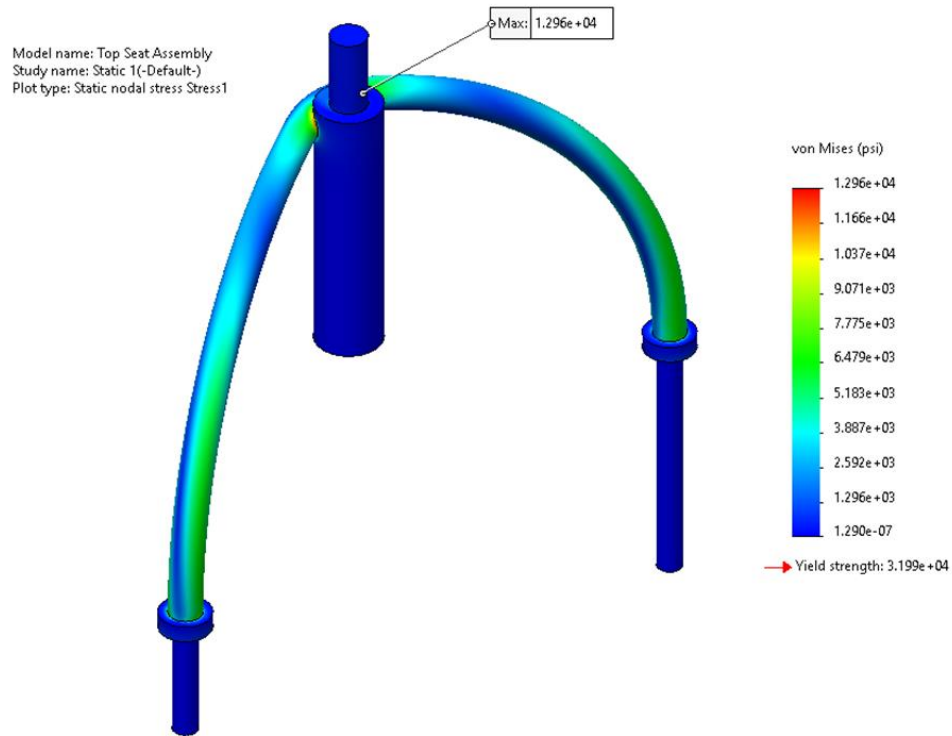


Figure 4.24: Trunk Trainer Seat von Mises Stress Plot (psi) – Zero Deformation Scale

Figure 4.25 shows the displacement of the trunk trainer seat from the 250 lbs. static FEA analysis. Note there is a deformation scaling factor of 50x applied to the plot to better depict how the trunk trainer seat deforms. A max displacement of 0.04 in. in a slightly horizontal direction is seen at the top side of the gas cylinder. This displacement is minimal, however, to increase durability of the trunk trainer seat a plate was added to the back of the gas cylinder as seen in Figure 4.19 reducing this displacement.

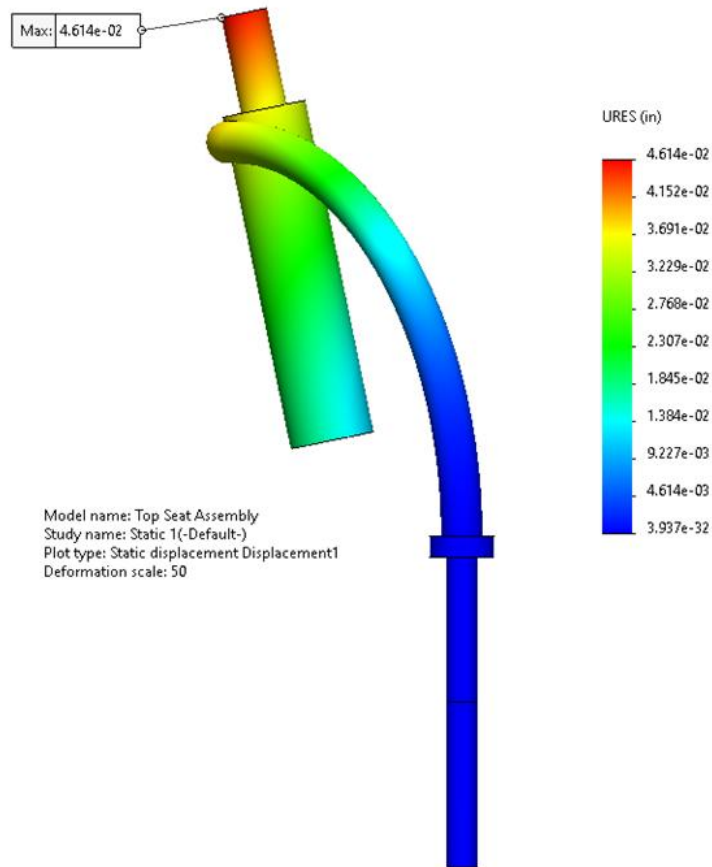


Figure 4.25: Trunk Trainer Displacement Plot (in) – 50 Deformation Scale

A factor of safety plot of the trunk trainer seat showed an overall FOS of 2.3 with 250 lbs. applied. This exceeds the design criteria of the trunk trainer seat being able to support 250 lbs. with a FOS of 1.5

Weight testing (195 lbs. volunteer + B + F) of the assembled trunk trainer seat for 10 minutes presented no failures, unusual deformation, or permanent deformation.

#### 4.5.3 Trainer Feedback on Seating/Footrests and Subsequent Iterations

Initial trainer feedback of the first iteration side seating design seen in Figure 4.18 presented a need to lower the seating so the top face of the base seating was sitting below the top surface of treadmill belt. The side seat cantilever arm design was updated to Revision 2 as shown in the left

picture in Figure 4.26. Revision 2 included an added 0.25 in. sheet metal plate with 0.3125 in. mounting holes allowing for lowering of the gas cylinder. A 0.25 sheet metal gusset was added to increase strength. The updated design allowed the top face of the base seat to sit 3 in. below the treadmill belt.



Figure 4.26: Rev. 2 Cantilever Side Seating Arm (Left) and Installed Rev. 2 Side Seating (Right)

When reviewing the Revision 2 side seating (right picture in Figure 4.26) with trainers, the seating vertical position received much more positive reviews, however, another issue was presented not previously seen during the early stages of design criteria development. During LT, trainers often rotate positions i.e., moving from the right-side seat to the left side or vice versa. This presents a need to be able to quickly adjust seating position while the trainer is still seating and supporting the patient's legs with at least one hand. Revision 2 seat design made this difficult because to adjust the seat fore/aft the trainer had to remove their body weight from the seat, lift to disengage the rack, and slide the seat to position. This was expressed as very cumbersome and not ideal.

Based on this feedback a Revision 3 side seat design was created as seen in Figure 4.27. The design intent was to use the existing linear bearing plus an external linear sliding sleeve that would eliminate the grooved rack and the need to lift the seat up to disengage before adjustment.

The design incorporated a steel plate with slots externally mounted to the treadmill side panel. The slots would be locking adjustment points for a plunger labeled in Figure 4.27. The trainer would simply pull the plunger to release the seat, use their feet to push or pull the seat into position and release the plunger to lock in place. This could be done with one hand while keeping another hand safely on the patient's legs as described during the train feedback session previously mentioned.

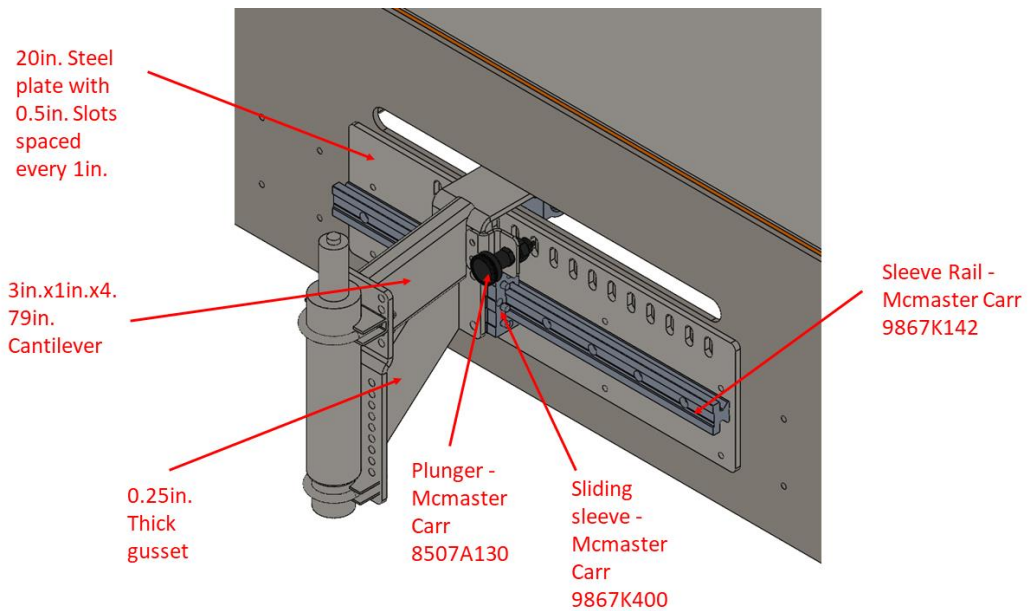


Figure 4.27: Updated Rev. 3 Side Seat Design

Trainer feedback from the assembled rev. 3 side seating design seen in Figure 4.28 showed an improvement in seat functionality but still presented some issues. Trainers felt the seating adjustment was still slightly cumbersome and the combination of the sliding sleeve and linear bearing system at times was not as smooth as anticipated. It was determined further iterations would be needed which is discussed in the future work section 5.1.



Figure 4.28: Rev. 3 Cantilever Side Seating Arm (Left) and Installed Rev. 3 Side Seating (Right)

Regarding the Revision 1 footrest design seen in the left picture in Figure 4.29, trainer feedback presented a couple of issues. It was determined that the footrest was too close to the seating system and often the trainer would simply rest their feet on the back bypassing the footrest. Additionally, the footrest linear bearing adjustability feature was not really utilized and needed during fitment testing. With this feedback, a much simpler rev. 2 footrest was designed as shown in the right picture in Figure 4.29. The design was a bent 0.25 in. thick sheet metal component with a 11.75 in x 8 in. footrest surface. It was mounted directly to the treadmill side panel using 0.25 in. mounting holes. Trainer feedback on the Revision 2 design was positive and determined no further iteration was needed.





Figure 4.29: Rev. 1 Footrest Installed (Left) and Rev. 2 Footrest Installed (Right)

## 4.6 Stabilizing Decks

### 4.6.1 Front/Rear Deck Dimensional Verification and Visual Analysis Results

The modularity aspect of the front deck can easily be observed in the left picture in Figure 4.30. This component was installed around the motor housing with no interferences. The deck was determined to be level and dimensional verification of the deck length showed it was 52 in.



Figure 4.30: Modular Front Deck Install (Left) and Installed Front Deck (Right)

surpassing the design requirement as seen in APPENDIX V: Front/Rear Decks Design Criteria and Verification Results.

The back deck was bolt to the rear treadmill flanges as seen in the left picture of Figure 4.31. The deck was determined to be level and dimensional verification of the deck length showed it was 52 in. surpassing the design requirement. The right picture in Figure 4.31 shows the installed 0.5-inch slew ring mounting plate satisfying the design requirement for a study crane mounting location. Dimensional verification along with slew ring test fitment showed the mounting holes were properly spaced and the required 0.5 in. diameter.



Figure 4.31: Modular Back Deck Install (Left) and Back Deck Leveling Feet with Crane Plate (Right)

Upon installation of the back deck TRESPA top surface and stairs as discussed in section 4.6.2, dimensional verification of the stair height at 6 in. satisfied the initial design requirement.



Figure 4.32: Installed Front and Back Decks

All further dimensional verification and visual inspection results can be seen in APPENDIX V: Front/Rear Decks Design Criteria and Verification Results

#### **4.6.2 Front/Rear Deck TRESPA Install and Weight Testing Results**

The left picture in Figure 4.33 shows the ball socket TRESPA attachments. The TRESPA plates were removed and “snapped in” three times to confirm functionality with no issues. The right picture in Figure 4.33 shows the complete TRESPA install with no instability seen satisfying the requirement for the front and back decks to have stable rigid top surfaces.



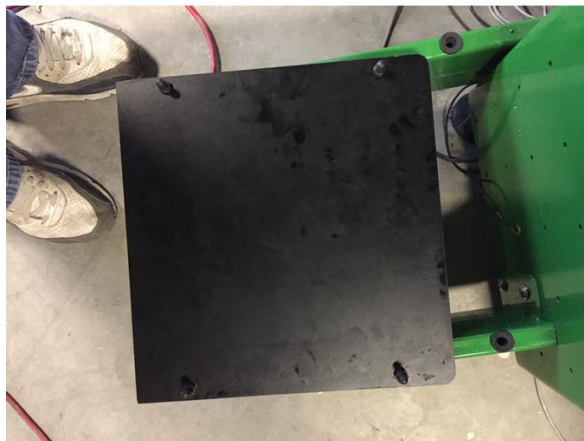


Figure 4.33: TRESPA Ball Sockets (Left) and Rear Deck TRESPA Installed Showing Patient Stairs (Right)

Figure 4.34 shows the weight testing of the back deck patient stairs. No failures or deformation was seen therefore passing the design criteria of the patient stairs will be able to



Figure 4.34: Rear Deck Patient Stairs Weight Testing

support up to 300 lbs. to ensure a patient or trainer can safely stand in place. The same weight was used to test both the right and left front deck platforms and no failures or deformation was observed.

## 4.7 Crane

### 4.7.1 Crane Dimensional Verification and Slew Ring Functionality Testing

The left picture in Figure 4.35 shows the fully assembled two-piece crane received from Winston Industries, Inc. The right picture in Figure 4.35 shows the BWS bracketry including three pulley mounts and the cylinder box support. A fitment check ensured the components allowed for complete mounting of the BWS components with no interference. Dimensional verification of the entire BWST height showed the system height was 8.67 ft. meeting the design requirement of less than 9 ft. Additionally, the crane passed all dimensional verification, functionality testing, and visual inspection as seen in APPENDIX VI: Crane Design Criteria and Verification Results.



Figure 4.35: Fully Assembled Crane (Left) and BWS Support Brackets and Pulley Brackets (Right)

Figure 4.36 shows the successful attachment point of the crane to the slew ring and subsequent rear deck. With the attachment of the slew ring power supply, the crane was rotated to the neutral position or the position over top the treadmill during a patient training session. Measurement from the plumb bob to the motor housing was 19.38 in. and the measurement from the edge of the treadmill belt to the plumb bob was 6.88 in. This position was determined to be the correct central position over the treadmill thus showing the crane meets the design criteria. Further slew ring functionality testing showed the crane successfully rotated the 150 degrees needed to reach a patient from their wheelchair on the rear side of the BWST. As well, this rotation took 23 seconds which equates to 6.5 degrees per second satisfying the design criteria of less than 20 degrees/s.



Figure 4.36: Slew Ring and Crane Attachment Point to Rear Deck

#### **4.7.2 Gusset vs. Non-gusset Static FEA results**

Figure 4.37 shows the von Mises stress results from the 120 lbs. gusset crane design static FEA simulation. The max stress that was seen was 9,786 psi found on the bolt hole located on the

crane mounting plate directly below the cantilever lever boom. This stress is significantly below the yield stress of carbon steel - 31,994.45 psi. Additionally, a neutral stress line can be seen located on two side of the bottom mast and up to the gusset attachment point on the top mast.

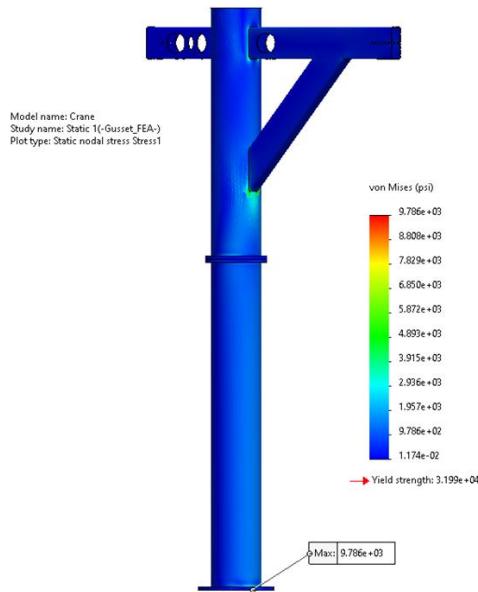


Figure 4.37: Gusset Crane Static FEA von Mises Stress Plot (psi) – Zero Deformation Scale

Figure 4.38 shows a close-up view of the top mast, crane boom, and the gusset steel tube. A stress concentration can be seen at the attachment of the gusset to the top mast with a von Mises stress hovering around 4,893 psi. Additionally, a slight stress concentration can be seen around the front and back attachment points of the cantilever crane boom. However, the added gusset did seem to almost dissipate any stress completely along the front cantilever crane boom.

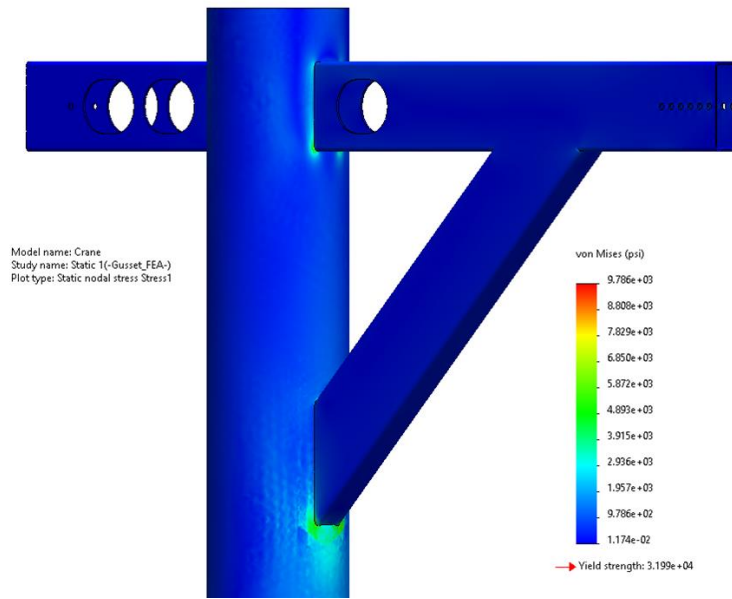


Figure 4.38: Gusset Crane Close-up von Mises Stress Plot (psi) – Zero Deformation Scale

Figure 4.39 shows the displacement of the gusset crane design 120 lbs. static FEA analysis. Note there is a deformation scaling factor of 50 set on the plot to better depict how the gusset crane deforms. A displacement of 0.06 in. is seen at the very end of the cantilever crane boom. This displacement is minimal and shows the proper frontal leaning from the load applied vertically down as expected from the design.

A factor of safety plot of the gusset crane design showed an overall FOS of 2.5 with 120 lbs. applied. This exceeds the design criteria of the crane being able to support 120 lbs. with a FOS of 1.5.

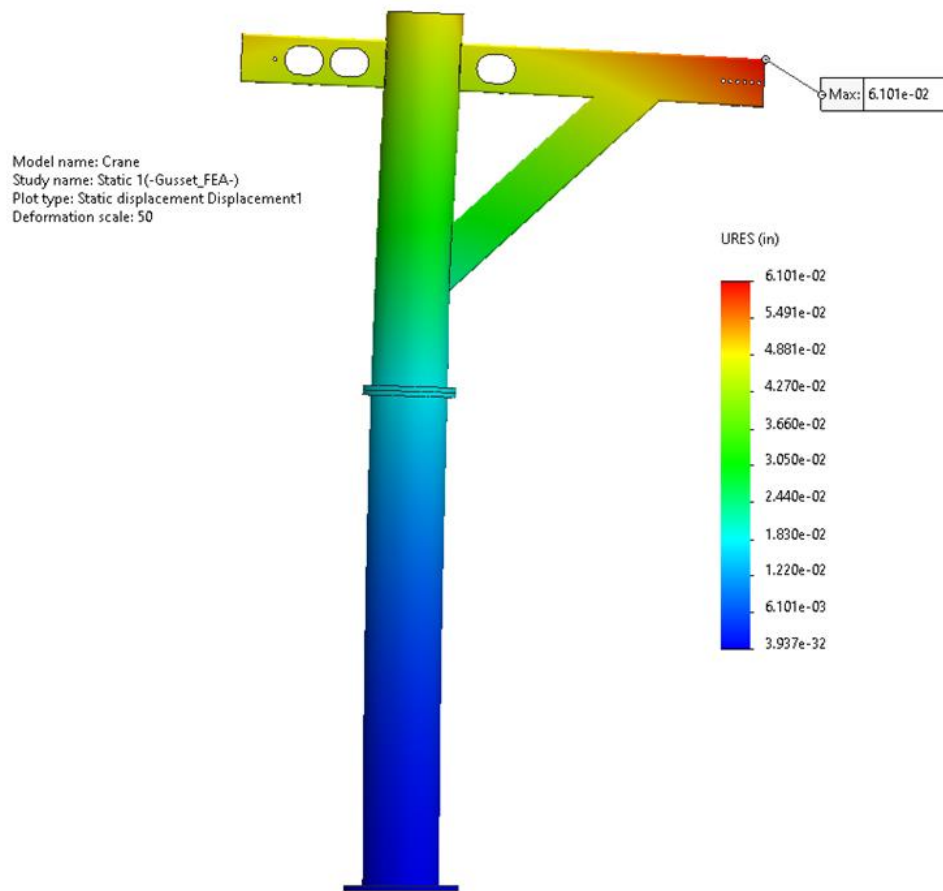


Figure 4.39: Gusset Crane Static FEA Displacement Plot (in) – 50 Deformation Scale

Figure 4.40 shows the von Mises stress results from the 120 lbs. non-gusset crane design static FEA simulation. The max stress that was seen was 9,502 psi less than the max stress of the gusset crane design seen in Figure 4.37 and found in the same location directly below the cantilever lever boom on the crane mounting plate bolt hole. This stress is significantly below the yield stress of carbon steel - 31,994.45 psi. A neutral stress line can be seen located on two sides of both the bottom and top mast. Without the gusset applying pressure to the top mast, a more even stress concentration can be seen throughout the non-gusset stress plot.

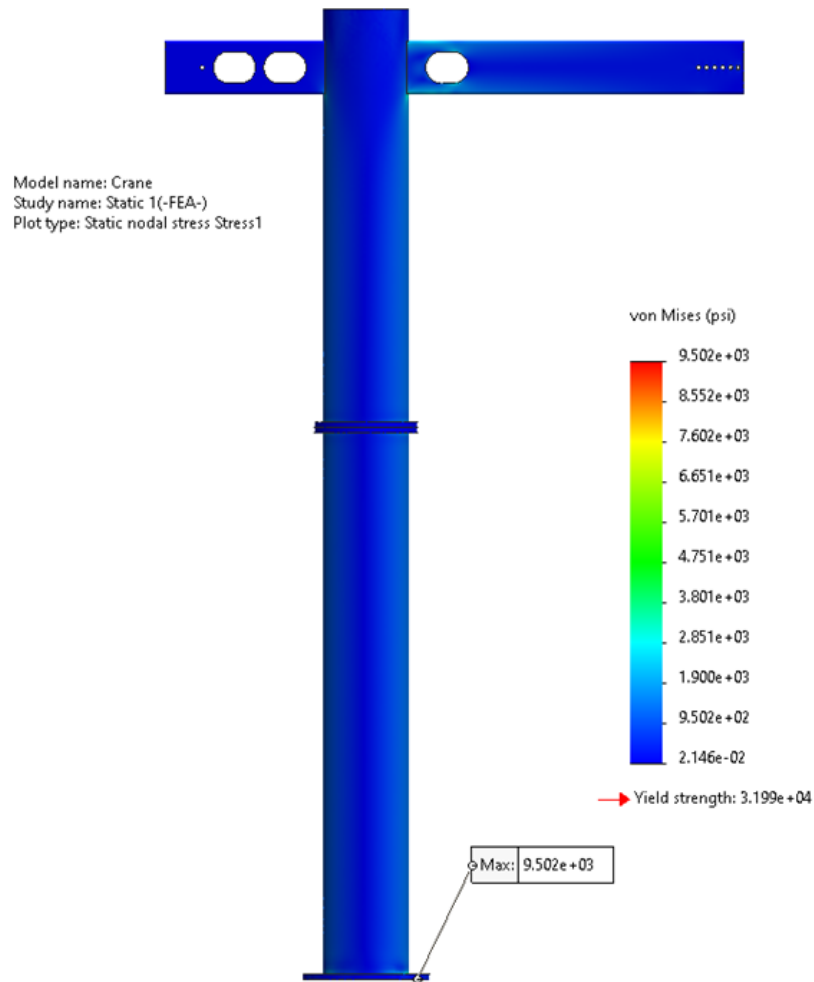


Figure 4.40: Non-gusset Crane Static FEA von Mises Stress Plot (psi) – Zero Deformation Scale

Figure 4.41 shows a close-up view of the top mast can cantilever crane boom. A stress concentration can be seen at the attachment of the boom to the top mast and along the top/bottom 1 in. side of the boom rectangular tubing near the top mast connection point - von Mises stress hovering around 5,701 psi. Furthermore, stress of the rectangular steel crane boom transitions from minimal at the boom end to around 2,852 psi. around the top mast connection point. With the removal of the gusset, it can be seen there is added stress on cantilever crane boom.



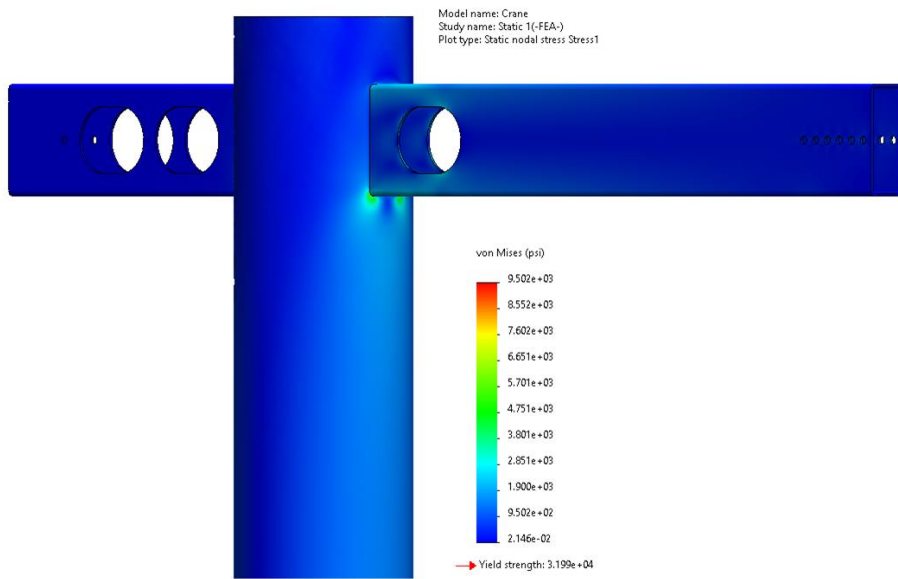


Figure 4.41: Non-gusset Crane Close-up von Mises Stress Plot (psi) – Zero Deformation Scale

Figure 4.42 shows the displacement of the non-gusset crane design 120 lbs. static FEA analysis. Note there is a deformation scaling factor of 50x applied to the plot to better depict how the gusset crane deforms. A displacement of 0.07 in. is seen at the very end of the cantilever crane boom. This displacement is still minimal but slightly larger than seen with the gusset crane design. As seen in the gusset FEA displacement plot, the non-gusset has a very similar frontal leaning from the load applied vertically down as expected from the design.

A factor of safety plot of the non-gusset crane design showed an overall FOS of 3.4 with 120 lbs. applied. This significantly exceeds the design criteria of the crane being able to support 120 lbs. with a FOS of 1.5. With the higher FOS, negligible stress and displacement differences, and additional ease of manufacturing, it was determined the non-gusset crane design will be integrated in the complete BWST design.



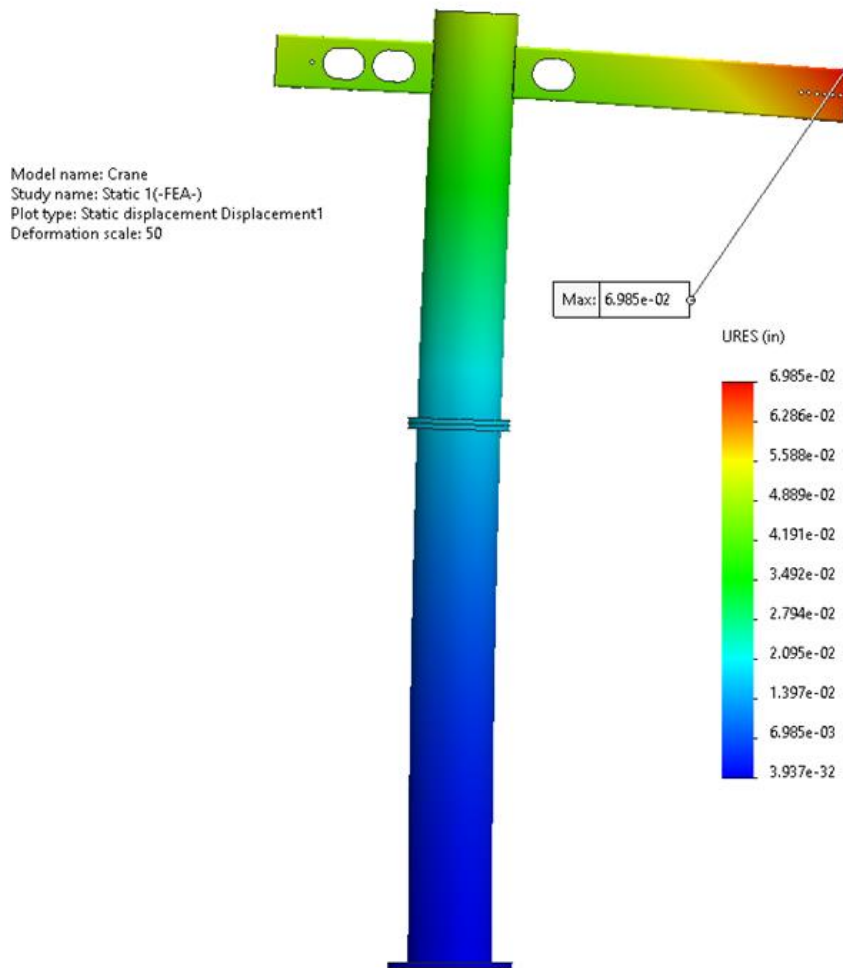


Figure 4.42: Non-gusset Crane Static FEA Displacement Plot (in) – 50 Deformation Scale

### 4.7.3 Non-gusset Modal Frequency Analysis and Linear Dynamic FEA Results

As described in section 3.8.2, a modal frequency analysis was performed on the non-gusset crane design to ensure the frequency of a child walking on the system would not be resonant with the natural mechanical frequency of the system. The two lowest natural frequencies found are Mode 1 - 19.57 Hz and Mode 2 - 19.89 Hz shown in Figure 4.43. The second mode shape is very similar to similar the frontal leaning deformation that will be shown during application of the

load. However, the 2.5 Hz cyclic stepping load is well below the frequency of Mode 2 (approximately 1/10) showing a dangerous mechanical resonance will not occur.

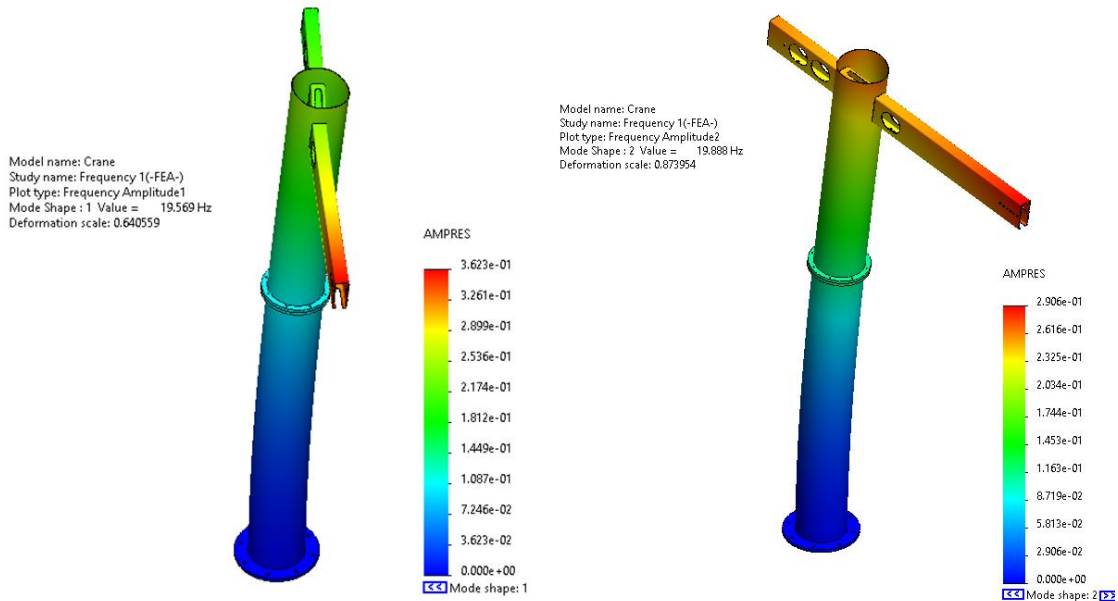


Figure 4.43: Non-gusset Crane Mode Shape 1 (19.57Hz)(Left) and Mode Shape 2 (19.89Hz)(Right)

Even though mechanical resonance is unlikely, a modal time history linear dynamic FEA was completed to better characterize the non-gusset crane design. Von Mises stress results graph as a function of time of is included in APPENDIX IX: Crane Modal Time History von Mises Stress Graphs. All von Mises stress graphs show a consistent stress curve comparative to the input data seen in Figure 3.59. Additionally, all graphs showed an impulse stress response from the initial ramp of load on the system during the first second of the simulation. This quickly dissipates to resemble the stepping force curve from the input data. The cantilever end (Node 13108) experienced von Mises stress around 1 psi, cantilever mast joint (Node 111750) experienced von Mises stress around 600 psi, crane mast joining flange plate (Node 95003) experienced von Mises stress around 15 psi, and crane mounting plate (Node 103353) experienced von Mises stress around 1,100 psi.

#### 4.7.4 Crane Weight Testing and Subsequent Electric Cylinder Support Box Redesign

Weight testing of the assembled BWST crane can be seen in Figure 4.44. During weight testing of the crane, a failure assumed to be related to insufficient welding was observed and is shown in Figure 4.45. The cylinder box support failed causing the electric cylinder to detach from the crane. Upon inspection, it was very clear the quality of the welded box joints was not sufficient. It appeared only the outer surface of the box edges was welded, and no weld beads could be seen internally.



Figure 4.44: Assembled Crane Weight Testing



Figure 4.45: Rev. 1 Cylinder Support Box Bracket Failure

Due to the box support failure during testing, a Revision 2 design was created. A 0.12 in. thick 4.5 in. x 2.25 in. weight distribution support piece was added at the box attachment to the crane as seen in the left picture in Figure 4.46. This was designed to help transfer some of the load over a larger surface area. In addition, weld joints will be pinpointed and described to the manufacturer to ensure quality welds are achieved internally and externally.

A static FEA was performed using the updated Revision 2 design attached to the crane mounting bar. The load was applied to the electrical cylinder attachment point represented by the purple arrows in the left picture of Figure 4.46. The load applied was 240 lbs. which is twice the max patient weight of 120 lbs. because of the pulley system configuration explained in section 873.9.1. The fixture points of the model are represented by the green arrows in the left picture of Figure 4.46. Mesh density of the analysis is shown in the right panel

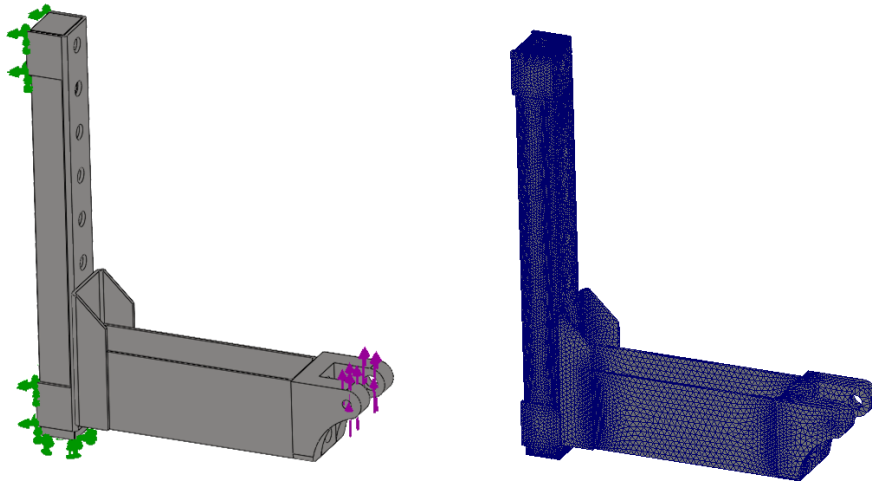


Figure 4.46: Rev. 2 Static FEA Fixture Points and Force Location (Left) and Mesh Density (Right)

After running the static FEA simulation, stress, displacement, and FOS plots were created. Figure 4.47 shows the von Mises stress plot of the Revision 2-cylinder box bracket design. A max stress of 16,180 psi. can be seen around the connection of the cylinder box support to the mounting bar attached to the crane. The FOS of the updated design was determined to be 2 and had an overall max displacement on cylinder attachment end of the box of 0.01 in. Based on the static FEA results, it was determined this design was sufficient to proceed to fabrication of a testable prototype.

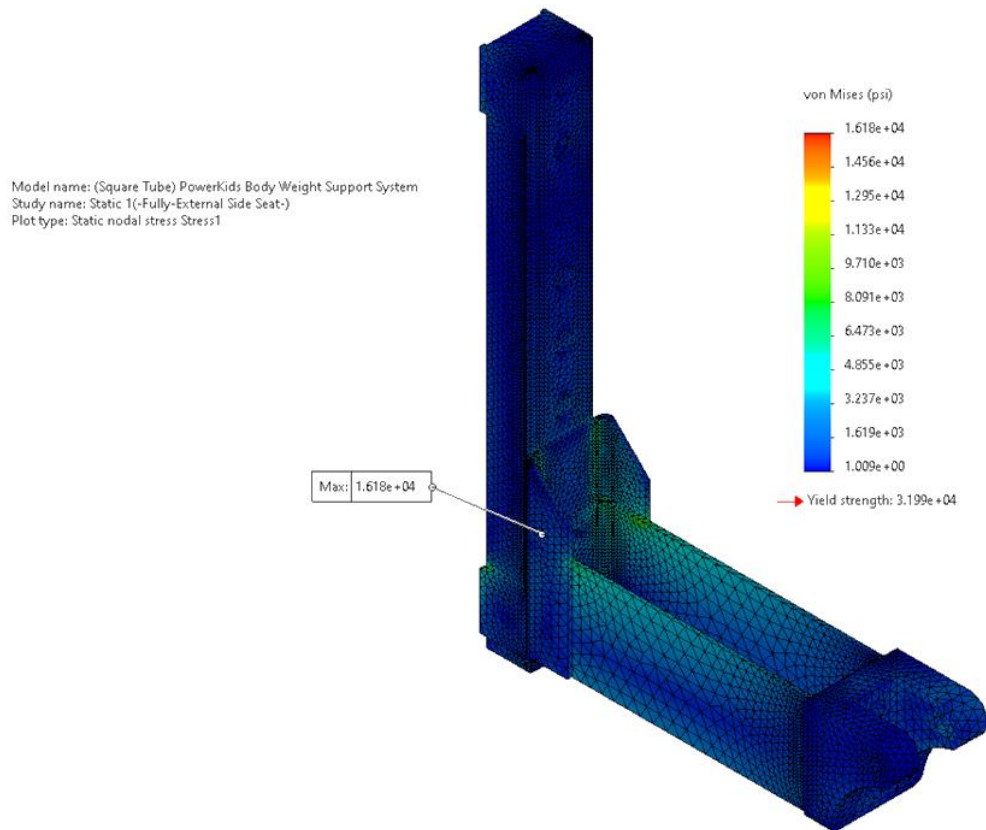


Figure 4.47: Rev. 2 Cylinder Support Box von Mises Stress Plot (psi) – Zero Deformation Scale

The Revision 2 design was manufactured at Winston Industries, Inc. Certain weld points were chosen and communicated to the manufacturer to ensure a strong durable part was created as designed. The final installed support box is shown in Figure 4.48. Weight re-testing using the same 325.24 lbs. (small chain + large chain + yoke and carabiner + parts F, G, H, I, J, K, L) and setup for 10 minutes seen in Figure 4.44 showed no system instability, deformation, or mechanical failure.



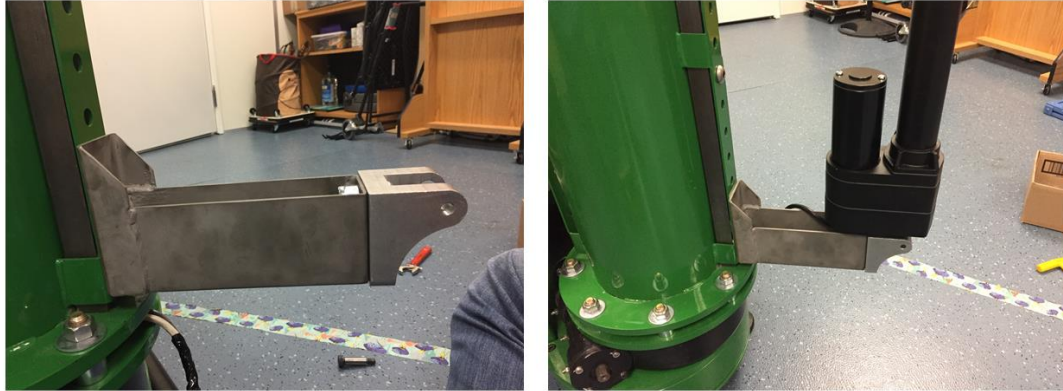


Figure 4.48: Installed Rev. 2 Cylinder Support Box Bracket

## **4.8 Body Weight Support and Control System**

### **4.8.1 BWS Dimensional Verification**

Figure 4.49 shows the completed BWST control system and installed BWS on the non-gusset crane – load cell, pneumatic small cylinder, and the large electric actuator. The BWS passed all dimensional verification, visual inspection, and functionality testing seen in APPENDIX VII: BWS/Control System Design Criteria and Verification Results.



Figure 4.49: Installed Complete BWS, Control System, and Computer

Dimensional verification was performed to ensure the system could accommodate patient height ranges from 1' 8" to 5' 6" and is shown in Figure 4.50. The high point measured directly under the center of the yoke measured 67.5 in. and the low point measured 20 in. thus meeting the design requirement. Additionally, the lowest point for patient pickup was measured at 37 in. to the floor seen in Figure 4.51.





Figure 4.50: Yoke Height Dimensional Verification – High Point (Left) and Low Point (Right)



Figure 4.51: Yoke Height Low Point Dimensional Verification in Patient Pickup Location

## 4.8.2 BWS Functionality Testing

The digital multimeter reading of the 24V power supply and the 12V power supply were 23.9V and 11.6V, respectively, and both within tolerance and ensuring proper power to the system. The completed pneumatic and electrical control system is shown in Figure 4.52 and the electrical schematic is shown in APPENDIX XII: BWST Control System Schematic.



Figure 4.52: Completed BWST Pneumatic and Electrical Control System

Functionality testing of the emergency stop button showed that with the engagement of the stop button, the treadmill stopped instantly and the BWS actuators locked correctly. Additionally,

the crane slew ring motor was still active and able to rotate the complete 90 degrees as stated in the testing procedure. This will allow for safe removal of the patient from the system if needed. Once the stop button was engaged reactivation of the BWS software was not possible until the emergency button was disengaged meeting all design requirements.

Figure 4.53 show the completed slew ring control circuit with H-bridge adapter and microcontroller attached.

Whisker switch and centering proximity switch functionality was tested and performed as designed. Figure 4.54 shows the whisker switch (uninstalled) on the left and the installed proximity sensor switch on the right.

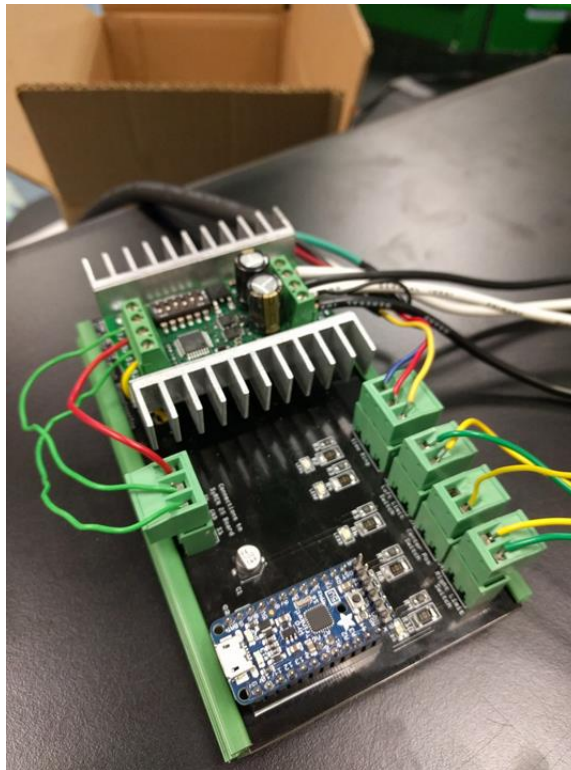


Figure 4.53: Slew Ring Control Circuit Board



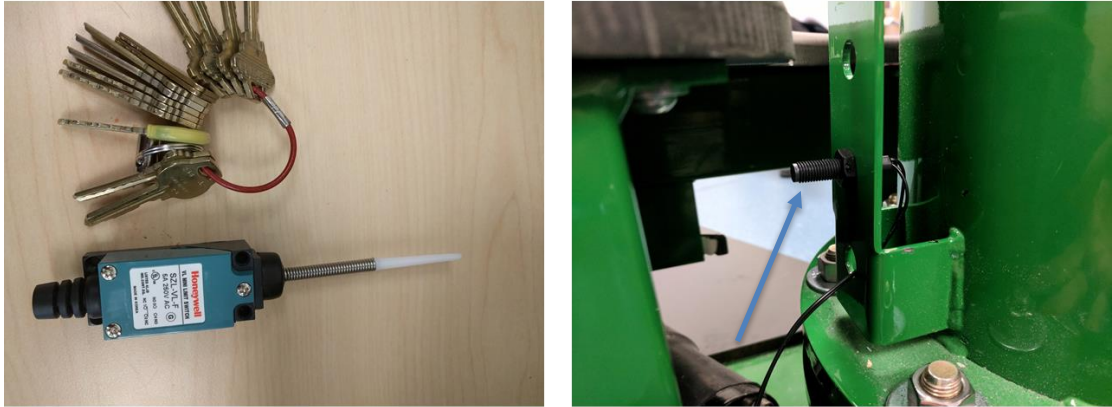


Figure 4.54: Whisker Limit Switch (Left) and positioning Switch (Right)

### 4.8.3 Load Cell Installation and Verification Testing

Figure 4.55 (left panel) shows the fully assembled load cell attached to the back of the crane boom. A successful calibration of the load cell was completed of the load cell as described in section 3.9.3. The freely hanging pneumatic small cylinder can be seen in the right picture in Figure 4.55.



Figure 4.55: Installed Load Cell (Left) and Pneumatic Small cylinder (Right)

Incremental weight testing of the load cell produced the graph shown in Figure 4.56 which plots the actual weight applied to the load cell compared to the BWS software load reading. The graph shows a linear trend which confirms the calibration of the load cell and the ability for the system to properly read the force across the desired patient range (up to 120lbs.). The average standard deviation of the load cell reading compared to the actual weight applied was 0.98 lbs. which was determined to be negligible.

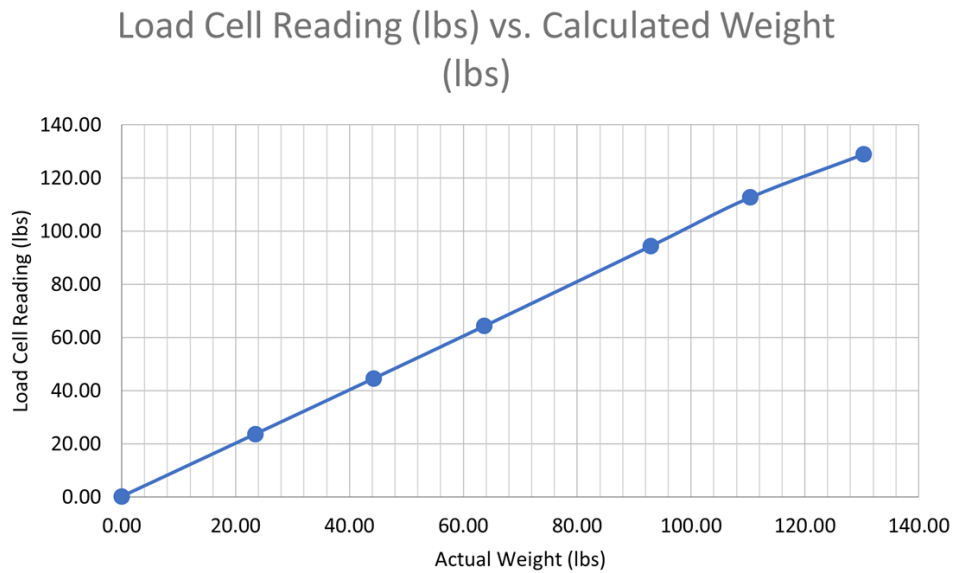


Figure 4.56: Load Cell Linearity and Verification Test Results

## **V. CONCLUSION & FUTURE WORK**

### **5.1 Considerations for Further Development and Validation**

One of the main limitations to this study was a lack of fatigue testing or durability testing over time. Static safety testing indicated a safe and robust system, but additional computer simulated fatigue testing and observation over time would provide additional information for system improvements regarding increasing durability over time and reducing overall needed system maintenance.

As described in section 4.5.3, the trainer side leg seating movement and functionality was still considered not as optimal during trainer seat rotations for the duration of a LT session. Another design iteration has been proposed to use electric actuators and a foot switch to move the seats fore and aft allowing for full hands-free control.

To reduce overall slew ring control complexity and cost, the next iteration slew ring should include a hall effect sensor within the motor. This will allow for precise slew ring control integrated into the BWS software without the need for any control hardware (center position, limit switches).

The BWST reported in this thesis has been verified for patient safety and overall functionality, however, the BWS system and computer software has yet to be completely validated for the pediatric population. In addition, this is a beta prototype and further improvements and iteration based on any feedback from patient validation testing will lead to the final product.

### **5.2 Conclusion**

The designed pediatric BWST is consistent with an emerging paradigm shift in rehabilitation from compensation to recovery-based strategies. This study showed the development, fabrication,

and successful verification testing of a pediatric BWST based current user and pediatric patient needs. This analysis led to an updated design which allows for proper BWS for locomotor training within the pediatric population via proper patient body mechanics via the optimized system structure and treadmill, the rotating crane to hoist the patient from their wheelchair, and appropriate trainer seating/positioning via the ergonomically designed seating structure.

Design computer simulation and mechanical weight testing showed the system can easily support the desired patients ranges with factor of safeties above the design criteria. Pre patient system functionality testing showed the BWS was safe for patient use and met all control system design criteria. Future patient validation testing will help further validate the BWS for use with pediatric patients. The trainer feedback and dimensional evaluation showed improved body mechanics and future iterations should further improve the trainer seating for use during rigorous LT sessions.

The symmetric modular design allowed for the system structure to contain fewer subcomponents thus allowing easy assembly/disassembly and transportation/shipping of the system the clinic. With the DFM and state-of-the art manufacturing techniques considered, a significant system cost reduction was possible making it more affordable for clinics to purchase and implement locomotor training for the pediatric population. The designed pediatric BWST can be easily transferred to manufacturing for commercialization efforts to take place.

## VI. REFERENCES

- Argetsinger, L. C., Singh, G., Bickel, S. G., Calvery, M. L., & Behrman, A. L. (2020). Spinal cord injury in infancy: activity-based therapy impact on health, function, and quality of life in chronic injury. *Spinal Cord Ser Cases*, 6(1), 13. <https://doi.org/10.1038/s41394-020-0261-1>
- Behrman, A. L., Bowden, M. G., & Nair, P. M. (2006). Neuroplasticity after spinal cord injury and training: an emerging paradigm shift in rehabilitation and walking recovery. *Phys Ther*, 86(10), 1406-1425. <https://doi.org/10.2522/ptj.20050212>
- Behrman, A. L., Nair, P. M., Bowden, M. G., Dauser, R. C., Herget, B. R., Martin, J. B., Phadke, C. P., Reier, P. J., Senesac, C. R., Thompson, F. J., & Howland, D. R. (2008). Locomotor training restores walking in a nonambulatory child with chronic, severe, incomplete cervical spinal cord injury. *Phys Ther*, 88(5), 580-590. <https://doi.org/10.2522/ptj.20070315>
- Cook, R. D., Malkus, D. S., Plesha, M. E., & Witt, R. J. (2002). *Concepts and Applications of Finite Element Analysis*. John Wiley & Sons, Inc.
- Foundation, C. a. D. R. (2006). *One Degree of Separation: Paralysis and Spinal Cord Injury in the United States*.
- Fox, E. J., Tester, N. J., Kautz, S. A., Howland, D. R., Clark, D. J., Garvan, C., & Behrman, A. L. (2013). Modular control of varied locomotor tasks in children with incomplete spinal cord injuries. *J Neurophysiol*, 110(6), 1415-1425. <https://doi.org/10.1152/jn.00676.2012>
- Fryar, C. D., Kruszon-Moran, D., Gu, Q., & Ogden, C. L. (2018). Mean Body Weight, Height, Waist Circumference, and Body Mass Index Among Adults: United States, 1999-2000 Through 2015-2016. *Natl Health Stat Report*(122), 1-16.
- Gordon, K., Svendsen, B., Harkema, S. J., & El-Alami, S. (2008). Closed-Loop Force Controlled Body Weight Support System 7381163).
- Harkema, S. J., Behrman, A. L., & Barbeau, H. (2011). *Locomotor Training: Principles and Practice*. Oxford University Press.
- Harkema, S. J., Hurley, S. L., Patel, U. K., Requejo, P. S., Dobkin, B. H., & Edgerton, V. R. (1997). Human lumbosacral spinal cord interprets loading during stepping. *J Neurophysiol*, 77(2), 797-811. <https://doi.org/10.1152/jn.1997.77.2.797>
- Harkema, S. J., Schmidt-Read, M., Lorenz, D. J., Edgerton, V. R., & Behrman, A. L. (2012). Balance and ambulation improvements in individuals with chronic incomplete spinal cord injury using locomotor training-based rehabilitation. *Arch Phys Med Rehabil*, 93(9), 1508-1517. <https://doi.org/10.1016/j.apmr.2011.01.024>



- Howland, D., Trimble, S. A., & Behrman, A. (2014). Neurological Recovery and Restorative Rehabilitation. In H. M. Hart (Ed.), *Spinal Cord Injury in the Child and Young Adult* (pp. 399-410). Mac Keith Press.
- Howland, D. R., Fox, E. J., Tester, N. J., Trimble, S., Senesac, C., Spierre, L., Johns, J., Kleim, J., Reier, P. J., & Behrman, A. L. (2010, 14 November). Responses to locomotor training and identification of functional long tracts in children with severe, chronic spinal cord injury Society for Neuroscience, 40th Annual Meeting, San Diego, CA.
- Howland, D. R., Fox, E. J., Trimble, S., Tester, N. J., Suter, S. P., Spiess, M., & Behrman, A. L. (2011, 13 November). Robust walking response to locomotor training despite disparate SCI etiologies, ages, and chronicity in pediatrics Society for Neuroscience, 41st Annual Meeting, Washington, DC.
- Kreutz, D. (2000). Standing Frames and Standing Wheelchairs: Implications for Standing. *Topics in Spinal Cord Injury Rehabilitation*, 5(4), 24-28. <https://doi.org/10.1310/p8yc-wgeh-clvp-2vc1>
- MacKay-Lyons, M. (2002). Central pattern generation of locomotion: a review of the evidence. *Phys Ther*, 82(1), 69-83. <https://doi.org/10.1093/ptj/82.1.69>
- Maria, R. (2016). Summary of Safety Criteria in Design. <https://doi.org/10.13140/RG.2.1.1501.5285>
- McKinley, W., Santos, K., Meade, M., & Brooke, K. (2007). Incidence and outcomes of spinal cord injury clinical syndromes. *J Spinal Cord Med*, 30(3), 215-224. <https://doi.org/10.1080/10790268.2007.11753929>
- Mothe, A. J., & Tator, C. H. (2012). Advances in stem cell therapy for spinal cord injury. *J Clin Invest*, 122(11), 3824-3834. <https://doi.org/10.1172/jci64124>
- Rowland, J. W., Hawryluk, G. W., Kwon, B., & Fehlings, M. G. (2008). Current status of acute spinal cord injury pathophysiology and emerging therapies: promise on the horizon. *Neurosurg Focus*, 25(5), E2. <https://doi.org/10.3171/foc.2008.25.11.E2>
- Roy, R. R., Harkema, S. J., & Edgerton, V. R. (2012). Basic concepts of activity-based interventions for improved recovery of motor function after spinal cord injury. *Arch Phys Med Rehabil*, 93(9), 1487-1497. <https://doi.org/10.1016/j.apmr.2012.04.034>
- Schottler, J., Vogel, L. C., & Sturm, P. (2012). Spinal cord injuries in young children: a review of children injured at 5 years of age and younger. *Dev Med Child Neurol*, 54(12), 1138-1143. <https://doi.org/10.1111/j.1469-8749.2012.04411.x>
- Services, U. S. D. o. H. a. H., & Administration, F. a. D. (2006). Q9 Quality Risk Management. Taylor, Z., & Ranganathan, S. (2013). Six Sigma Tools for Predictive Engineering. In *Designing High Availability Systems* (pp. 278-301). <https://doi.org/https://doi.org/10.1002/9781118739853.ch14>

Verbecque, E., Vereeck, L., Van de Heyning, P., & Hallems, A. (2017). Gait and its components in typically developing preschoolers. *Gait Posture*, 58, 300-306.  
<https://doi.org/10.1016/j.gaitpost.2017.08.012>

Zahid, F. B., Ong, Z. C., & Khoo, S. Y. (2020). A Review of Operational Modal Analysis Techniques for In-service

Modal Identification. *Journal of the Brazilian Society of Mechanical Sciences and Engineering*, 42. <https://doi.org/10.1007/s40430-020-02470-8>



**VIII. APPENDIX II: Overall BWST Design Criteria and Verification Results**

<b>Item</b>	<b>User Need/Design Criteria</b>	<b>Pre-Assembly Design Evaluation</b>	<b>Test Method/ Verification</b>	<b>Results</b>
1	Modularity	N/A	Visual Confirmation of five sub-assemblies	Pass
2	Commercialization/DFM	N/A	Cost reduction comparison to adult system (\$100,000)	PASS, State of the art manufacturing, <\$50,000
3	The device should support up to 600 lbs. to account for the patient and trainers.	N/A	Weight Testing, Load the crane with 120 lbs. while one trainer stands on the motor housing, one trainer seats on each seat (two side seats and trunk trainer seat). (ensure weight is greater than or equal to 600lbs)	Pass, 120 lbs. plus four trainers on system for 10 mins
4	Device should not tip	Solidworks Motion Analysis, 120 lbs. with FOS 1.5	Weight Testing, Cantilevered weight testing, 325 held for 15 minutes	Pass, Motion analysis FOS 7.98
5	Crane behind patient – allows for more patient interaction and less intimidating	N/A	Visual Inspection	Pass
6	Symmetric Footprint	N/A	Visual Inspection	Pass, treadmill midline, have crane on right or left
7	Footprint Reduction	N/A	Dimensional Verification, Compare to adult system (9’10” H x 4’ 9” W x 18’ L)	Pass, floating seating system. Eliminated ramp, (8.5’ H x 6.25’ L x 4.33’ W)
8	Easy install and transport	N/A	Visual Inspection	Pass, two-piece crane, limited palettes
9	Ergonomic	N/A	Visual Inspection	Pass

Item	User Need/Design Criteria	Pre-Assembly Design Evaluation	Test Method/ Verification	Results
10	Made for child patient size	N/A	Pediatric manikins	Pass

**IX. APPENDIX III: Treadmill Design Criteria and Verification Results**

<b>Item</b>	<b>User Need/Design Criteria</b>	<b>Pre-Assembly Design Evaluation</b>	<b>Test Method/ Verification</b>	<b>Results</b>
<b>1</b>	The device should feature a robust level central treadmill weight at least 350lbs. to stabilize the entire body weight support treadmill	mass properties calculations on SolidWorks	Check with 4-foot level	Pass, system is level, weighs 409.87 lbs.
<b>2</b>	A stabilizing fore and aft deck should be able to be attached to the front and back of the treadmill	N/A	Visual Inspection	Pass
<b>3</b>	Motor housing should be 2 cubic feet to able to house the electrical and mechanical components for the treadmill as well as a platform for trainer to stand	N/A	Dimensional Verification	Pass, 3.67 ft <sup>3</sup> (2.08' x 1.33' x 1.33')
<b>4</b>	The motor housing should be able to support up to 300lbs.	N/A	Weight testing for 10 minutes, 309.96 lbs. (E, F, G, H, I, J, K)	Pass, no failure
<b>5</b>	motor housing contains breakout electrical panel, 220V input and 1 220 outputs for treadmill motor and 2 120 outputs for the control panel, slew ring motor, the electric actuator	N/A	Visual Inspection	Pass
<b>6</b>	Treadmill must be able to be controlled by a computer and reach a speed of 6 mph with 0.1 mph per increments in under a second	N/A	Functionality testing, ramp treadmill to 6 mph, ensure 0.1 mph increments when ramping, and starts and stops on command	Pass
<b>7</b>	Treadmill should stop in < 2s when prompted during motion.	N/A	Functionality Testing	Pass, stops instantly

<b>Item</b>	<b>User Need/Design Criteria</b>	<b>Pre-Assembly Design Evaluation</b>	<b>Test Method/ Verification</b>	<b>Results</b>
<b>8</b>	Treadmill deck should support 120lb max patient weight with a 1.5 factor of safety	Treadmill deck and 4x mounting brackets Static FEA, FOS 2.1	Weight testing, Stand on deck for 10 minutes	Pass, 195 lbs. on deck for 10 minutes with no noticeable failures
<b>9</b>	Device treadmill surface should have at minimum 40" exposed belt length and between 12.5" and 14" in exposed belt width	N/A	Dimensional Verification	Pass, 40" L x 14" W
<b>10</b>	Device chassis width should be 13.5"-15".	N/A	Dimensional Verification	Pass, 14.5" W
<b>11</b>	Robust roller and treadmill belt design to reduce maintenance over time	Large custom roller, robust durable motor	Functionality Testing over time	Let treadmill run for 45 mins confirming proper installation, Full validation will occur over time
<b>12</b>	Treadmill belt should not have slippage or side to side movement	N/A	Functionality Testing after proper tensioning of belt	Pass, 195lbs. person walked on belt after tensioning with no slippage
<b>13</b>	Includes integrated adjustable right/left trainer seating at least 17" fore/aft and right/left trainer footrest system at least 8" fore/aft	N/A	Visual Inspection and Dimensional Verification	Pass, includes linear bearing and rack system, 17" slot for seats and 8" slot for footrests
<b>14</b>	Treadmill must be safe, durable and must not have any sharp/jagged edges.	N/A	Visual Inspection	Pass, rounded corners, bent steel edges, back side of treadmill is left open to not get patients feet/clothing stuck
<b>15</b>	No treadmill incline feature	N/A	Visual Inspection	Pass

**X. APPENDIX IV: Seating/Foostrest Design Criteria and Verification Results**

<b>Item</b>	<b>User Need/Design Criteria</b>	<b>Pre-Assembly Design Evaluation</b>	<b>Test Method/ Verification</b>	<b>Results</b>
<b>1</b>	Device must contain two chairs on either side of the treadmill and one seat for the trunk trainer	N/A	Visual Inspection	Pass
<b>2</b>	All trainer seats (leg and trunk trainer seats) should support trainers up to 250 lbs.	Seating cantilever arm Static FEA, FOS 1.9 and Trunk trainer seat Static FEA, FOS 2.3	Weight Testing	Pass, each tested with student - 195 lbs. holding B + F
<b>3</b>	integrated seating into the treadmill for easier install and smaller overall footprint	N/A	Visual Inspection	Pass
<b>4</b>	The center of each leg trainer seat should be within $17 \pm 1$ in. from the midline of the treadmill	N/A	Dimensional Verification	Pass, right 18 in. and left 17.75 in.
<b>5</b>	Leg trainer seats need to have a $5 \pm 1$ in. chair height adjustment range	N/A	Dimensional Verification	Pass, right 4 in. and left 4 in.
<b>6</b>	The leg trainer seats should be adjustable $17 \pm 1$ in. fore and aft	N/A	Dimensional Verification and Functionality testing	Pass, moved as designed, right 16 in. and left 16 in.
<b>7</b>	Trunk trainer seat height should be adjustable $3 \pm 1$ in.	N/A	Dimensional Verification	Pass, 4 in.
<b>8</b>	The center of the trunk trainer seat should be within $24 \pm 2$ inches from patient position on the treadmill	N/A	Dimensional Verification using plumb bob from crane boom	Pass, 22.5 in.



<b>Item</b>	<b>User Need/Design Criteria</b>	<b>Pre-Assembly Design Evaluation</b>	<b>Test Method/ Verification</b>	<b>Results</b>
<b>9</b>	The seat for trunk trainer must be removable for getting patient on and off treadmill and to use stairs in back	N/A	Functionality Testing	Pass, seat rotated and was easily removed
<b>10</b>	Footrests for leg trainers should be adjustable by 5 ± 1 in. fore and aft	N/A	Dimensional Verification and Functionality testing	Pass, moved as designed, right 4.75 in. and left 4.75 in.
<b>11</b>	Each footrest should be minimum 6 in. long and 2 in. wide	N/A	Dimensional Verification	Pass, 10.5 in. by 9 in. TRESPA platform
<b>12</b>	Each footrest should be able to support up to 125 lbs.	Can use seating static FEA to justify footrests meet design criteria since same bracketry is used	Can use seating weight testing to justify footrests meet design criteria since same bracketry is used	Pass

**XI. APPENDIX V: Front/Rear Decks Design Criteria and Verification Results**

<b>Item</b>	<b>User Need/Design Criteria</b>	<b>Pre-Assembly Design Evaluation</b>	<b>Test Method/ Verification</b>	<b>Results</b>
<b>1</b>	Overall rear deck length is $\geq 50$ in.	N/A	Dimensional Verification	Pass, 52 in.
<b>2</b>	Overall front deck length is $\geq 50$ in.	N/A	Dimensional Verification	Pass, 52 in.
<b>3</b>	A sturdy slew ring motor attachment point should be integrated to the aft deck to allow for crane rotation	N/A	Visual Inspection	Pass, 0.5 in. crane plate
<b>4</b>	Device must have stairs for patient of step height 5 in. $\pm$ 1 in. that can support up to 300 lbs.	N/A	Dimensional Verification and Weight testing for 10 minutes, 309.96 lbs. (E, F, G, H, I, J, K)	Pass, 6 in., no failure, or deformation seen
<b>5</b>	Fore deck should have a step to allow trainers on the motor housing unit platform that supports up to 300 lbs.	N/A	Weight testing for 10 minutes, 309.96 lbs. (E, F, G, H, I, J, K)	Pass, 10.5 in., no failure, or deformation seen
<b>6</b>	Decks should extend past central treadmill to provide lateral stabilization	N/A	Visual Inspection	Pass
<b>7</b>	Decks should be level and include leveling feet for adjustment	N/A	Visual Inspection and Check with 4-foot level	Pass
<b>8</b>	Rigid top platform	N/A	Visual Inspection	Pass, TRESA installed with no instability seen
<b>9</b>	Modularity	Modular front and rear deck attachment design	Visual Inspection	Pass

<b>Item</b>	<b>User Need/Design Criteria</b>	<b>Pre-Assembly Design Evaluation</b>	<b>Test Method/ Verification</b>	<b>Results</b>
<b>10</b>	Aft deck has symmetrical slew ring attachment	N/A	Dimensional Verification and Visual Inspection	Pass, crane plate installed on right or left side, 11 x 0.5 in. mounting holes, ability to flip slew ring worm drive
<b>11</b>	TRESPA removable with ball and socket for potential storage	N/A	Visual Inspection	Pass, ball sockets installed
<b>12</b>	Front/rear decks do not have any sharp/jagged edges.	N/A	Visual Inspection	Back deck passed, Front deck has squared off edges – patient will not be near front deck, will be updated with manufacturer in next iterations

## XII. APPENDIX VI: Crane Design Criteria and Verification Results

Item	User Need/Design Criteria	Pre-Assembly Design Evaluation	Test Method/ Verification	Results
1	The device should include a sturdy two-piece crane for patient hoisting that is attached to the slew ring motor on the aft deck	N/A	Visual Inspection	Pass, crane can break down into two pieces and is attached to slew ring
2	The crane should have attachment points and brackets for body weight support treadmill	N/A	Visual Inspection and Fitment	Pass, 3 pulley mounts and cylinder support box
3	Entire BWST including crane should be under 9 ft. tall.	N/A	Dimensional Verification	Pass, 8.67 ft.
4	Crane should include slew ring for placing child on/off treadmill	N/A	Visual Inspection	Pass
5	Crane should rotate clockwise from neutral position 150 deg to be able to reach a patient in a wheelchair at the rear the BWST	N/A	Dimensional Verification and Functionality Testing	Pass
6	Crane rotation speed should not be more than 20 deg/sec	N/A	Functionality Testing	Pass, 23s for complete 150 degrees rotation, 6.5 degrees/sec

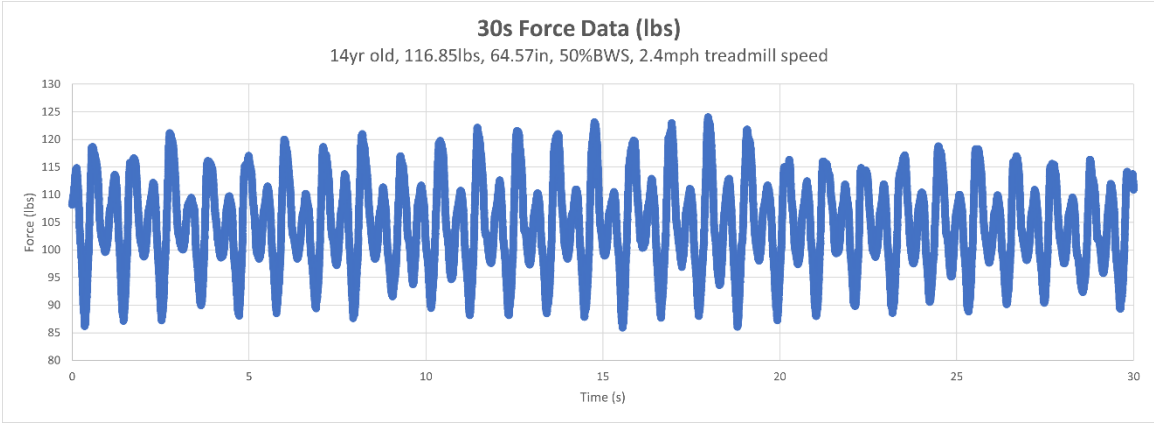
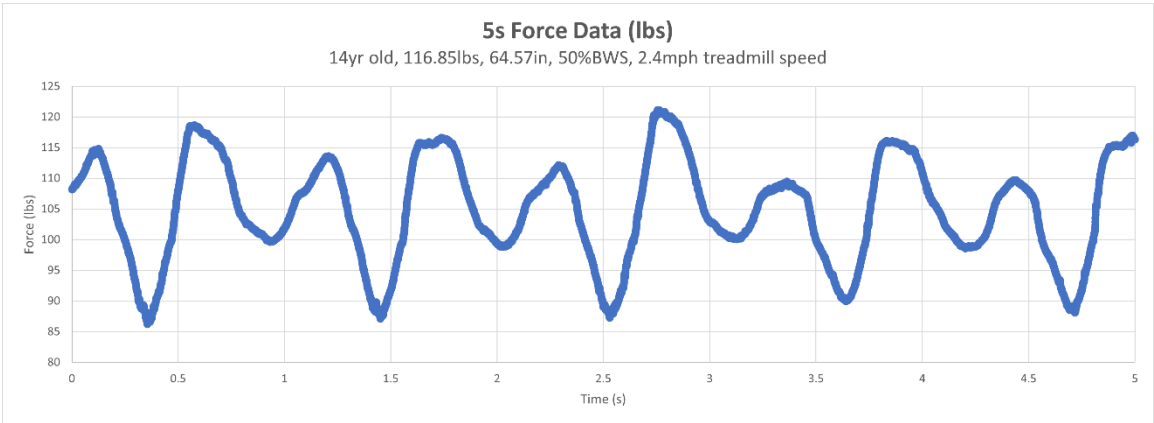
Item	User Need/Design Criteria	Pre-Assembly Design Evaluation	Test Method/ Verification	Results
7	The device crane arm should be able to hold at minimum 300 lbs. or 120-pound max patient weight with a factor of safety of 1.5	Gusset crane Static FEA, FOS 2.5 and Non-gusset crane Static FEA, FOS 3.4	Weight Testing for 10 minutes, 325.24 lbs. (small chain + large chain + yoke and carabiner + parts F, G, H, I, J, K, L)	<ul style="list-style-type: none"> <li>• 1st attempt - fail, cylinder support box broke, required redesign</li> <li>• Pass, static FEA of rev. 2 support, FOS 2</li> <li>• Pass, weight testing rev. 2</li> </ul>
8	Device crane must center the patient on the treadmill	N/A	Dimensional Verification using plumb bob	Pass, 19-3/8 in. from motor housing and 6-7/8 in from treadmill belt

**XIII. APPENDIX VII: BWS/Control System Design Criteria and Verification Results**

<b>Item</b>	<b>User Need/Design Criteria</b>	<b>Pre-Assembly Design Evaluation</b>	<b>Test Method/Verification</b>	<b>Results</b>
<b>1</b>	Control system should have a closed loop force feedback algorithm for body weight support control	N/A	N/A	Pass, control system includes BWS computer software previously used in adult BWST
<b>2</b>	Load cell must have a 1:1 force ratio to the patient weight	N/A	Incremental Weight Testing	Pass, load cell incremental weight testing graph is linear
<b>3</b>	Must include yoke, cable, and a safety cable	N/A	Visual Inspection	Pass, previous yoke, cable, safety cable design used from Alpha Peds BWST
<b>4</b>	Cable extension from the crane should accommodate 1'8" - 5'6" patient heights from the connection to yoke	N/A	Dimensional Verification	Pass, Treadmill position – 67.5 in. H and 20in. L, Patient pickup position 37 in. L
<b>5</b>	Crane must have neutral position sensor and two limit switches		Dimensional Verification and Functionality Testing	Pass
<b>6</b>	The device should have a hoist system that includes a yoke attached to a rope/cable that runs through a gross actuator, then a fine actuator terminated at a load cell.	N/A	Visual Inspection	Pass
<b>7</b>	The device should feature a control panel to has DAQ and allows for control of treadmill, slew ring, and hoist system.	N/A	Visual Inspection	Pass
<b>8</b>	Device emergency stop button should lock treadmill and BWS.	N/A	Functionality Testing	Pass, treadmill stopped instantly and BWS locked up

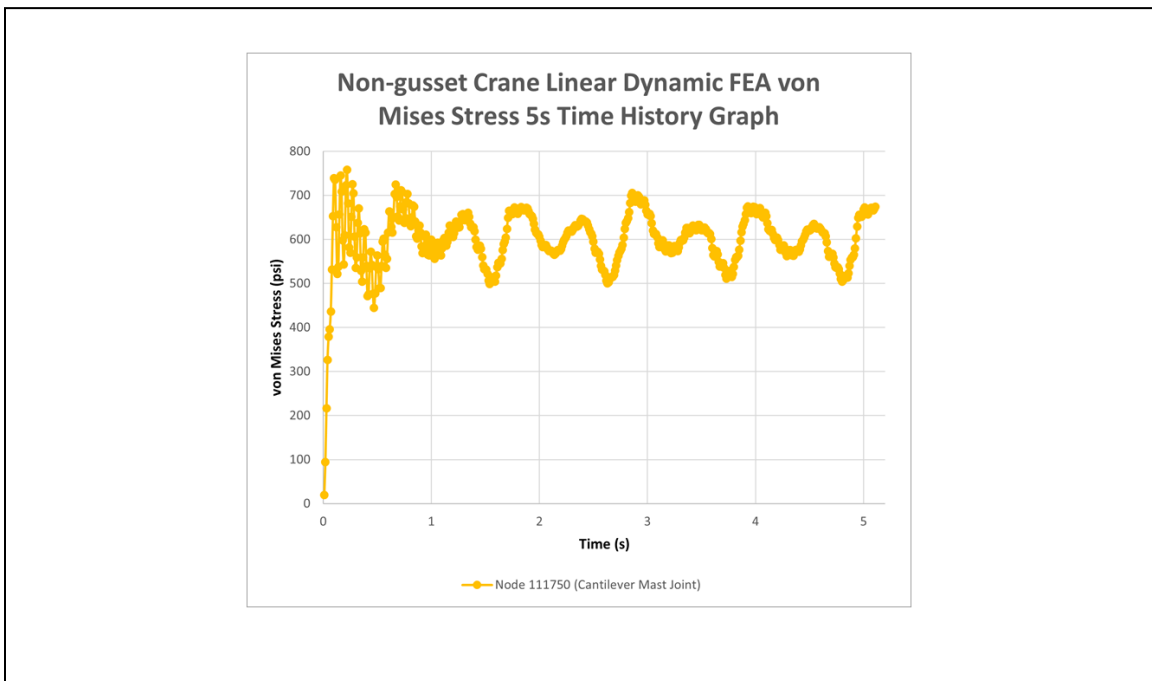
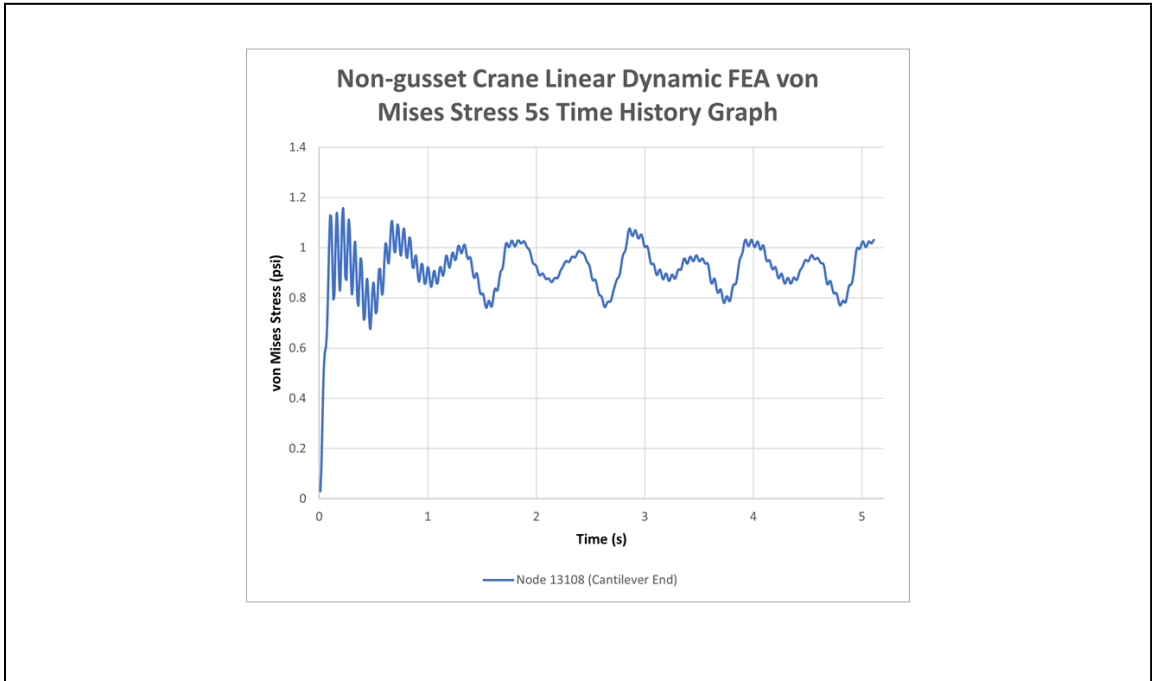
<b>Item</b>	<b>User Need/Design Criteria</b>	<b>Pre-Assembly Design Evaluation</b>	<b>Test Method/Verification</b>	<b>Results</b>
<b>9</b>	Device emergency stop button should not lock crane rotation.	N/A	Functionality Testing	Pass, crane successfully moved 90 degrees clockwise and counterclockwise back to starting position
<b>10</b>	Device emergency stop button should lock the computer software.	N/A	Functionality Testing	Pass, display indicates emergency stop and reactivation was not possible until emergency button was disengaged
<b>11</b>	Device contains 24V 20A power supply for the control panel, slew ring motor and controller.	N/A	Multimeter	Pass, Mean Well SDR-480-24, 20 A rated, 110V, 20A, measured 23.9V, tolerance is +-1.2%
<b>12</b>	Device contains 12V 19A power supply for the gross actuator.	N/A	Multimeter	Pass, 11.6 V
<b>13</b>	Air compressor should be able to output pressures between 90 and 115psi., have at least an 8 gal. air tank	Spec Sheet Evaluation	Functionality Testing	Pass
<b>14</b>	Dynamic body weight support treadmill tuned to child weighing 20-120lbs	N/A	Software Validated in further testing over time	N/A

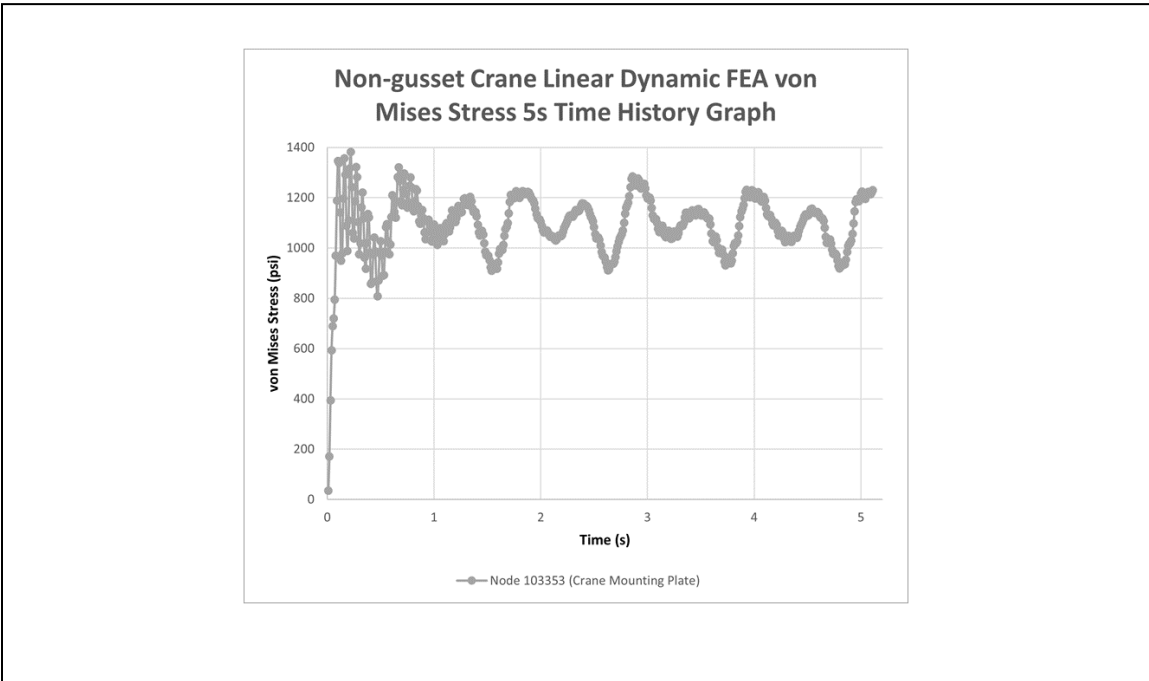
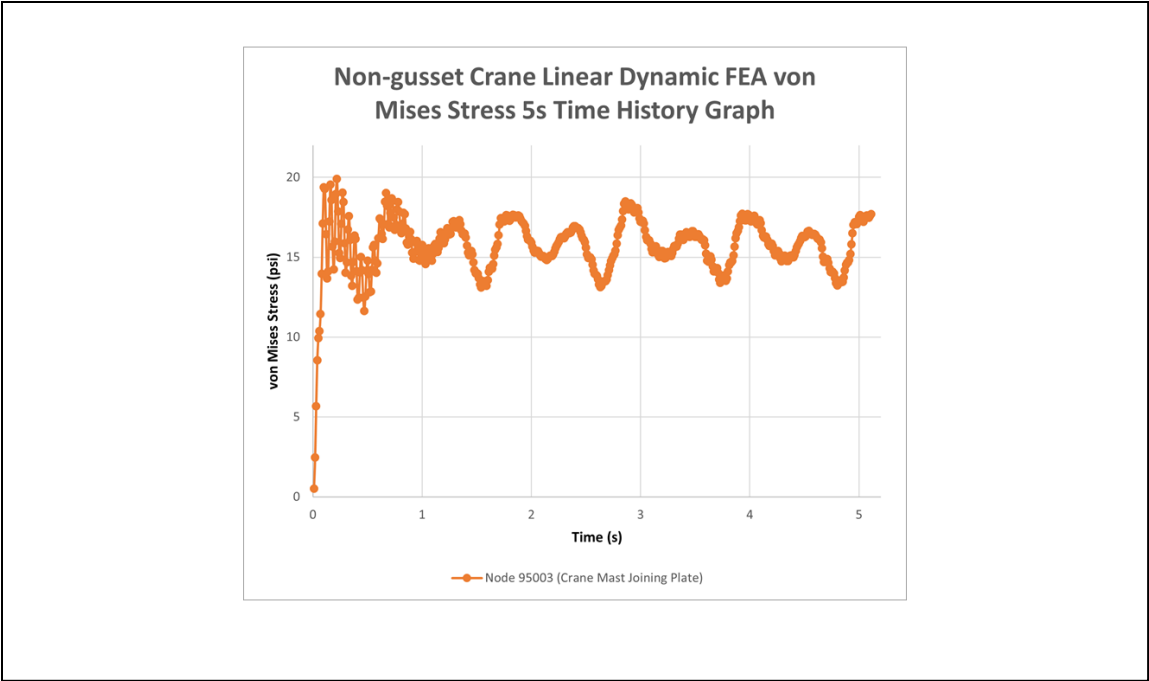
**XIV. APPENDIX VIII: Original Patient Force Data for FEA Dynamic Analysis**





**XV. APPENDIX IX: Crane Modal Time History von Mises Stress Graphs**





**XVI. APPENDIX X: High-level Cost Structure**

<b>Item</b>	<b>Cost</b>
Treadmill	\$ 15,089.00
Fore and Aft Decks	\$ 1,776.64
Crane	\$ 1,485.29
TRESPA	\$ 300.00
Side Seats	\$ 188.74
Trunk Trainer Seat	\$ 500.00
Footrests	\$ 190.34
Air compressor	\$ 11,789.04
Pneumatic Cylinder and Equip.	\$ 3,829.24
Electric Cylinder	\$ 436.97
Hardware	\$ 595.26
Rope, Cable , yoke	\$ 378.44
Electronics	\$ 5,806.84
Powder Coat	\$ 625.00
<b>Total</b>	<b>\$ 42,990.80</b>

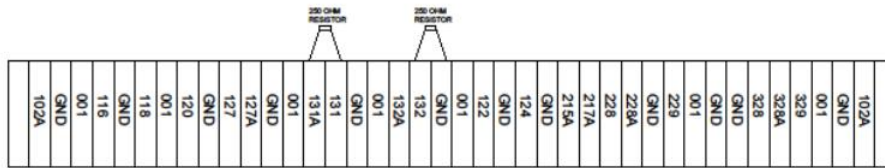
**XVII. APPENDIX XI: Pediatric SCI Patient Metrics Reference**

<b>Pediatric SCI Patient Age, Height, and Weight</b>		
<b>Age</b>	<b>Height (ft)</b>	<b>Weight (lbs.)</b>
6	4.15	48.61
4	3.63	39.90
14	5.38	116.84
3	3.19	33.07
5	3.90	108.14
6	3.80	53.24
6	3.58	77.71
4	3.33	33.95
5	3.66	42.99
4	2.75	27.12
<b>Average</b>	<b>5.70</b>	<b>58.16</b>

# XVIII. APPENDIX XII: BWST Control System Schematic

PRODUCED BY AN AUTODESK EDUCATIONAL PRODUCT

PRODUCED BY AN AUTODESK EDUCATIONAL PRODUCT

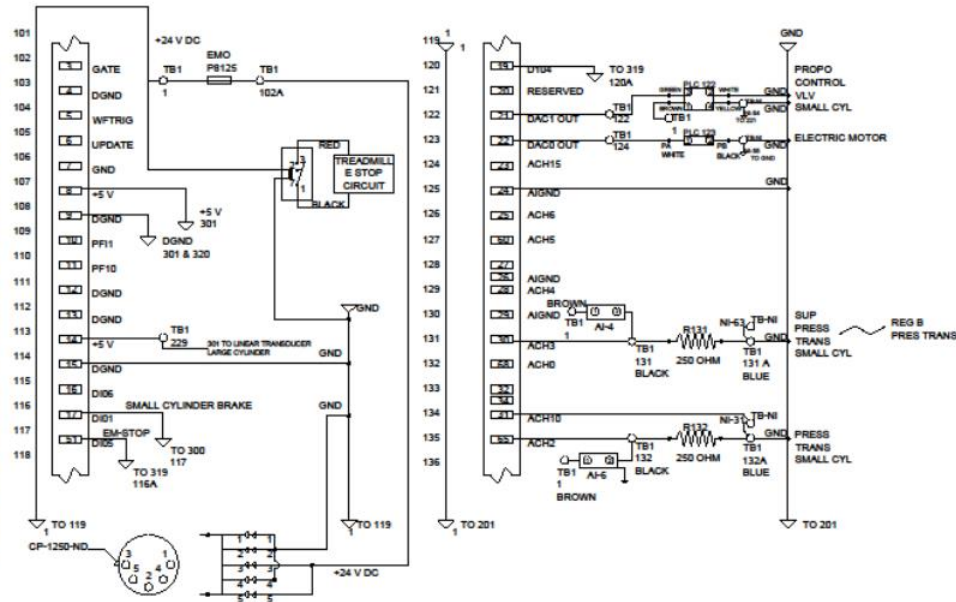


TERMINAL STRIP (TB1)

PRODUCED BY AN AUTODESK EDUCATIONAL PRODUCT

PRODUCED BY AN AUTODESK EDUCATIONAL PRODUCT

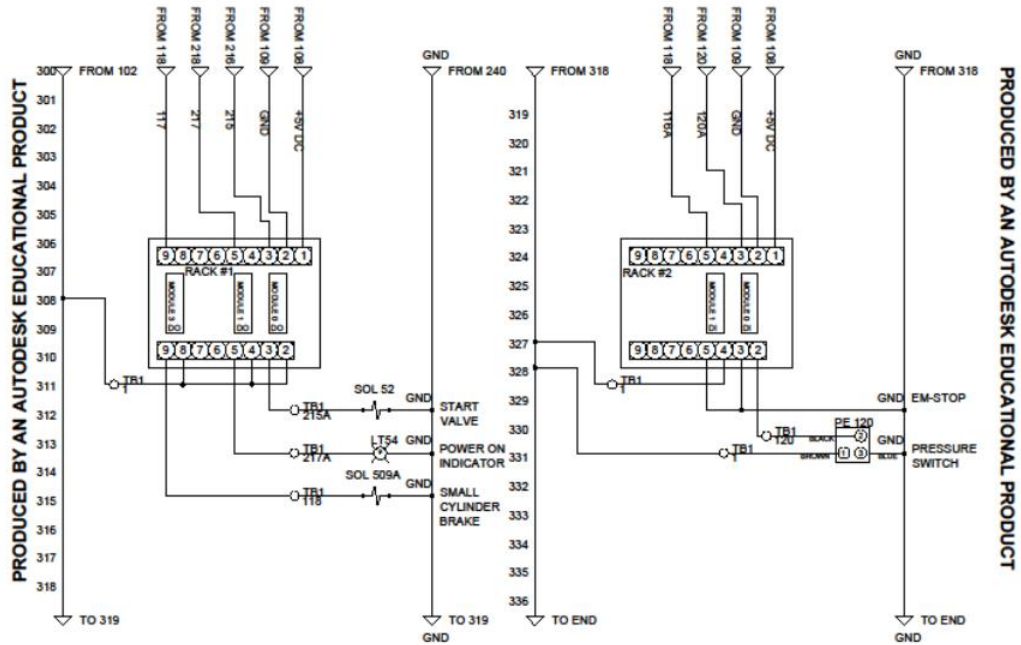
PRODUCED BY AN AUTODESK EDUCATIONAL PRODUCT



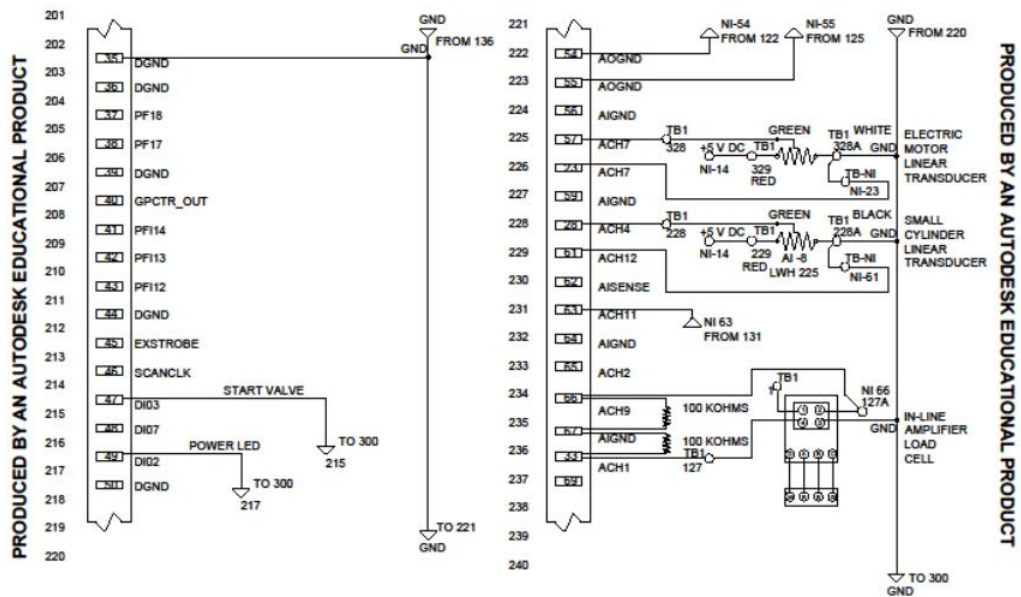
PRODUCED BY AN AUTODESK EDUCATIONAL PRODUCT

PRODUCED BY AN AUTODESK EDUCATIONAL PRODUCT

PRODUCED BY AN AUTODESK EDUCATIONAL PRODUCT



PRODUCED BY AN AUTODESK EDUCATIONAL PRODUCT  
 PRODUCED BY AN AUTODESK EDUCATIONAL PRODUCT



PRODUCED BY AN AUTODESK EDUCATIONAL PRODUCT